IMPACT OF *BIFIDOBACTERIUM* AND ITS METABOLITES ON ATOPIC DERMATITIS VIA MODULATION GUT MICROBIOTA AND HOST IMMUNITY

KEXIN ZHANG

PhD

The Hong Kong Polytechnic University

2026

The Hong Kong Polytechnic University

Department of Food Science and Nutrition

Impact of Bifidobacterium and Its Metabolites on Atopic Dermatitis Via Modulation Gut Microbiota and Host Immunity

Kexin Zhang

A thesis submitted in partial fulfillment of the requirements for the degree of Doctor of Philosophy

August 2025

CERTIFICATE OF ORIGINALITY

I hereby declare that this thesis is my own work and that, to the best ofmy knowledge and belief, it reproduces no material previously published or written, nor material that has been accepted for the award of anyother degree or diploma, except where due acknowledgment has been made in the text.

Signature: _____

Name of Student: Kexin ZHANG

Abstract:

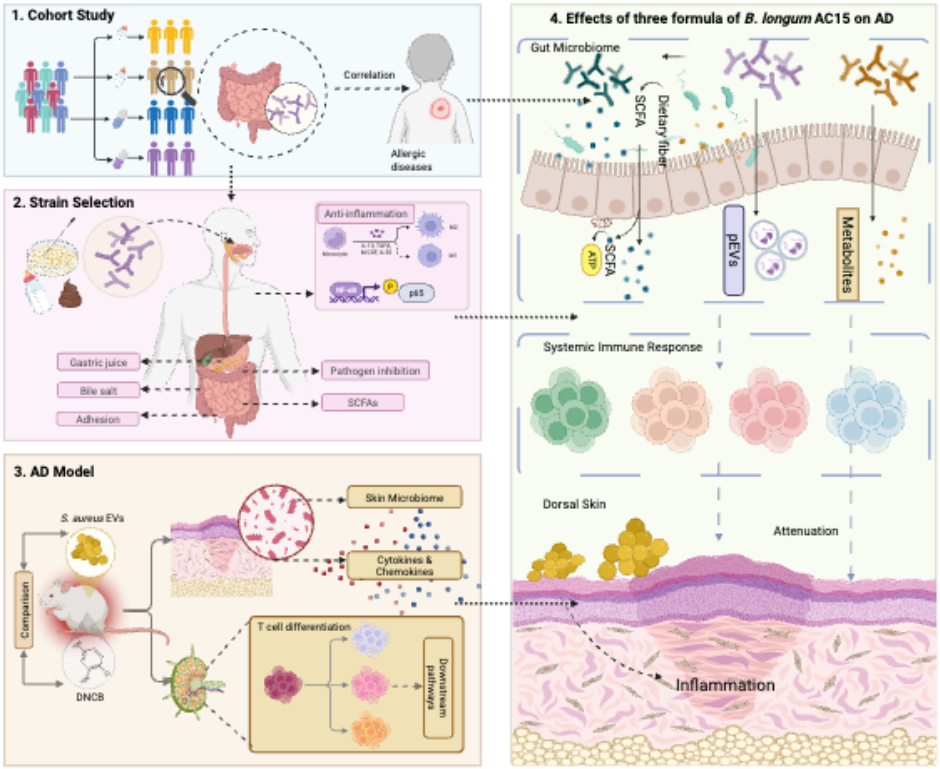

Figure 1 Study design of thesis

Bifidobacteria have garnered scientific interest since their discovery because of their extensive physiological benefits for the host. As persistent colonizers across the human lifespan, they perform important functions, such as modulating immune responses, enhancing intestinal barrier integrity, and competitively excluding pathogens. Their role as pivotal commensals is especially significant in early infancy, during which they dominate the gut microbiota and contribute fundamentally to immunological programming and tolerance development. The genus encompasses a wide diversity of species and strains, many uniquely adapted to metabolize human milk oligosaccharides (HMOs), reflecting a co-evolutionary relationship with humans. This integral niche within the microbiome, together with their ability to produce immunomodulatory metabolites like short-chain fatty acids (SCFAs), establishes bifidobacteria as promising therapeutic targets for immune-mediated diseases. Building on this foundation, they are considered as the key modulators of the Gut-Skin Axis. Their depletion or altered composition is mechanistically linked to the immune dysregulation and impaired tolerance observed in atopic dermatitis (AD). Consequently, strategies aimed at restoring or modulating bifidobacterial populations have become a major focus of contemporary research into this complex, chronic inflammatory skin disorder.

Therefore, this study was structured into four distinct yet interconnected sections to investigate the relationship between bifidobacteria and AD. The first section presented a cohort study analyzing the correlation between AD and gut microbiota composition, with a focus on *Bifidobacterium* and its specific subspecies. It also examined the influence of delivery modes and feeding patterns on the development of the infant gut microbiome. Our data

indicated that breastfeeding is the best source of high diversity of *Bifidobacterium spp.* to infant gut microbiota. A specific synbiotic mixture (*B. breve* M16-V with scGOS/lcFOS 9:1 prebiotic mixture) restored the delayed colonization of infant-type *Bifidobacterium spp*. and increased gut microbiota diversity in C-section born infants to levels closer to those observed in healthy, vaginal-born, breastfed infants. Besides, it helped the development of strict anaerobes in the C-section born infants' gut, which helps with digestion, nutrient absorption, SCFAs production and immune system development.

The second section was designed to isolate, screen, and characterize bifidobacteria obtained from human breastmilk and feces. The biological functions of these isolates were examined through *in cellulo* and *in vitro* assays, with the focuses on gastrointestinal resilience, adhesion to intestinal epithelium, pathogen exclusion capability, antimicrobial activity, and anti-inflammatory effects. Our data showed that different species exhibited distinct capabilities that benefit host health through diverse mechanisms. Overall, *B. longum* AC15 demonstrated outstanding performance amongst all, especially the adhesion ability to enterocyte (6.0±1.1 bacteria/Caco-2 cell), tolerance to acid (Log (CFU/mL) decreased from 7.95 to 6.57), and anti-inflammatory on macrophage via suppressing the phosphorylation of p65 in the NF-κB signaling pathway. Those evidences suggested it might be a potential candidate in modulating immune responses and potentially serve as a therapeutic strategy to mitigate inflammatory diseases, which provided a potential option for the subsequent investigation of skin inflammatory disease.

Different from the golden standard DNCB (2,4-Dinitrochlorobenzene) induction assay, , AD animal model was established using *Staphylococcus aureus*-derived extracellular vesicles (SA-EVs) in section 3. SA-EVs created a thickened epidermis, enlarged skin draining lymph nodes (SDLNs), and increased level of total IgE in serum, which are comparable to the characteristics of DNCB-induced one. Data from the combinational analysis of transcriptome and proteome indicated that the underlying mechanisms between two disease models varied. SA-EVs mainly triggered immune responses via IL-17 signaling pathway, while DNCB influenced pathways related to parasites. Moreover, DNCB induced severe dysbiosis of skin microbiome, while SA-EVs led to over colonization of *S. aureus* but maintained overall skin microbiome diversity. Collectively, the SA-EVs model generates an AD phenotype more closely aligned with real-world disease pathology, providing a solid foundation for subsequent investigation into potential AD therapies.

The last section evaluated the beneficial effects of the primary screened isolate, *B. longum* A15, on AD mice induced by SA-EVs and its underlying mechanism. In this part, three forms of *B. longum* AC15, including live, heat-inactivated (HI), and EVs, were investigated. The most promising dosage was determined through preliminary titration experiments. Results from this study demonstrated that pre-treatment and co-treatment of 10^9 CFU of live/HI *B. longum* AC15 and 100 μg EVs of *B. longum* AC15 sufficiently alleviated the AD symptoms. Notably, the ameliorative effects were mediated through the suppression of Th17 cell differentiation and the downregulation of Th2- and Th17-related cytokines, subsequently modulating the immune system through SDLNs. Taken together, these results suggest that *B. longum* AC15 could be a promising candidate for the AD attenuation.

Acknowledgement:

I would first like to express my deepest gratitude to my research supervisor, Professor Amber Chiou Jiachi, of the Department of Food Science and Nutrition. Her expert guidance, unwavering patience, and invaluable insights were the cornerstone of this research journey. Professor Chiou's profound knowledge and critical feedback challenged me to refine my ideas and deepen my analysis, for which I am eternally thankful. This thesis would not have reached its completion without her steadfast support and mentorship.

I extend my sincere appreciation to the members of my thesis committee for their time, engaging questions, and constructive suggestions, which significantly strengthened the quality of this work. My thanks also go to the technical and support staff of University Research Facility in Life Science for their indispensable assistance with qPCR, GC-FID and MS-HPLC analysis and for always providing a helping hand. I am grateful to my fellow colleagues and lab mates, especially Dr. Lilong JIANG, Dr. Tim-Fat SHUM, and Mrs Xiaoqing KUANG for creating a stimulating and supportive research environment. Our collaborative discussions, shared struggles, and camaraderie made the long hours in the lab not only productive but also enjoyable. On a personal note, I owe my profoundest thanks to my family. To my parents, Mrs Jun GAO and Mr. Guobin ZHANG, thank you for your unconditional love, endless encouragement, and for always believing in me.

Finally, I dedicate this work to all those who seek to understand the profound connection between food, science, and human health.

Table of Contents

List of Figures:

List of tables

List of Supplementary Figures/Tables

List of abbreviation

Abbreviation	Definition
AD	Atopic dermatitis
VDB	Vaginal born babies who were given breast milk
CSB	C-section babies who were given breast milk
CAP	C-section babies who were given synbiotic supplements
CCO	C-section babies who were not given synbiotic supplements
C-section	Cesarean section
HMOs	Human Milk Oligosaccharides
RTC	Randomized Controlled Trial
BL	Selective medium used for the cultivation and maintenance of Bifidobacterium
RCM	Reinforced Clostridial Medium
BSM	*Bifidobacterium* Selective Media
TPY	Tryptone Peptone Glucose Yeast Extract
MRS	De Man–Rogosa–Sharpe agar
B. lactis	*Bifidobacterium lactis*
B. longum	*Bifidobacterium longum*

B. breve	*Bifidobacterium breve*
***B. breve* M16-V**	*Bifidobacterium breve M16-V*
B. bifidum	*Bifidobacterium bifidum*
B. adolescentis	*Bifidobacterium adolescentis*
B. catenulatum	*Bifidobacterium catenulatum*
B. pseudocatenulatum	*Bifidobacterium pseudocatenulatum*
L. acidophilus	*Lactobacillus acidophilus*
L. gasseri	*Lactobacillus gasseri*
L. crispatus	*Lactobacillus crispatus*
S. aureus	*Staphylococcus aureus*
E. coli	*Escherichia coli*
SA-Sp	*S. aureus* cultured supernatant
SA-Sp >100KDa	Supernatant above 100KDa and ultracentrifuged pellet
SA-Sp <100KDa	Supernatant below 100KDa fraction
SA-EVs	*Staphylococcus aureus*-derived extracellular vesicles
BL15-EVs	*B. longum* AC15-derived extracellular vesicles
OMVs	Outer membrane vesicles
PEVs	Probiotic-derived EVs

SEAP	Secreted embryonic alkaline phosphatase
EF-Tu	Elongation factor Tu
Tal	Transformalase
Hsp20	Heat shock protein 20
scGOS	Short-chain Galacto-oligosaccharides
lcFOS	Long-chain Fructo-oligosaccharide
GI tract	Gastrointestinal tract
SCFAs	Short-Chain Fatty Acids
LDL	Low-density lipoprotein
HDL	High-density lipoprotein
SDLN	Skin draining lymph nodes
APC	Antigen presenting cells
IgE	Immunoglobulin E
PFA	Paraformaldehyde
H&E staining	Hematoxylin-Eosin Staining
TMB	Tetramethylbenzidine Solution
LOD	Limit of detection
PBS	Phosphate buffered saline

Th1	Type 1 T helper
Th2	Type 2 T helper
Th17	Type 17 T helper
GATA-3	GATA Binding Protein 3
FOXP3	Forkhead box P3
RORγt	RAR-related orphan receptor gamma
CD4$^+$	Cluster of differentiation of 4
CD8$^+$	Cluster of differentiation of 8
TSLP	Thymic stromal lymphopoietin
DCs	Dendritic cells
IFN	Interferon
TNF- α	Tumour necrosis factor alpha
MIP-1α	Macrophage inflammatory protein-1α
MCP-1	Monocyte chemoattractant protein-1
TARC/CCL17	Thymus and activation-regulated chemokine
MDC/CCL22	Macrophage-derived chemokine
RANTES/CCL5	Regulated upon activation, normal T cell expressed and secreted
CCL	Chemokine (C-C motif) ligand

IL	Interleukin
K	Keratin
TSLP	Thymic stromal lymphopoietin
GC	Gas chromatograph
FID	Flame Ionization Detection
qPCR	Quantitative real-time polymerase chain reaction
RT-qPCR	Reverse transcription-quantitative polymerase chain reaction
PGN	Peptidoglycan
DNCB	2,4-Dinitrochlorobenzene
SIJ	Simulated intestinal juice
SGJ	Simulated gastric juice
Caco-2	Colon epithelium cells
HaCaT	Human skin epidermis cells
HI	Heat-inactivated
PVDF	Nitrocellulose filters
DEGs	Differentially expressed genes
FDR	False Discovery Rate
LC-MS	Liquid Chromatography-Mass Spectrometry

RWE	Real-World Evidence
MF	Molecular function
CC	Cellular components
GO	Gene ontology
CAD	Chronic atopic dermatitis
SAD	Subacute atopic dermatitis
AAD	Acute atopic dermatitis
C/EBPβ	CCAAT/enhancer-binding protein beta
AP-1	Activator protein 1
MAPK	Mitogen-activated protein kinases
NF-κB	Nuclear factor-kappa B

Chapter 1: Introduction

The human gastrointestinal tract hosts a diverse and complex community of microorganisms, collectively termed the gut microbiota [1]. These microbial communities play a pivotal role in modulating host health and influencing pathophysiological processes [2]. In light of their profound significance for human health, substantial scientific research has been directed toward developing strategies to therapeutically manipulate this internal ecosystem. Within this domain, a specific group of beneficial microorganisms known as probiotics has emerged as a major focus in nutritional science and clinical microbiology [3,4]. Furthermore, the bioactive compounds produced by these probiotics, often referred to as postbiotics, have also increasingly garnered significant research attention.

The word “probiotic”, derived from a combination of the Greek “*bios*” (life) and the Latin prefix “*pro”* (for), has undergone significant refinement since its early informal use [5]. The currently authoritative definition, provided by the International Scientific Association for Probiotics and Prebiotics (ISAPP), states that probiotics are “live microorganisms that, when administered in adequate amounts, confer a health benefit on the host”. Postbiotics, on the other hand, are defined as “preparation of inanimate microorganisms and/or their components that confer a health benefit on the host”[6]. Crucially, postbiotics must be deliberately inactivated, and their production process must be characterized and controlled [7]. This category encompasses a diverse range of bioactive compounds, including but not limited to cell wall fragments, peptidoglycans, extracellular polysaccharides, and short-chain fatty acids (SCFAs) synthesized by the microbiomes [8]. Probiotics and postbiotics represent two complementary yet distinct classes of biotherapeutic agents for modulating host health through microbial interventions. The fundamental difference between viability and non-viability reflecting their respective mechanisms of action, stability, and applications.

A genus of exceptional importance in the category of probiotics is *Bifidobacterium*. These bacteria are known to benefit the host through multifaceted mechanisms, including competitive exclusion of pathogens, production of antimicrobial substances, and modulation of the host immune system [9,10].

Regarding the competitive exclusion, bifidobacteria inhibit the colonization and proliferation of pathogens by occupying adhesion sites on the surface of intestinal epithelial cells, competing for nutrients, and altering the local microenvironment. For instance, *B. longum* can specifically bind to the mucin layer of the intestinal mucosa, physically blocking the attachment of pathogenic bacteria such as *E. coli* and *Salmonella* [11]. Moreover, its efficient metabolism of dietary fibers depletes available carbon sources in the gut, creating a "nutrient competition" against pathogens with similar nutritional demands[12]. Additionally, its metabolites, acetate and lactate, significantly lower intestinal pH, creating an acidic environment unfavourable for the survival of most pathogens, thereby further consolidating their competitive advantage[13]. Acetate also acts as a proton carrier that penetrates the pathogen's cell membrane, disrupting the transmembrane proton motive force and leading to the collapse of cellular energy metabolism[14]. Beyond directly inhibiting the growth of pathogens via metabolites, bifidobacteria also synthesize specific bacteriocin-like compounds. Certain strains such as *B. bifidum* can produce bifidocin, a bacteriocin that directly compromises the integrity of pathogen membranes, causing leakage of intracellular contents and cell death [15].

Bifidobacteria also can modulate the host immune system by engaging intestinal immune cells through pattern recognition receptors, thereby finely balancing immune responses [16]. For instance, peptidoglycan and lipoteichoic acid within the cell wall of *B. breve* can be recognized by TLR2 on dendritic cells (DCs), further promoting the differentiation of regulatory DCs. This enhances the secretion of anti-inflammatory cytokines, while suppressing pro-inflammatory factors [17]. Meanwhile, SCFAs produced by bifidobacteria, particularly butyrate, act directly on intestinal epithelial cells and immune cells. By inhibiting histone deacetylases (HDACs) and activating G-protein-coupled receptors (e.g., GPR43 and GPR109a), they promote the differentiation and proliferation of regulatory T cells (Tregs) [18]. This helps suppress excessive Th2 immune responses and maintains immune tolerance. Additionally, bifidobacteria enhance intestinal epithelial barrier function by upregulating the expression of tight junction proteins such as occludin and claudin, while stimulating the production of secretory immunoglobulin A[19]. Together, these actions form a robust immune defence, collectively maintaining intestinal homeostasis and health.

In addition to their live form, the heat-inactivated *Bifidobacterium* and its derived extracellular vesicles (EVs) are also capable of delivering documented health benefits in a highly stable, safe, and shelf-stable format, which eliminates challenges associated with microbial viability in production and storage and enhances safety for immunocompromised populations [20]. Thus, postbiotics derived from *Bifidobacterium* offer a practical strategy to deliver the established benefits of this genus, such as immunomodulation and barrier enhancement, through the direct application of its bioactive components, without relying on microbial colonization or viability.

Outer membrane vesicles (OMVs) from Gram-negative bacteria are the most extensively studied [21–24], while the investigation into EVs from Gram-positive bacteria has exploded recent years, particularly regarding probiotic-derived EVs (PEVs), moving from fundamental characterization into mechanistic elucidation and therapeutic investigation. They carry various vital biomolecules and membrane receptors originating from their parent cells, including proteins, nucleic acids, peptidoglycans, lipids, metabolites, and organelles [25]. Many researchers have reported that PEVs play a vital role as delivery vehicles of host-microbe interactions, owing to their nanoscale dimensions, biocompatibility compared to synthetic drug delivery systems, the ability to cross biological barriers, and capacity to protect cargo from harsh *in vivo* environments [26].

PEVs protect the host by inhibiting the overgrowth of pathogens, blocking the interaction between pathogens and the host, and enhancing the adhesion and colonization of probiotics against pathogens. Proteomic analysis revealed that PEVs are rich in bacteriocins, which are the antibacterial compounds that can kill other bacteria [27]. For instance, *L. acidophilus* ATCC 53544-derived EVs protected bacteriocins from digestion of protease and inactivation by compounds in the intestine, so the EVs were precisely delivered to the target and effectively eliminated them [28]. Dynamic EVs produced by *B. longum* NCC2705 harbor various mucin-binding cytoplasmic proteins, such as phosphoketolase, GroEL, elongation factor Tu (EF-Tu), phosphoglycerate kinase, transaldolase (Tal), and heat shock protein 20 (Hsp20), which in turn promote its adhesion to the gastrointestinal tract [29]. EVs generated from *L. crispatus* and *L. gasseri* sufficiently prevented the infection of HIV-1 to host cells through reducing the virus accessibility of a viral envelope protein (gp120) to the host target cells [30].

PEVs boost the immune responses of the hosts, which brings their great potential in working as novel adjuvants treating immune disorder diseases. Studies proved that PEVs enhanced innate immunity by increasing the secretion of pro-inflammatory cytokines from host immune cells [31]. For instance, *L. plantarum*-derived EVs promoted the differentiation of human monocytic THP1 cells towards an anti-inflammatory M2 macrophage phenotype, which alleviate hyperinflammatory skin conditions [32]. Other research showed PEVs successfully suppressed the release of IgE via influencing T cells and mast cells. As López et al. demonstrated in their research, exposure of DCs to EVs derived from *B. bifidum* LMG13195 not only accelerated differentiation of functional $CD25^{high}FOXP3^{high}CD127^{-/low}$ Treg cells but also increased secretion levels of the pro-inflammatory cytokines IFN-γ, TNF-α, and IL-17 [33].

PEVs have promising prospective as a potent bioactive nanotherapeutics, while significant challenges in standardization, manufacturing, and regulation remain. The components, features and physicochemical properties of each PEV are strain- and species- dependent. Their yield relies on peptidoglycan (PGN) content in PEVs, and their component depends on the growth conditions such as pH, oxygen and agitation rate. Apart from the obstacles of standardized production protocol, they also face the challenges of the post-translational modifications effects when work as immune adjuvants, which will address adverse immune responses of the hosts. Moreover, based on our current knowledge, the underlying mechanism of how those PEVs modulate immune system and further benefit human health remain poorly understood.

Recently, the concept of the "Gut-Skin" axis has been proposed, with accumulating studies suggesting that alter the intestinal microenvironment, representing a promising target for the prevention and treatment of atopic dermatitis (AD)[34]. Studies have demonstrated the effects of bifidobacteria on AD are strain-dependent. For instance, certain strains ameliorate DNCB-induced AD by suppressing Th2 polarization, regulating the gut microbiota and SCFAs metabolism[35]. Others produce metabolites like Indole-3-carboxaldehyde (I3C) that reduce AD severity [36]. Consequently, it is necessary to conduct targeted investigations into the functionalities of various species to elucidate their specific potential in the prevention and treatment of AD. On the other hand, research on the effect of postbiotics, particularly PEVs, on AD remains remarkably scarce.

However, translating these promising scientific insights into tangible therapies faces a fundamental translational barrier: the regulatory governance of such novel preparations exhibits profound legislative heterogeneity, creating a fragmented landscape for research translation and market entry.

In Mainland China, the regulatory framework is shifting towards a formalized inclusion of non-viable bacterial products. While traditional probiotics are governed under established strain lists, PEVs often fall under the scope of "New Food Raw Materials," requiring rigorous safety assessment and approval by the National Health Commission (NHC) if the specific strain or extraction process lacks a history of safe use (NHC, 2013). A significant development occurred with the implementation of the group standard T/CIFST 006-2022 (Probiotic Lactic Acid Bacteria Postbiotics), which standardizes the definition of inanimate microorganisms and their cellular components, effectively providing a technical category for PEVs (CIFST, 2022). However, functional health claims remain strictly limited to products that undergo the extensive "Blue Hat" registration process overseen by the State Administration for Market Regulation (SAMR)[37]. Conversely, Taiwan employs a risk-based paradigm centered on

ingredient novelty. Under the Act Governing Food Safety and Sanitation, PEVs are typically categorized as "non-traditional food ingredients" if they lack a significant history of consumption. Consequently, the Taiwan Food and Drug Administration (TFDA) mandates a comprehensive safety dossier, including genotoxicity and subchronic toxicity studies, before market entry is permitted (TFDA, 2020). Furthermore, specific therapeutic or physiological claims (e.g., immunomodulation) are prohibited unless the product secures the "Green Mark" certification, which demands rigid scientific substantiation through not only animal but also human trials [38]. Hong Kong presents a juxtaposed regulatory environment characterized by high market accessibility but stringent post-market surveillance. Lacking specific legislation for postbiotics or novel foods, PEVs are regulated as general food products under the Public Health and Municipal Services Ordinance (Cap. 132), bypassing pre-market safety approval (Centre for Food Safety, 2018). However, commercial viability is constrained by the Undesirable Medical Advertisements Ordinance (UMAO), which strictly proscribes advertisements claiming to treat or prevent specific diseases, thereby creating a precarious environment for communicating the clinical efficacy of bioactive vesicles (Department of Health, 2012) [39]. Collectively, this regulatory divergence necessitates a stratified compliance strategy, balancing the toxicology-heavy requirements of Mainland China and Taiwan with the claim-restrictive marketing framework of Hong Kong.

Looking ahead, future research should focus on several key areas to bridge the current gaps. First, systematic, comparative studies are needed to elucidate the strain-specific efficacy and mechanisms of both live bifidobacteria and their postbiotic fractions, particularly PEVs, in AD models and human trials. Second, establishing standardized protocols for the production, characterization, and quality control of PEVs is paramount to ensure reproducibility and safety. Finally, fostering interdisciplinary dialogue between scientists, industry stakeholders, and regulatory bodies is essential to develop more harmonized and adaptive regulatory frameworks. Such frameworks must evolve to accommodate the unique nature of these novel biotherapeutic agents, ensuring that innovative and evidence-based microbiome interventions can be safely and effectively translated to benefit human health. All in all, this research project aims to 1) examine the influence of delivery modes and feeding patterns on the development of infant gut microbiota with the focus on Bifidobacteria in Hong Kong populations; 2) isolate and characterize human-sourced *Bifidobacterium* based on both *in vivo* and *in vitro* experiments; 3) explore the characterization and composition of SA-EVs and *B. longum* AC15. 4) establish and compare AD models induced by SA-EVs and DNCB through various aspects; and 5) investigate the beneficial effects of *B. longum* AC15 and its EVs on SA-EVs-induced AD and its underlying mechanism.

Chapter 2: Methodology

2.1 An Observational Study to evaluate associations between early life feeding-pattern, delivery modes, and gut microbiota development of Chinese babies in Hong Kong

2.1.1 Study design:

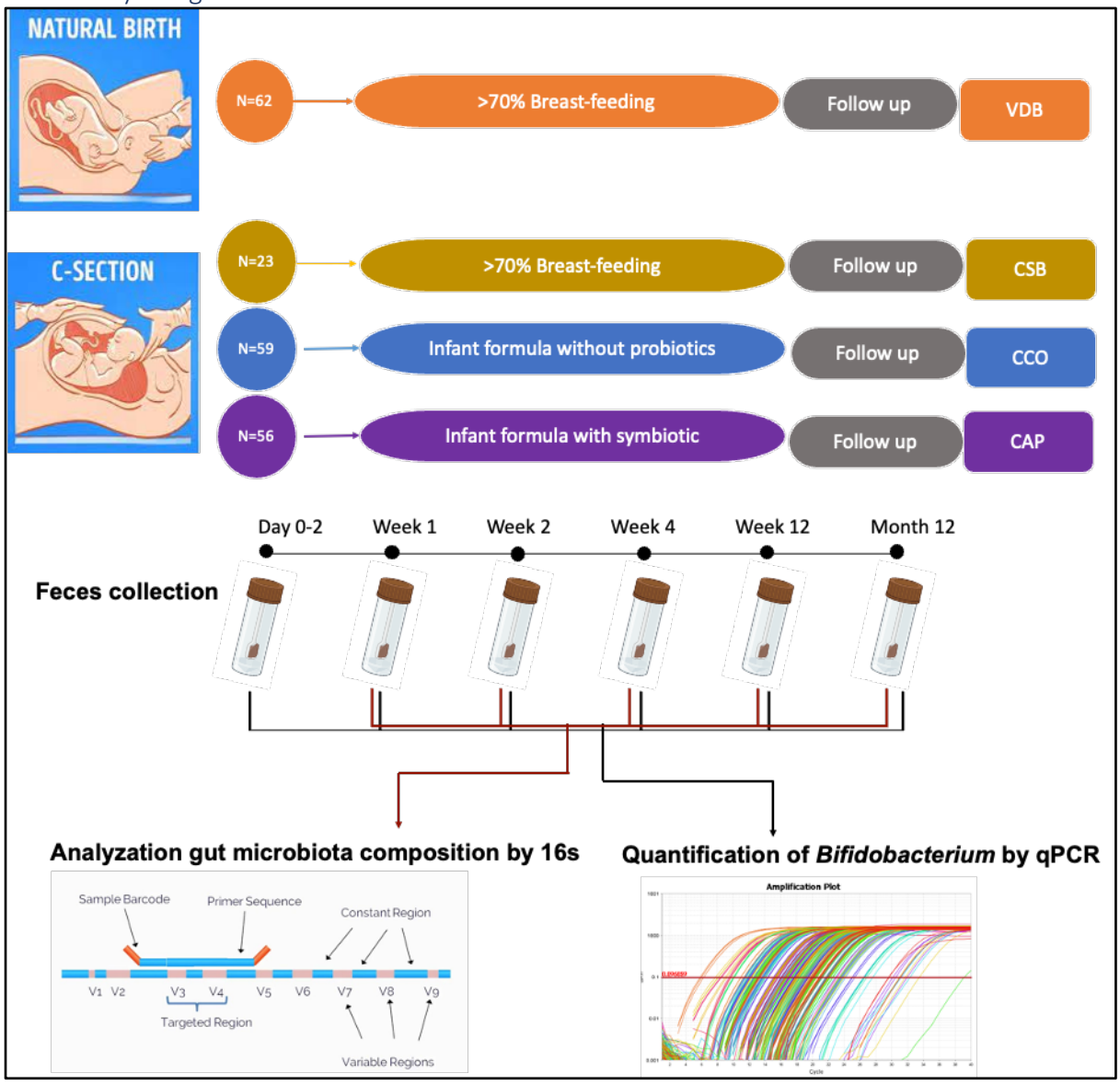

Figure 2.1 Illustration the study design of observational study. 16s sequencing and qPCR were used to investigate the functional impact of delivery mode and early life nutrients on the development of infant gut microbiota.

A total of 200 newborn eligible babies in Hong Kong were recruited in this study project between June 2021 and December 2023. They were grouped into four study arms, which are C-section born infants fed with over 70% of infant formula consisting of a synbiotic (CAP), C-section born infants fed with over 70% of infant formula without synbiotic (CCO), C-section born baby fed with over 70% of breastfeeding (CSB) and vaginal born baby fed with over 70% of breastfeeding (VDB). The synbiotic is 5.4 g scGOS/lcFOS (9:1) and $3x10^9$ CFU of *B. breve* M16-V in per 100 g infant formula. The percentage of feeding was determined based on the volume of infant formula or breastmilk. Total 6 fecal samples of Day 0-2, Week 1, Week 2, Week 4, Week 12 and Month 12 were collected from each participant. The abundance of total bacteria and targeted *Bifidobacterium* species in their feces were quantified by quantitative

real-time PCR (qPCR). To further investigate their gut microbiota composition, DNA of fecal samples at Week 1, Week 2, Week 4, Week 12, and Month 12 were analysed through 16S sequencing.

2.1.2 Sample collection and preparation

Infant stool samples were collected by nurses or parents and stored immediately in 95% ethanol. All samples were transported to laboratory at room temperature, where they were stored at -80°C until further analysis. For DNA extraction, 0.2 g fecal samples were weighted and extracted using Fast DNA Stool Mini Kit (Cat#51604, QIAGEN, Hilden, Germany) according to the manufacturer's instruction with some modification by adding a bead-beating step. Approximately 200 mg of 0.1 mm glass beads were added to 200 mg of stool sample and re-suspended in QIAGEN ASL buffer, bead-beating was performed using homogenizer (Precellys Evolution touch homogenizer, Bertin Technologies, Paris, France) for 3 repetitions of 1 minute bead-beating with 5 min incubation on ice. Samples were then heated at 95°C for 15 min before centrifugation at 20,000 g for 1 min. The supernatant was transferred into a clean tube containing InhibitEX tablet and vortexed to mix proceeding with manufacturer instructions. Isolated fecal genomic DNA were eluted in 50 µL AE buffer, checked with Nanodrop (Thermo Scientific™ NanoDrop™, Wilmington, Delaware, USA), and stored at -20°C until use in further analyses.

2.1.3 Analysis of the early colonization of *Bifidobacterium* in the gut by qPCR

The absolute gene copy numbers of total bifidobacteria and several *Bifidobacterium* species including the *B. longum, B. breve, B. breve* M16-V*,* and *B. bifidum* were assessed with qPCR. Two qPCR chemistries (SYBR Green and TaqMan) were selected and performed on Applied Biosystems QuantStudio 7 Flex Real-Time PCR System (Applied Biosystems, California, USA). SYBR Green PCR master mix (Cat#RR420A, TAKARA, Kusatsu, Japan) and TaqMan universal master mix (Cat#360, TAKARA, Kusatsu, Japan) were used for their respective assays. Primers were selected and/or designed to amplify specific regions of the 16S rRNA gene or the 16S-23S intergenic spacer region or specific genomic region (*B. breve* M16-V) with their respective optimized qPCR conditions (Appendices:

Supplementary Table 1) Standards for each *Bifidobacterium* target were generated from their respective genomic DNA by endpoint PCR with their respective primer pairs. The specificity of the amplified PCR product was checked using gel electrophoresis prior to purification. The

concentrations of the purified amplicons were measured using NanoDrop (Thermo Scientific™NanoDrop™, Wilmington, Delaware, USA) and the copy number/µL were calculated before dilution to a range of 10^1-10^9 copies/µL of standards used in each assay. In brief, fecal genomic DNA was diluted 1-, 10-, 100-, 1,000-fold. qPCR conditions were stage 1 denature of heating 2.63°C/s to 95°C maintain 30 s, stage 2 and 3 Annealing and Extension of maintaining 3 s and decrease to 60°C with the decreasing rate of 2.42°C/s and fluorescence reading collected at the last step for melting curve analysis in SYBR Green assays. For TaqMan assays, the conditions were set at 1 cycle of 95°C for 30 s, followed by 40 cycles of amplification at 95°C for 3 s and 64°C for 30 s (Applied Biosystems QuantStudio™ 7, Foster city, California, USA) was used to visualize and check abnormality of curves deviating from standard amplification. Raw data were then exported into Excel, where the Ct values were recalculated for log Copy numbers/g feces. The results were then used for statistical analysis.

2.1.4 Analysis of gut microbiota composition by 16s sequencing

Total genomic DNA from collected infant fecal samples were extracted using TIANamp Stool DNA kit (Cat#4992205, TIANGEN, Beijing, China) according to the manufacturer's protocol. The V3-V4 region of 16S rRNA were sequenced using primers 338F and 806R. 16S rDNA sequencing was performed by BGI using DNBSEQ sequencer. For sequence analysis, primer sequences were trimmed, and raw data was analysed by using QIIME2 (QIIME2-Amplicon 2024.02) with High Performance Computing platform provided by Information Technology Services Office, The Hong Kong Polytechnic University. Paired-end sequences with quality were denoised by Deblur pipeline. Taxonomy was assigned by SILVA classifier (138.1 Ref NR 99). Alpha diversity indices including Shannon index and Faith's pd, beta-diversity analyses weighted UniFrac and Bray-Curtis PCoA plots were generated within QIIME2. Taxonomy heatmaps were generated by RStudio with *gplots* and *ggplot2* packages.

2.2 Isolation and Characteristics of extracellular vesicles

2.2.1 Isolation of EVs from culture supernatant.

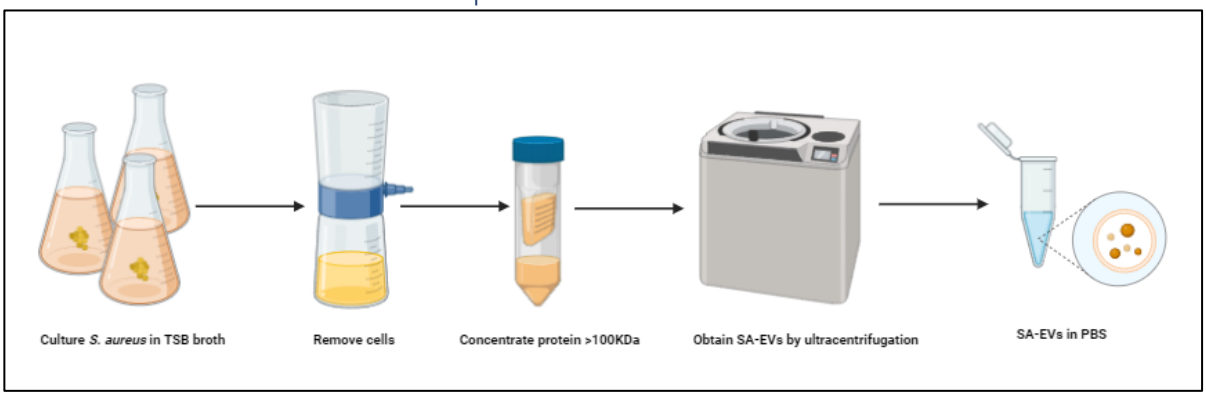

Figure 2.2 Procedure of EVs isolation

The isolation protocol of EVs was adapted from Jun et al. with some modification [40]. Briefly, bacteria were inoculated in culture broth incubated at 37℃ under vigorous shaking overnight. The overnight cultured bacteria were sub-cultured into fresh broth to mid-log phase for use. After bacterial cells were removed by centrifugation at 8,000 g for 20min at 4℃, the supernatants were filtered with 0.22 μm membrane to remove residual bacteria and cellular debris. And then they filtered supernatant were concentrated with a 100 KDa Amicon centrifugal filter (Cat#UFC910008, Millipore, Darmstadt, Germany). The EVs fractions were centrifuged at 150,000 g for 3 hr at 4℃, and the purified EVs were resuspended in phosphate-buffered saline (PBS). The protein concentration was determined using the BCA assay (Cat#23250, Thermo fisher, San Diego, California, USA). The isolated EVs was filtered through 0.22 μm membrane and stored at -80℃ until used.

2.2.2 Visualization of EVs by Transmission electron microscopy (TEM)

EVs were fixed in 1% glutaraldehyde solution, transferred to a clean copper mesh, and stained with 2% uranyl acetate solution. After that, the samples were visualized on a TEM (JEOL Model JEM-2010, JEOL Ltd, Akishima, Tokyo, Japan).

2.2.3 Measurement of size distribution of EVs through Nanoparticle Tracking Analyzer (NTA)

NTA is used to visualize and measure nanoparticles in suspension in the range of 10-1000 nm based on the analysis of Brownian motion. Particles in the sample are visualized by the illumination with a laser beam. The scattered light of the particles is recorded with a light sensitive CCD or CMOS camera, which is arranged at a 90-degree angle to the irradiation plane. Using a special algorithm, particles are detected, and their path registered. EVs were diluted 100 times by PBS before analysis. 1 mL of sample was injected into the sample measurement window of NTA (Nanoparticle (405nm) Tracking Analyzer) (NanoSight NS300, Malvern Panalytical, Malvern, Worcestershire, United Kingdom).

2.2.4 Identification of pathogenetic protein via SDS PAGE and Western blot analysis

The target protein of EVs was separated by SDS PAGE and identified by Western blot. The isolated SA-EVs sample was mixed with 4X sample buffer and boiled at 95℃ for 3 min for denaturation. Then, they were loaded onto precast gels (4% stacking gel and 12% separation

gels). The running time of SDS PAGE was 3 hr at 120 mA. Further, the gel was transferred to nitrocellulose membrane (BioRad, Hercules, California, USA) for 1.5 hr at 80 V in the cold room. The membrane was blocked with 5% non-fat milk powder in Tris-Buffered Saline-Tween (TBST) at 4℃ for 1 hr. The blocked membrane was incubated with primary antibody (anti-α hemolysin) (Cat#ab190467, Abcam, Cambridge, United Kingdom) at 4℃ overnight. The membrane was washed 3x15 min in TBST buffer prior to incubation with HRP-conjugated goat anti-mouse secondary antibody (Cat#G21040, Invitrogen, California, USA) for 2 hr at 4℃. All antibodies were diluted in 5% non-fat milk powder in TBST. Finally, the membrane was washed 3 times for 15 min in TBST followed by the development with ECL Substrate detection kit (Cat#1705060, BioRad, Hercules, California, USA) for 5 min. The digital detection was made using the ChemiDoc system with Images Lab software (Bio-Rad, Hercules, California, USA).

2.2.5 EVs composition analysis via proteomics

EVs were lyzed by RIPA buffer supplemented with two cocktails tablets, and then ultra-sonicated at 50% amplitude for 30 s and paused for 30 s. In total, ran for 4 cycles. Total protein was extracted from EVs, and concentration determined using the Pierce™ BCA protein quantification kit (Cat#23225, Thermo fisher, Waltham, USA). Subsequently, 100 μg of protein was taken for proteolysis according to the EasyPep™ MS sample preparation kit (Cat#A40006, Thermo fisher, Waltham, USA). The final peptides were analysed using Ultimate 3000 UPLC coupled with Thermo Orbitrap Fusion ultra-high resolution 3-in-1 mass spectrometry. Chromatographic separations were performed using a C18 reverse column and water and acetonitrile containing 0.1% formic acid in the mobile phase. The mobile phase gradient, temperature, scanning resolution, etc. were optimized to determine the optimal parameters. The protein results were analysed by Spectronaut, and the statistical results were based on the corrected p-value of < 0.05 and the fold difference greater than 50%.

2.3 Isolation and characterization of human-sourced *Bifidobacterium*

2.3.1 Isolation and optimization of cultural conditions for *Bifidobacterium*:

A cohort of nine participants was recruited for specimen collection. Fresh fecal samples were obtained from six adult individuals (comprising three females and three males) aged 26–33 years, as well as from one child aged 5 years. Additionally, fresh breastmilk samples were provided by three lactating mothers from Hong Kong during the postnatal period. Six *Bifidobacterium spp.* were successfully isolated by using five broths, Tryptic Soy broth (TSB) (Cat#HB8570-1), BL broth (Cat#HB0395), Bifidobacterium-selective media (BSM) broth (Cat#HB0396-1) purchased from Hope Bio-Technology (Qingdao, China), Reinforced Clostridial Medium(RCM) (Cat#CM0149B, OXOID Ltd, Ireland, UK) and De Man, Rogosa & Sharpe(MRS) (Cat#LA4360, Solarbio, Beijing, China). Those agars were supplemented with 100 mg/L of mupirocin (Cat#T1465-100MG, TargetMol, Boston, USA), and 90 mg/L of 8-hydroxyquinoline (Cat#H6878-100g, Sigma Aldrich, St. Louis, Missouri, USA). Table 2.1 detailed the one commercial *Bifidobacterium* and six isolated *Bifidobacterium spp.* enrolled in the study. They belong to three groups, *B. longum*, *B. adolescentis* and *B. pseudocatenulatum*. As the six selected isolates were isolated from RCM broth, a 200 μL aliquot of each *Bifidobacterium* stock was inoculated into 10 mL RCM broth. Cultures were then incubated anaerobically at 37°C in an atmosphere of 5% CO_2, 5% H_2, and 90% N_2 using an anaerobic chamber (Concept 400, Baker Ruskinn, Troisdorf, Germany). Taxonomic

identification in Table 2.1 was double confirmed by matrix assisted laser desorption ionization-time of flight mass spectrometry (MALDI-TOF) (Ultraflextreme, Bruker, Billerica, Massachusetts, USA) and sequencing of PCR-amplified 16S rDNA using the universal pair of primers 27F (5'-AGAGTTTGATCCTGGCTCAG-3') and 1492R (5'-TACGGCTACCTTGTTACGACTT-3') [41] .

Table 2.1: Description of the Bifidobacterium cultures used in this study

No.	Isolates in this study	Source	Identification method
1	*B. longum* CICC6186	American Type Culture Collection (ATCC)	/
2	*B. longum* AC15	Human milk	16S sequencing
3	*B. longum* AC16	Human milk	16S sequencing
4	*B pseudocatenulatum* AC17	Human feces	16S sequencing
5	*B. longum* AC18	Human feces	16S sequencing
6	*B. adolescentis* AC19	Human feces	MALDI-TOF
7	*B. longum* AC20	Human feces	MALDI-TOF

2.3.2 Monitor the Growth Curve of *Bifidobacterium*

Bifidobacterium isolates were cultured as previously described for 24 hr and then subcultured into fresh medium before monitoring the growth curve. The optical density at OD_{600nm} was monitored every hour for 12 hr starting at OD_{600nm} of 0.2 until the cultures reached to the stationary phase. The corresponding RCM broth without bacteria was used as a negative control during the observation to control for non-biological change in the medium, such as abiotic turbidity or color change. All the experiments were conducted with three independent biological replicates. The average generation time was calculated using the following equation:

$$n = \frac{\mathrm{Log}\left(\frac{OD600nm\_Tn}{OD600nm\_T0}\right)}{\mathrm{Log}(2)}$$

- OD_{600nm}_Tn is the final value of OD_{600nm} at time n.
- OD_{600nm}_T0 is the initial value of OD_{600nm}.
- n is the number of generations
- The factor of 2 is used because bacteria typically divided by binary fission, where one cell becomes two.

2.3.3 Determination of Simulated Gastric Juice and Simulated Intestinal Juice tolerance ability of *Bifidobacterium*

Bifidobacterium isolates were cultured as described above into the mid-log phase. The culture was centrifuged at 8,000 g for 10 min and the pellets were incubated in the Simulated Gastric Juice (SGJ) for 2 hr and then transferred into Simulated Intestinal Juice (SIJ) for 3 hr. The formulation of SGJ and SIG were adopted from A. Abadelazez et al. with some modification [42] . The compositions of SGJ and SIJ were shown in Table 2.2. The bacteria were taken out

every hour to determine the CFU. Optimal diluted bacteria suspension was spread on RCM plates. This procedure was performed in duplicate for each bacteria type.

Table 1.2 Composition of Simulated Gastric Juice and Simulated Intestinal Juice

Name	Composition	Duration
Simulated Gastric Juice	Dissolve 3.0 g NaCl, 1.1 g KCl, 0.15 g $CaCl_2$, and 0.60 g $NaHCO_3$ in 1 L of distilled water and adjust pH to 3. Final concentration of 3.0 g/L porcine stomach mucosa pepsin (Cat#P7125-100G, Merck, Darmstadt, Germany) is added to the autoclaved solution.	2 hr
Simulated Intestinal Juice	Dissolve 5.0 g NaCl, 0.60 g KCl, 0.30 g $CaCl_2$, and 0.60 g $NaHCO_3$ in 1 L of distilled water and adjust pH to 7.3. Bile salt (Cat#B8756-50G, Sigma Aldrich, St. Louis, USA) at 3.0 g/L are added into autoclaved solution.	3 hr

2.3.4 Adhesion and Competitive Adhesion Ability of *Bifidobacterium* on colon epithelium cells

Total number of 2 X 10^4 cells of colon epithelium cells (Caco-2 cell) were seeded in 24-well plates and cultured at 37°C in 5% CO_2 incubator for 24 hr. Complete media (DMEM+10% FBS) was changed every other day for at least 14 days until a monolayer of Caco-2 cells were formed. Seven *Bifidobacterium spp., S. aureus* ATCC6538 and *E. coli* ATCC8739 were cultured in RCM and TSB broths overnight, respectively. All of them were sub-cultured to mid-log phase in incubator or an anaerobic chamber (Concept 400, Baker Buskinn, Troisdorf, Germany) at 37°C. Supernatants were removed after centrifugation and replaced by phosphate-buffered saline (PBS). 100 µL of each bacteria suspension was applied to the Caco-2 cells monolayer, followed by incubation in the anaerobic chamber for 2 hr. After incubation, Caco-2 cells were washed by PBS for three times and lysed by 100 µL of 0.5% Saponin (Cat#sc-280079, Santa Cruz, California, Unites States) for 15 min. Optimal serial dilution of cell suspension was spread on RCM or TSB agar plates and incubated at 37°C. This procedure was performed in triplicate for each bacteria type.

2.3.5 Determination of Short Chain Fatty Acids produced by *Bifidobacterium*

The SCFAs analysis method was adapted from Li et al. with some modification (Li et al., 2022). Bifidobacterium isolates were cultured as described above into mid-log phase. The supernatant of 1 mL bacteria culture was collected by centrifugation and filtered via 0.22 µm membrane. The pH was adjusted to 2-3 by hydrochloric acid before analysis using a column (DB-FFAP 123-3232, Agilent, Santa Clara, USA) on the gas chromatography (GC) with flame ionization detector (FID) (Agilent 7890B, Santa Clara, USA). Oven temperature was set at 80°C for 2 min followed by ramping 6°C per minute until 180°C, and then held for 2 min. Concentration of different SCFAs, including acetate, propionate, butyrate, isobutyrate, valerate, and isovalerate, were calculated from standard curves of each SCFA. A standard solution containing a mixture of acetate, propionate, butyrate, isobutyrate, valerate, and isovalerate was prepared, with each constituent at a concentration of 50 mM. This stock was subsequently subjected to a series of two-fold dilutions using Milli-Q water, yielding final concentrations of 25 mM, 12.5 mM, 6.25 mM, 3.125 mM, and 1.5625 mM. The standard curve

was constructed by plotting the known concentration of each target analyte against its corresponding mean chromatographic peak area. This test was performed with three biological replicates. The calculated mean concentration of each SCFA among isolates was analysed using Student's T-test.

2.3.5 Antimicrobial ability of *Bifidobacterium*

The spot-on-law antibacterial assay was adopted from Yada and Tiwari et al. [43]. Briefly, *Bifidobacterium* isolates were cultured as described above into mid-log phase, and 2 µL of cultures was applied as a single spot on the nutrient agar plates which kept or removed the glucose and starch. Semisoft nutrient broth (Cat#CM0110A, Neogen, Lansing, USA) agar (0.7%) mixed with 10^5 CFU/mL of overnight cultured pathogens, including *S. aureus* ATCC6538 and *E. coli* ATCC8739, were overlaid on the RCM plates. Inhibition zones were recorded after 48 hr of incubation at 37°C. All experiments were conducted with three independent biological replicates. The mean inhibition zone of isolates cultured on agar plates with glucose and starch (w-GS) was compared to that of isolates cultured on agar plates without these carbohydrates (w/o-GS) using Student's T-test.

2.4 Establishment of *in vitro* AD model

2.4.1 SA-EVs dosage titration on HaCaT/RAW-BLUE™

Human skin epidermis cells (HaCaT) (Cat# 300493, Cytion, Heidelberg, Germany) cells were cultured in complete media (DMEM+10% FBS+2mM L-glutamine) and sub-cultured with a 0.05% EDTA solution at 37°C for 3-5 min and then detached with 0.05% Trypsin at 37°C for 2-3 min. Passing cells for 2-3 passages until they reach good condition for the following experiments. Total number of 2 X 10^5 cells of HaCaT were seeded in 24-well plates and cultured at 37°C in 5% CO_2 incubator for 24 hr. The optimized induction condition was determined through the dosage titration of SA-EVs. Cell viability was analysed via MTT assay. Proinflammatory markers secreted by HaCaT cells, including IL1b, TNFA, IL6, TSLP, CCL17, CCL22, FLG, and IL8 were analysed via RT-qPCR. For HaCaT differentiation, cells were cultured with DMEM supplemented with calcium chloride at 0.00 mM, 0.03 mM (Low-Ca^{2+}) and 2.8 mM (High-Ca^{2+}) final concentration. Low/high Ca^{2+} content medium was added after 24 hr of seeding and changed with fresh medium every two days until its differentiated. The makers of suprabasal and basal layers were detected by RT-qPCR. Primer sequences could be found in Supplementary Table 2. For RAW-BLUE™, 2x10^4 cells were seeded in 96-well plate and incubated for 24 hr at 37°C in a humidified atmosphere containing 5% CO_2. The optimized induction condition was determined through the dosage titration of SA-EVs. Cell viability was analysed via MTT assay. The inflammatory statues were determined by the reaction of QUANTI-BLUE™.

2.4.2 Anti-inflammation capacity of Heat-inactivated *Bifidobacterium* on RAW-BLUE™

Seven isolates were cultured as described above into mid-log phase. The supernatant was removed by centrifugation at 8000 g for 5 min. The bacteria pellet was washed twice and resuspended in PBS for heat-inactivation at 70°C for 30 min. The efficiency of heat deactivation was checked via plate count.

The commercially available NF-κB/AP-1 reporter RAW-BLUE™ cell line (Cat# raw-sp)was used to assess anti-inflammation capacity of *Bifidobacterium* isolates. RAW-BLUE™ cell was originating from the murine macrophage cell line RAW-264.7 and bearing a reporter construct for secreted alkaline phosphatase (SEAP), which the expression is inducible when NF-κB and AP-1 attach to the consensus sequences in the promoter. RAW-BLUE™ cells were cultured in Growth medium. The growth medium was DMEM, supplemented with 4.5 g/L glucose, 2 mM L-glutamine, 10% (v/v) heat-inactivated fetal bovine serum, 100 U/mL penicillin, 100 µg/mL streptomycin, 100 µg/mL Normocin™ (Cat#an-tnr-05) or Normocin™ and Zeocin™(Cat# an-zn-05). All the above mentioned reagents were purchased from InvivoGen (San Diego, California, USA). Briefly, $2x10^4$ cells were seeded in 96-well plate and incubated for 24 hr at 37°C in a humidified atmosphere containing 5% CO_2.

RAW-BLUE™ cells were pre-treated with three dosages (10^5, 10^6 and 10^7 CFU/well) of each heat-inactivated (HI) *Bifidobacterium spp.* for 24 hr and induced by SA-EVs for 16 hr. The supernatant was collected for inflammation analysis. Levels of secreted embryonic alkaline phosphatase, a reporter protein widely used to study promoter activity or gene expression, were monitored by QUANTI-BLUE™ solution (Cat# rep-qbs) and read via Microplate Reader. The results of QUANTI-BLUE™ were normalized to total protein of the cells. Each test was performed in triplicate.

2.4.3 The influence of HI *Bifidobacterium* on the polarization of M1 Macrophage via NF-KB pathway

Raw 264.7 cells were cultured same as previously described, total RNA was extracted with RNAIso (Cat#9112, TAKARA, Kusatsu, Japan). The extracted RNAs (1000 ng) (n = 3 replicates) were reverse transcribed into cDNA with PrimeScript™ RT Master Mix (Perfect Real Time) (Cat#RR360A, TAKARA, Kusatsu, Japan), followed by quantitative analysis of qPCR (Applied Biosystems QuantStudio 7 Flex Real-Time PCR System, Thermo Fisher, Waltham, USA). The sequences of primers were listed in Table 2.3.

The total protein was extracted by RIPA lysis buffer supplemented with protein inhibitor and phosphorylate inhibitor, respectively. To determine p65, pp65 and TNF alpha, 30 µg of cell extracts were resolved on 8% SDS-polyacrylamide stacking gels and 12% SDS-polyacrylamide separation gel. After the gels, the proteins were electro-transferred onto nitrocellulose filters (PVDF), probed with rabbit monoclonal Ab against p65 (Cat#3033), pp65 (Cat#8242) and TNF alpha (Cat#6945s) purchased from Cell signaling (Danvers, USA), and detected by chemiluminescence (Cat# RM00021P, ABclonal Technology, Woburn, USA). The bands obtained were quantitated using ImageJ.

Table 2.3 Primer sequence for qPCR analysis

	Forward primer 5'-3'	Reverse primer 5'-3'
CD80	TGG CTC TGC AAA CAC GGT TC	AGC AAA TGT GCA AAT CGT CCC
TNFA	AGC CAG GAG GGA GAA CAG A	CAG TGA GTG AAA GGG ACA GAA C
CD206	GTG GAG TGA TGG AAC CCC AG	CTG TCC GCC CAG TAT CCA TC
Arg1	AGG GTC CAC CCT GAC CTA TG	ACA GGT TGC CCA TGC AGA TT

2.4.4 Confocal microscopy analysis

Sterile coverslips were placed in a 24 well plate and treated with 0.1% gelatin diluted in sterile water for 45 min at 37°C. In each well, 2.5 x 10^4 cells were plated and incubated at 37 °C and 5% CO_2 for 24 hr. HI *B. longum* AC15 with concentration at 10^4 to 10^7 CFU/mL were incubated with HaCaT cells for 24 hr and then FM™4-64-labelled SA-EVs (15 μg/mL) were added and further incubated for 4 hr. Fluorescein filters were suitable for FM™4-64 detection. The labeling of EVs with FM™ 4-64 was performed applying the manufacturer's instructions. Briefly, SA-EVs was incubated with 5 μg/mL of FM™ 4-64 dissolved in HBSS on ice for 30 min. Excessed FM™4-64 was removed by ultra-centrifugation at 39880 rpm for 1 hr. SA-EVs was washed by PBS and removed via ultra-centrifugation at 39880 rpm for 1 hr for two times. The concentration of FM™ 4-64-labelled SA-EVs was measured by BCA assay.

After SA-EVs treatment, HaCaT cells were fixed with 4% paraformaldehyde at RT for 30 min. Fixed cells were washed by PBS three times and sealed with mounting media. Samples were stored in 4˚C avoiding light before imaging by Leica TCS SPE Confocal Microscope (Leica Microsystems, Wetzlar, Germany). On the white light laser, excitation wavelengths were set at 608 nm for the excitation of FM™ 4-64-labelled SA-EVs. DAPI staining was visualized by the 405-diode laser. The signal of the FM™ 4-64-labelled SA-EVs was detected using a classic PMT detector. Recordings were performed using a 63 × water immersion objective. Images were taken with a pixel size of 1024 × 1024. Pixel saturation was prevented by adjusting the laser intensities and amplifier gains of the detectors. All detectors use grey levels, and thus the colours observed are pseudo-colours.

2.5 Establishment of *in vivo* AD model

2.5.1 Generation of AD model via SA-EVs and DNCB

Balb/c mice are easily triggered by immunization and demonstrate Th2- based immune response. 6- to 10-week-old male Balb/c mice were used in this study for model establishment. Before applying the SA-EVs, the dorsal skin of mice was stripped five to six times by using medical tape. And then 5 μg, 10 μg and 15 μg of SA-EVs or 1% dissolved into PBS or 1% DNCB dissolved in the mixture of olive oil: acetone (1:9) were applied onto the disrupted dorsal skins. SA-EVs or DNCB were applied onto dorsal skin for induction purpose. After sacrifice, the spleen, skin draining lymph nodes, dorsal skins and serum were collected and stored in -80° C fridge for further analysis.

2.5.2 Measurement of AD severity

The severity of AD symptoms will be assessed according to the Eczema Area and Severity Index (EASI) scoring system. The dorsal skin will be assessed as the key sign of AD including edema, erythema, excoriation, and lithification. The degree of skin edema could be represented and quantified via naked eyes.

2.5.3 RNA extraction

The dermal fibroblasts, skin draining lymph nodes and splenocytes of Balb/c mice were preserved in RNAiso and stored in -80° C fridge. Before extraction, samples were homogenized by Bertin Precellys Evolution Homogenizer at 6000 rpm for 1 min and then 200 μL of chloroform were added to extract RNA. After centrifugation at 150,000 g for 15 min,

isopropanol was added to precipitate the RNA. Finally, pre-cold 70% ethanol was used to wash and further purify the RNA. The concentration of RNA was measured by Nanodrop (Thermo Scientific™Nanodrop™, Wilmington, Delaware, USA).

2.5.4 Tissue embedding and Histological analysis.

Dorsal skin samples of mice were fixed in 4% paraformaldehyde (PFA) for 48 hr and then stored in 70 % ethanol at room temperature. Dorsal skins were dehydrated through graded concentrations of ethanol, cleared in xylene, and embedded in paraffin (TP1020 Tissue Processor, Leica, Wetzlar, Germany). The above processes last 30 min of each step.

The Leica microtome was used to cut the dorsal skins into 4µm-thick sections for hematoxylin-eosin (H&E) staining. The slices were placed on glass slides, submerged in diluted ethanol concentrations, then deparaffinized using xylene. Several portions from each group were stained with H&E solution after being rinsed in distilled water. Following washing, the sections were cleaned with xylene, cover slid, and dehydrated using graded concentrations of ethanol. The images were taken by microscope and analysed by ImageJ. The statistical analysis was performed using Prism 9.

2.5.5 Evaluation of T-cells proliferation profile by flow cytometry

To study the immune profile of splenic T cells, four-color flow cytometry was performed. Freshly collected spleen or skin draining lymph nodes (SDLNs) were smashed with the piston of a syringe and wash through 70 µm cell strainer with 3 mL staining buffer. The final volume was adjusted to 10 mL and centrifuged at 450g for 7min at 37℃. And then 2 mL of Red Blood Cells lysis buffer (Cat#2725077, eBioscience™, San Diego, California, USA) were added after discarding the supernatant. For intracellular staining, cells were fixed and permeabilized using IC fix buffer (Cat#2560198, Invitrogen, California, USA) and Perm/Wash buffer (Cat#2582224, Invitrogen, California, USA), respectively. $1x10^7$ cells of splenocytes were blocked by Fc Block antibody (Cat#553141, BD Bioscience, Hong Kong, China) stained with the following antibodies combinations: CD4+, BV711/ FOXP3, PE/ GATA-3, Alexa-647/ RORγt, PerCp-Cy5.5 (Cat#563050/566881/560068/562683, BD Bioscience) according to the manufacturer's instructions. $1x10^7$ cells of SDLNs were blocked by Fc Block antibody (Cat#553141, BD Bioscience, Hong Kong, China), stained with the following antibodies combinations: Live/Dead cells/FVS440UV, CD4+/APC-H7, FOXP3/PE, Anti-GATA/PE-CF594, RORγt/R718, Tbet/RB705 (Cat# 566332/ 560181/ 560408/ 563510/ 567362, BD Bioscience, Hong Kong, China) according to the manufacture's instruction. Finally, $1x10^6$ cells were run and analysed on BD FACSymphony A3 Cell Analyzer (BD Bioscience, Hong Kong, China). The sensitivity of the fluorescence detectors was set using positive control. FSC and SSC measurements were made using linear amplifiers, whereas fluorescence measurements were made with logarithmic amplifiers. Flow cytometric two-parameter dot plots and quadrant statistics were generated using BD FACDiva 9.3.

2.5.6 Determination of serum total IgE by ELISA

Serum samples were prepared from mouse blood for analysis of the total serum IgE levels by ELISA (Cat#EM024-96, ExCell Bio, Suzhou, Jiangsu, China). Each well received serum from the experimental group diluted 1:2 and incubated at 37° C for 2 hr with gentle shaking at 300 rpm.

And then the plate was washed five times by washing buffer and added biotinylated antibody and enzyme conjugate, incubated at 37° C for 1 hr. After washing, the plates received 100 µL/well of tetramethylbenzidine solution (TMB) then the absorbance was measured at 450 nm with an automatic ELISA reader.

2.5.7 Analysis of typical AD-related pro-inflammatory mediators by RT-qPCR

The dermal fibroblasts, SDLN and splenocytes of Balb/c mice were preserved in RNAiso and stored in -80°C fridge. Before extraction, samples were homogenized by Bertin Precellys Evolution Homogenizer at 6000 rpm for 1 min and then 200 µL of chloroform were added to extract RNA. After centrifugation at 150,000 g for 15 min, isopropanol was added to precipitate the RNA. Finally, pre-cold 70% ethanol was used to wash and further purify the RNA. The concentration and quality of RNA was measured by Nanodrop (NanoDrop™, Thermo Fisher Scientific, Waltham, Massachusetts, USA).

2.5.8 Gut and skin microbiota composition analysis by 16S sequencing

Total genomic DNA from collected mice skin samples and feces were extracted using DNeasy PowerSoil Pro Kit (Cat#47014, QIAGEN, Germany) according to the manufacturer's protocol. The V3-V4 region of 16S rDNA were sequenced using primers 16S-338F and 16S-806R. 16S rDNA sequencing was performed by BGI using DNBSEQ sequencer. For sequence analysis, primer sequences will be trimmed, and raw data was analysed by using QIIME2 (QIIME2-Amplicon 2024.02) with High Performance Computing platform provided by Information Technology Services Office, The Hong Kong Polytechnic University. Paired-end sequences with quality were denoised by Deblur pipeline. Taxonomy was assigned by SILVA classifier (138.1 Ref NR 99). A-diversity indices including Shannon index and Faith's pd, beta-diversity analyses weighted UniFrac and Bray-Curtis PCoA plots were generated within QIIME2. Taxonomy heatmaps were generated by RStudio with gplots and ggplot2 packages.

2.5.9 Comparison the differential gene and protein expression through multi-omics analysis

Total RNA was extracted as above described and shipped to Novogene for library preparation and mRNA sequencing. Libraries were sequenced as 150 bp paired end reads on Illunina NovaseqX plus platform. The data analysis method was adopted from Wongvibulsin et al. 2021. The false discovery rate was calculated to control for multiple hypothesis testing. Differentially expressed genes (DEGs) were defined as genes with a log2 fold change >1 or < -1, and FDR adjusted p-value <0.05 [44].

Total protein was extracted from 0.2 g of skin tissue and assessed for concentration by Pierce™ BCA Protein Assay Kits (Cat#23225, Thermo Fisher Scientific, Waltham, Massachusetts, USA). Peptides were produced by using EasyPep™ MS Sample Prep Kits (Cat#A40006, Thermo Fisher Scientific, Waltham, Massachusetts, USA). Briefly, 100 µg of protein per sample was lysed, reduced, and alkylated, and then further digested by Enzyme Reconstitution solution containing Trypsin/Lys-C protease Mix. The peptides were cleaned up and dry by vacuum centrifuge. The obtained peptides were resuspended in 100 µL of 0,1% formic acid in MilliQ water for LC-MS analysis.

Chapter 3: Observational study

3.1 Introduction:

It is acknowledged that the first 1000 days of life are a crucial period to support infants' health through gut microbiome modulation and immune systems development. Any health issues arising during this timeframe could have a long-term impact on adult life. Numerous prospective longitudinal studies have examined the early-life gut microbiota in the Western populations, which highlighted the importance of gut microbiota on the prevention of skin disorders such as AD[45,46]. However, few studies conducted in this field focused on Asian populations. As the gut microbiome of infants is also affected by ethnicity, there is a research gap of conducting studies in other ethnic groups.

The maturation of infant gut microbiome is shaped by multiple prenatal and postnatal factors. For instance, two specific factors, mode of delivery and feeding pattern, have shown profound effects on the establishment of early-life gut microbiome [45,47] .

Currently, Cesarean section (C-section) birth rate remains relatively high in Hong Kong (38%) and China (46%), with elective C-section contributing to a high proportion [48,49]. Research illustrated that gut microbiota profiles between C-section and vaginal born infants are significantly different. Infants born C-section have decreased diversity and delayed colonization of beneficial bacteria, such as *Bifidobacterium*, in gut compared to those born vaginally. Vaginally born infants receive certain strains of *Bifidobacterium* transmitted from mothers through the vaginal canal and then colonize in infant's gastrointestinal tract [50]. Those Bifidobacteria carry out important activities in infant's gut, such as producing compounds that impart physiological benefits. Many studies also reported the beneficial effect of *Bifidobacterium* to attenuate the allergic reaction. According to the research by Liu et al, *B. lactis* alleviates allergic symptoms by regulating the balance of Treg and Th17 cells. Treg and Th17 cells, two main subsets of CD4+ T cells, are involved in the allergic responses. *B. lactis* controls the gut microbiota homeostasis by increasing the differentiation of Treg cells while suppressing that of Th17-type cells. In addition, the expression of FoxP3 and TGF-beta related to Treg cells were significantly increased [51]. The lack of exposure to maternal microbes during birth may lead to the immune system dysfunction and high risks of allergic diseases, such as asthma, rhinitis, and AD [52]. Yu et al. reported that the content of *Clostridium* in the intestine of infants with AD is relatively high, while the content of *Bifidobacterium* and *Lactobacillus* were comparatively higher in healthy infants than those with AD [53].

To restore the delayed colonization of *Bifidobacterium*, feeding pattern is an important factor influencing the gut microbiota difference in infants. Breastmilk is widely recognized as the best nutrients source for infants due to its unique composition that meets the biological needs of humans. It contains essential nutrients such as fat, protein, different immune-active chemicals, vitamins, minerals, microorganisms and human milk oligosaccharides (HMOs), which are vital for the growth and development of infants. The hypothesis of breastfeeding being positively associated with reducing risk of AD development remains controversial. Dattner et al. presented the evidence supporting the idea that breastfeeding during the first four months of life can reduce the incidence of AD in children [54]. On the other hand, Kim et al. published the negative results and showed that exclusive breastfeeding did not influence the risk of AD in infants during the first year of life [55]. The possible relationship between the development of AD and breastmilk required further investigation and validation through large cohort studies. In conclusion, a great deal of research has been conducted to assess the

connection between allergies and breastfeeding. The outcomes are inconsistent, ranging from protective immunity to no effects, or even an increased risk. Maternal immunity during pregnancy and nursing has a significant impact on the immune system in the early years of life. Therefore, more research concentrating on the properties of breastmilk using carefully planned randomized controlled trial (RCT) is required to elucidate these matters. Many studies have shown that supplementary of *Bifidobacterium* in the prenatal and postnatal period could reduce the risk of developing AD in infants [56].

Thus, this research project focuses on two areas: (1) to examine the effects of delivery modes and feeding patterns practice on the colonization of *Bifidobacterium* in infant gut, with a focus on total bifidobacteria and its four subspecies, including *B. longum*, *B. breve*, *B. breve* M16-V, and *B. bifidum*; (2) to investigate whether those two factors influenced the development of infant gut microbiota, including bacteria diversity, their phylogenetic distance and compositional changes.

3.2 Quantification of targeted *Bifidobacterium* in infants' gut via qPCR

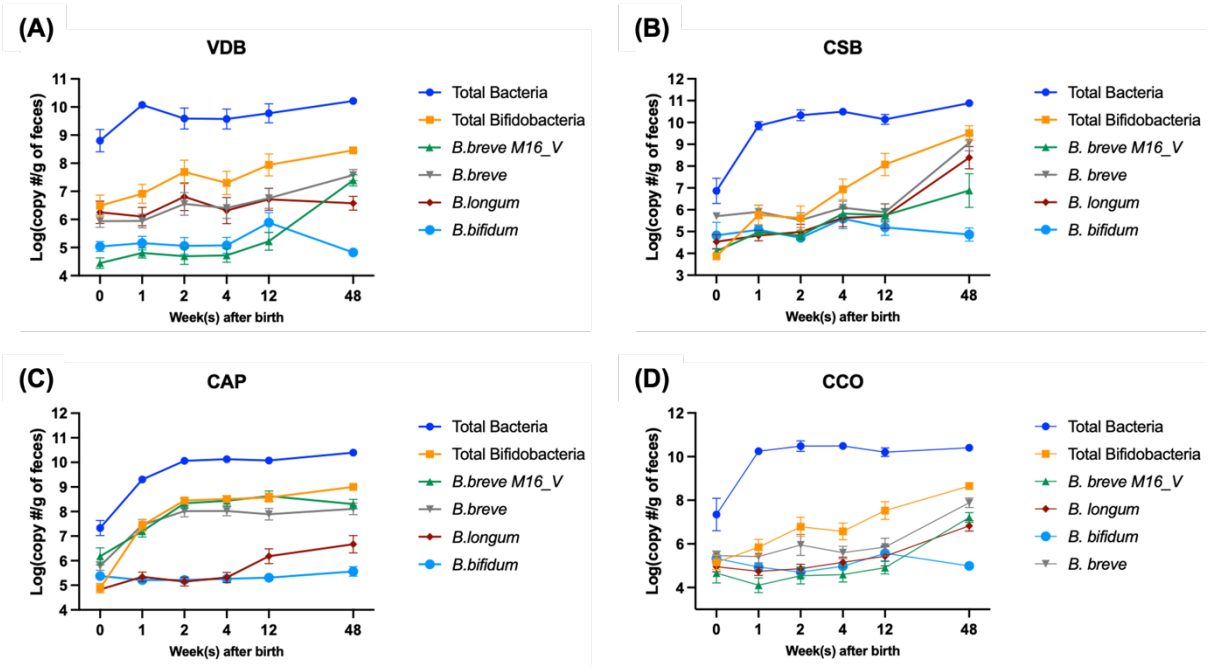

Figure 3.1: Effect of the delivery mode and feeding patterns on the development of infants' gut microbiota. At each timepoint, the mean log (copy number/g of feces) of targets, including total bacteria, total Bifidobacteria, B. longum, B. breve, B. breve M16-V, and B. bifidum, were quantified by quantitative real-time polymerase chain reaction (qPCR). Comparison of the effects of the delivery modes, vaginal and C-section birth on the infants' gut microbiota (A, B). Comparison the influence of different feeding patterns, which are breastmilk, infant formula with/without synbiotics, on the gut microbiota development of C-section-born infants (B, C, D).

The composition of *Bifidobacterium spp.* in four groups was different. During the first 12 weeks after birth, the level of *B. longum* was the highest in VDB group, followed by *B. breve* and *B. bifidum* (Fig 3.1 A). By contrast, *B. breve* was the most abundant species in CAP group, which was dominated by *B. breve* M16-V, throughout the whole observation period, while the amount of *B. longum* and *B. bifidum* were nearly below the limit of detection (LOD) (Fig 3.1 C). In the groups of CSB and CCO, the number of four targeted *Bifidobacterium spp*. were similar and remained at a relatively low level except for *B. breve*, which was slightly higher

than the other species (Fig 3.1 B and D). In week 48, the level of total bifidobacteria in four groups reached to the highest point and *B. breve* was the most prevalent species.

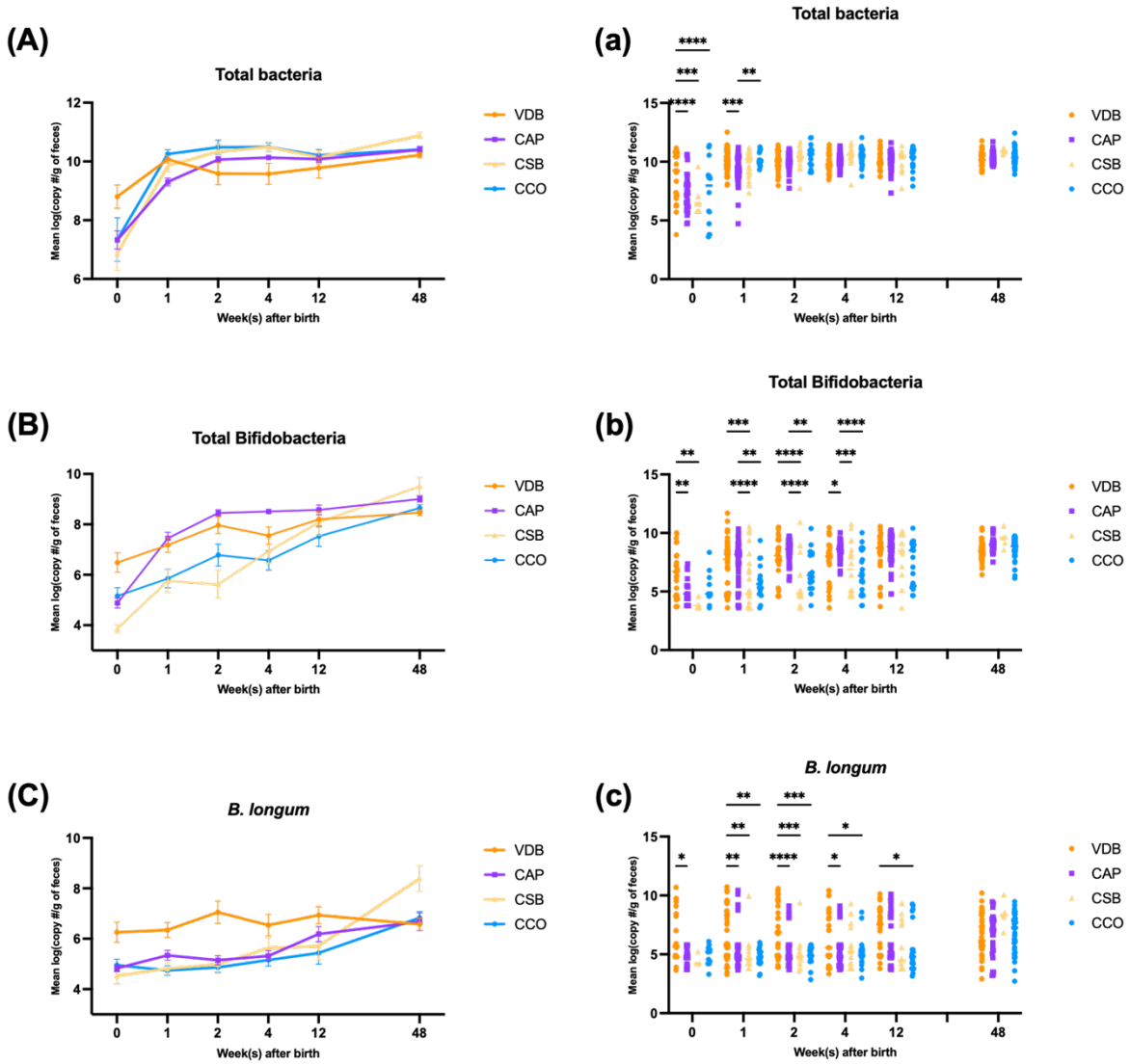

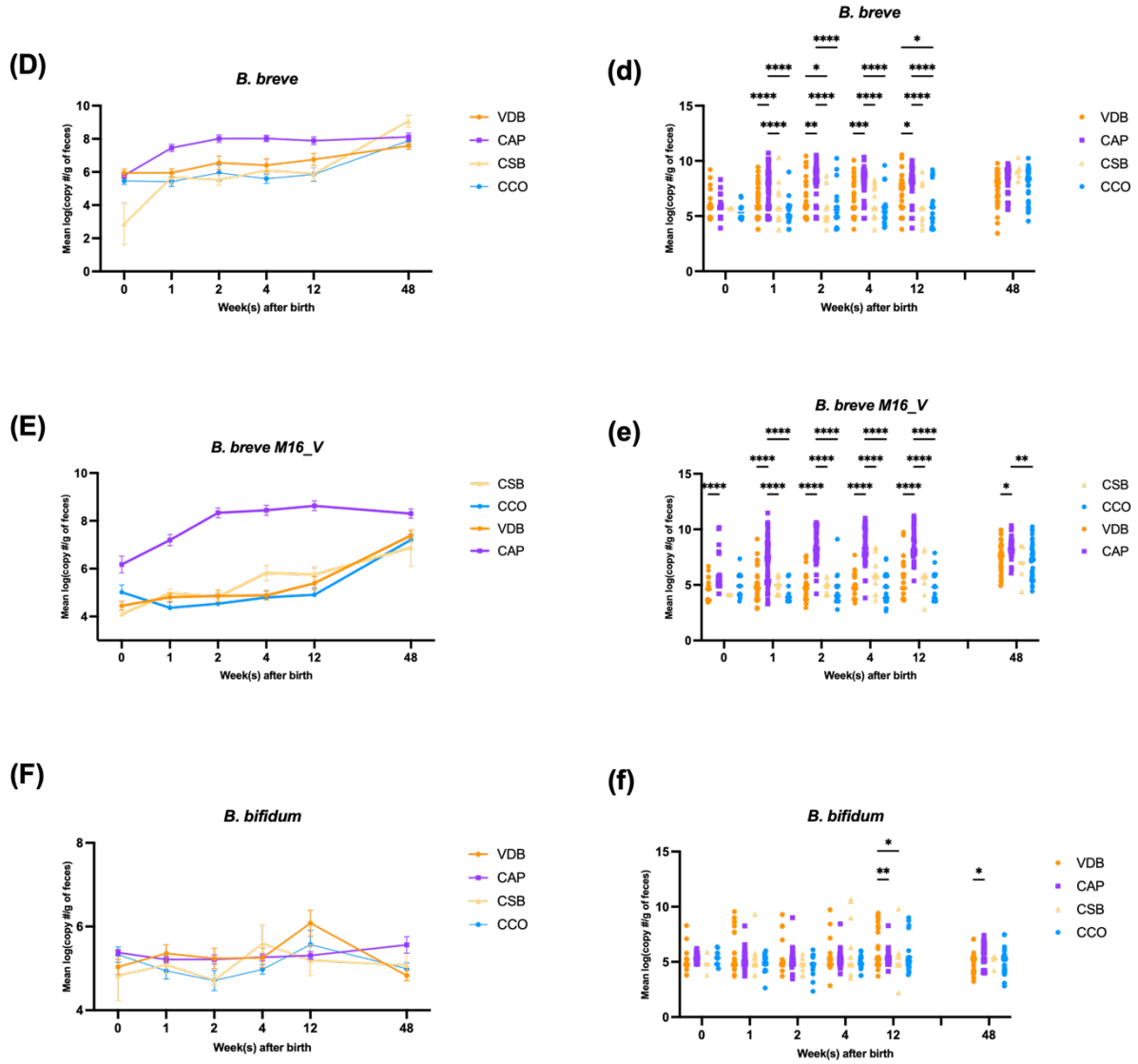

*Figure 3.2 Comparison of the abundance of different Bifidobacterium spp. in VDB, CSB, CCO and CAP groups. The mean log (copy number/g of feces) of each target v.s timepoints were plotted (A, B, C, D, E, F) and the statistically analysis were used TWO-ANOVA and multiple comparisons in Prism 9 (a, b, c, d, e, f), *p<0.05, **p<0.01, ***p<0.005, ****p<0.001.*

The colonization of *Bifidobacterium* was delayed in three C-section groups. Amongst four groups, only VDB group has detectable abundance of total bacteria and total bifidobacteria at the first timepoint, with mean log (copy number/g of feces) 8.80, and 6.49, respectively. After week 1, the rest three groups extended dramatically in total bacteria and showed no significant differences with VDB group, while only C-section born infants supplemented with synbiotics showed a boost in total bifidobacteria and caught up the gap with the VDB group. And the number of both CSB and CCO groups climbed gradually and reached merely around log 6. Finally, in the 12 weeks after birth, the level of total bifidobacteria of four groups eventually reached to a similar level with no statistical difference.

The VDB group alone exhibited measurable abundance of *B. longum* at the first timepoint and this value remained significantly higher until Week 2. Thereafter, the CSB and CAP groups increased gradually and began to make up the gaps by week 4 and week 12, respectively. In week 12, only the CCO group displayed a noticeably low level of *B. longum*. After that, there

were no appreciable variations in the abundance of *B. longum* across all groups, remaining at similar level.

The CAP has the highest abundance of *B. breve*, which is dominated by *B. breve* M16-V, among the four groups from week 0 to week 12. At week 48, the three groups that had fallen behind started to catch up with the VDB group, and there were no discernible differences. Yet, for the entire monitoring time, the particular strain, *B. breve* M16-V, stayed at the greatest level.

Both VDB and CCO groups showed dateable abundance of *B. bifidum* after week 12 and distinct variances from the other two groups. Interestingly, the levels dropped dramatically and remained the lowest within CSB subjects, while the CAP group began to rise gradually to the highest and differ significantly from the other groups.

In summary, the VDB group had the highest diversity and earliest colonization of *Bifidobacterium* in the guts of newborns. *B. longum* and *B. breve* appear to be the initial inoculum of infant gut microbiota most likely through vaginal birth while infant formula with *B. breve* partially compensates the abundance of *Bifidobacterium* in the gut microbiota of C-section born infants as early as week 1. The abundance of total *Bifidobacterium* in the CCO and CSB group could only reach a similar level of the CAP and VDB groups at week 12.

3.3 Alpha diversity and beta diversity of infants' gut microbiome

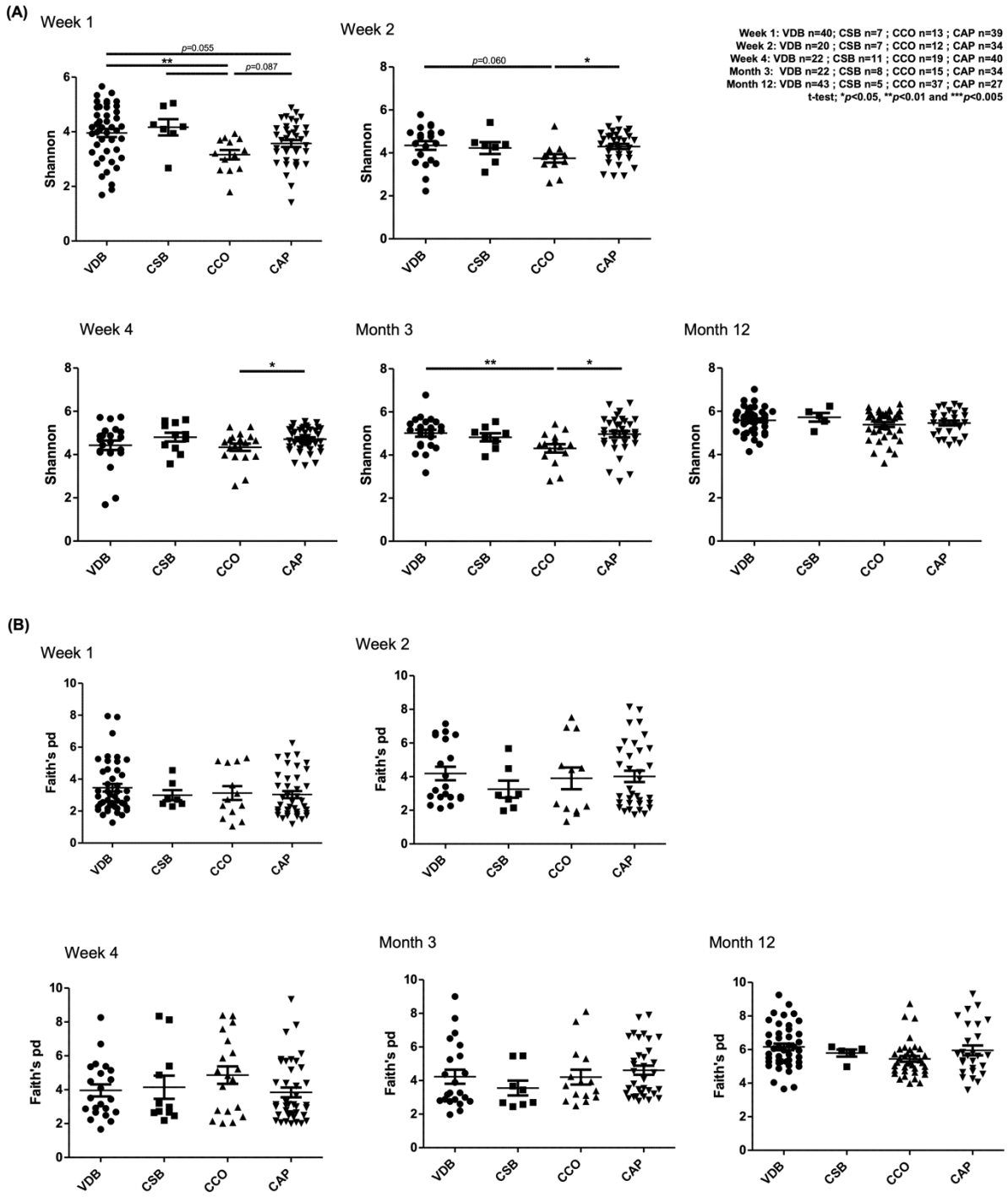

*Figure 3.3: Comparison the alpha diversity of infants' gut microbiota amoung four groups, VDB, CSB, CCO, and CAP. Shannon diversity index (A). Faith's phylogenetic diversity (B). *p<0.05, **p<0.01, ***p<0.005, ****p<0.001 by T test.*

To determine the distinct gut microbial communities affected by delivery modes and feeding pattern, the Shannon index and phylogenetic distance between each group were compared.

The gut microbiota in VDB and CSB groups showed the significant highest diversity amongst four groups at week 1. After that, only the CAP group's Shannon index raised to a level comparable to that of VDB and CSB groups. At week 12, none of them differed significantly

from the other two. In the aspect of phylogenetic distance, there were not significant difference among all groups throughout the whole observational period, indicating the gut microbiome communities of them were very similar.

*Figure 3.4: Comparison the beta diversity of infants' gut microbiota amoung four groups, VDB, CSB, CCO, and CAP. Weighted UniFrac (A). Bray-Curtis (B). *p<0.05, **p<0.01, ***p<0.005, ****p<0.001 by T test.*

The weighted UniFrac distance uses species abundance information and weights the branch length with abundance difference. In the graph, the VDB samples were grouped in the lower left corner in Week 1, indicating the phylogenetic distance of gut flora between VDB group and the rest three groups were far from each other at that time. They began to blend in with the other groups in week 2. By Month 12, they were nearly identical. The CAP was converged in the left side of the graph and didn't merge with the rest until month 12. This result revealed less gut microbial variation between four groups (Fig 3.4 A). These results suggested that the infants' gut flora composition was similar after 12-month development, regardless of the influence of delivery modes or early life nutrients.

Bray-Curtis dissimilarity measures the abundances of microbes that are shared between two samples, and the number of microbes found in each site. In the graph, the VDB and rest three groups were clustered in the upper right corner and bottom left corner in week 1, respectively. It showed that VDB group had much more bacteria than the others. The circumstances changed after week 2, samples of all four groups gathered and separated equal in the graph (Fig 3.4 B), indicating that the abundance of the other three groups increased significantly and reached to the similar level of VDB group.

3.4 The composition of infants' gut microbiota analysis by 16s sequencing

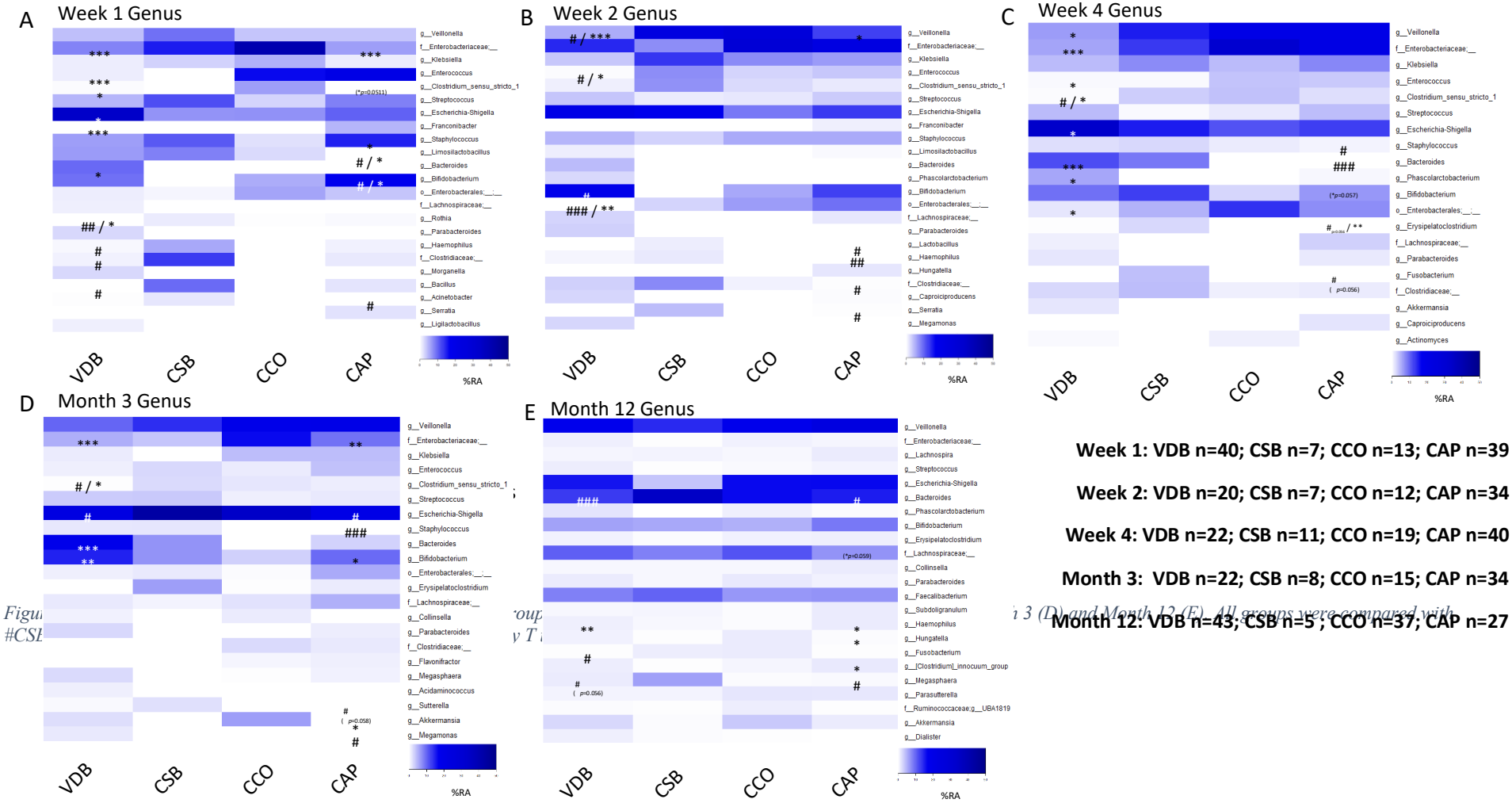

Figu… …oup… …n 3 (D) and Month 12 (E). All groups were compared with #CSB… …y T…

Week 1: VDB n=40; CSB n=7; CCO n=13; CAP n=39

Week 2: VDB n=20; CSB n=7; CCO n=12; CAP n=34

Week 4: VDB n=22; CSB n=11; CCO n=19; CAP n=40

Month 3: VDB n=22; CSB n=8; CCO n=15; CAP n=34

Month 12: VDB n=43; CSB n=5 ; CCO n=37; CAP n=27

In contrast to certain bacteria such as *Escherichia-shigella, Bifidobacterium,* and *Bacteroides* that remained the highest in VDB group over the entire time, other gut microbiota underwent fast changes within a short observational frame even within the same group.

In the first week. the VDB group had much higher quantities of *Bacteroides* and *Escherichia-shigella* than the CCO group while there was a considerable decrease in the abundance of *Enterobacteriaceae*, *Enterococcus*, *Clostridium*, *Franconibacter*, and *Rothia*. In comparison to CSB group, the levels of *Bacillus*, *Clostridiaceae*, *Rothia*, and *Heamophilus* were much lower in the VDB group. For the CAP group, the highest populations of bacteria were *Staphylococcus* and *Bifidobacterium* while relatively lower populations of *Enteracoccus*, *Limosilactobacillus*, and *Acinetobacter* were observed.

After one week of development, each group's gut microbiota underwent a considerable change in week 2. *Veillonella and Escherichia-shigella* both increased in the CSB and CCO groups. The former one deviated from the VDB and CAP groups with statistical differences while the later one did not. In comparison to the CSB and CCO groups, the VDB group's bifidobacteria abundance showed a notable rise, and the number of *Enterococcus* and *Enterobacterales* remained the lowest level among four groups. In the CAP group, the abundance of *Lactobacillus*, *Haemophilus*, *Clostridiaceae*, and *Serratia* was the lowest with significant difference among four groups.

In week 4, the amount of *Veillonella* in the VDB began to increase gradually, although it was still significantly different from the other three groups. By contrast, the abundance of *Enterobacteriaceae* had a declining tendency starting in Week 4 and continued to be low until Month 12. In VDB, *Bacteroides* were much more abundant than in CSB, while in CAP, they were significantly less abundant than that of CCO. The VDB group had the lowest level of *Clostridum* compared to the CSB and CCO groups, with notable differences.

As the observation time comes to Month 3, *Veillonella* in the VDB group didn't differ all that much from the others. Furthermore, the *Enterobacteriaceae* in the CSB and CAP declined sharply to a level comparable to the VDB and only had statistically significant variations with the CCO. Among the four groups, VDB subjects had the lowest level of *Clostridium*. Comparing the CSB and CCO groups to the VDB and CAP groups, there was a significant rise in *Escherichia shigella*. In comparison to the CSB and CCO groups, the VDB group's abundance of *Bifidobacterium* and *Enterobacteriales* increased dramatically in Month 3.

In the final stage of the observation study, the gut microbiota of four groups were getting close to each other except few bacteria, including *Bacteroides*, *Haemophilus*, *Hungatella*, and etc.

3.5 Significant results and implications

In the first part of this chapter, the infant cohort study was the first observational study, also considered as the Real-World Evidence (RWE), with around 200 participates to track the effects of feeding pattern and delivery methods on the development of the gut microbiota in Hong Kong newborns. The outcomes of this study are more likely to accurately represent the current state of affairs than interventional studies as the feeding pattern was not strictly stringent.

Maternal vaginal microbiome as a primary source to "inoculate" infant gut microbiota can be transmitted and colonize in the infant's intestine shortly after birth [57]. As shown in our result, infants born vaginally have the earlier and more diversified colonization of bifidboacteria compared with that of C-section born infants. Once infant passing through the vaginal canal, the newborn receives microbiome from their mothers, consisting mainly of *Proteobacteria* and *Actinobacteria* (mainly bifidobacteria). As bifidobacteria are able to metabolize the HMOs present in the human milk continuously, this genus of bacteria has an advantage and grows exponentially, reaching up to 50% of the total colonic microbial structure of infants [58].

Breastmilk has a substantial selection effect on *B. longum*, especially *B. longum* subspecies *infantis,* which eclipses any priority effects the initial colonizers have [59]. In the breastfed groups, the number of *B. longum* was relatively higher than in non-breastfed groups and it is the dominate species among them all before week 12. While the interesting finding is that *B. longum* suddenly no longer dominated the community and other *Bifidobacterium* species in week 48, such as *B. breve* reached higher absolute abundance, suggesting that *B. longum* only dominates the community as long as the infant is primarily breastfed [60].

The prebiotic in infant formula provides a selection pressure for bifidobacteria species. When comparing the outcomes of C-section babies who were given breast milk (CSB) and synbiotic supplements (CAP), it was found that two groups grew and reached to similar level at the end but at different rates over time. Despite the fact that the amount of bifidobacteria developed significantly faster in CAP than that in CSB, the diversity of bifidobacteia is lower in the CAP group when compared to CSB subjects. Unlike the HMOs in the breastmilk, infant formula usually provides the combination of plant-derived galacto and fructo- oligosaccharides which are naturally present in many plants. Together with the supplemented *B. breve* M16-V, the scGOS/lcFOS supports its growth and hence outnumbers the other types of *Bifidobacterium* spp. in the CAP group.

Another noteworthy phenomenon has been observed in groups of VDB, CSB, and CCO is that the abundance of *B. breve* and *B. bifidum* increased and decreased correspondingly in the first 12 weeks. One possible explanation is that the cell-surface-localized sialidases of *B. bifidum* are capable of degrading HMOs into sialic acid, which is further utilized as a carbon source for *B. breve*. However, the situation changed in week 48, the number of *B. breve* continuously grew while *B. bifidum* dropped significantly to below LOD. It is highly possible that the transmission of dietary from breastmilk to solid food and cow milk leads to the discontinuous

colonization of *B. bifidum* in infant's guts. Unlike *B. breve*, *B. bifidum* lacks the ability to break down the sialylated oligosaccharides [61]. *B. breve* has the ability to utilize both short- and long-chian GOS and FOS in the solid food. While without the support of the only carbon hydrate sources from HMOs, *B. bifidum* becomes less competitive in terms of colonization ability against other species and starts to disappear gradually.

With the help of 16s sequencing, the dynamics of the microbial flora composition and richness in the infants' guts can be better understood. The statical differences between the four groups were compared to evaluate the impacts of delivery modes and feeding patterns on the variation of gut microbiome during the observational period. The results demonstrated that the VDB group was positively associated with the level of *Escherichia-shigella*, *Bacteroides* and *Bifidobacterium*. Numerous researches have reported this phenomena may be due to the impact of delivery modes. The research group from Pat et al. found the similar results by comparing the gut microbiota composition between vaginal born and C-section born infants from 82 healthy subjects (39 boys and 43 girls) in China. It is reported that the genera *Bifidobacterium*, *Lactobacillus* and *Bacteroides* were dominated in vaginal delivery group, whereas *Staphylococcus*, *Streptococcus* and *Corynebacterium* were main observed in the C-section group. Those two cohort studies recruited subjects from different regions but showed the similar results, providing a strong evidence and foundation for further researches.

Bacteria predominated in VDB group are considered to be beneficial bacteria obtained from vaginal canal which help to maintain the hemostasias of the gut by producing various metabolites such as SCFAs that are involved in different physiological functions of hosts. Besides, those bacteria were shown to be more stable due to increased metabolic and biodegradation rates of vitamins, xenobiotics, and carbohydrates compared to C-section groups [62].

Besides, positive relationships were also found between *Veillonella, Enterobacteriacea*, and *Klebsiella* and the C-section group. These were the most prevalent, potentially hazardous, and pro-inflammatory microorganisms linked to the hospital environment [63]. In the three C-section groups, the abundance of certain beneficial bacteria such as bifidobacteria were stored shortly in the infant's gut of CSB and CAP infants, which were fed with breastmilk and formula containing the symbiotic respectively. Disparities in the composition of the gut microbiota and delivery method appear to have more noticeable effect shortly after birth which fade away over the course of the postnatal period.

To sum up, all the results showed that the best way to "inoculum" a high diversity of *Bifidobacterium spp.* in infants' gut microbiome is through vaginal birth and breastfeeding [64]. Continuous breastfeeding which supplements *Bifidobacterium* to newborns helps to train their immune system and could reduce skin disorders such as AD.

Chapter 4: Characterization of *Bifidobacterium* and probiotic-derived EVs, along with their *in vitro* functions.

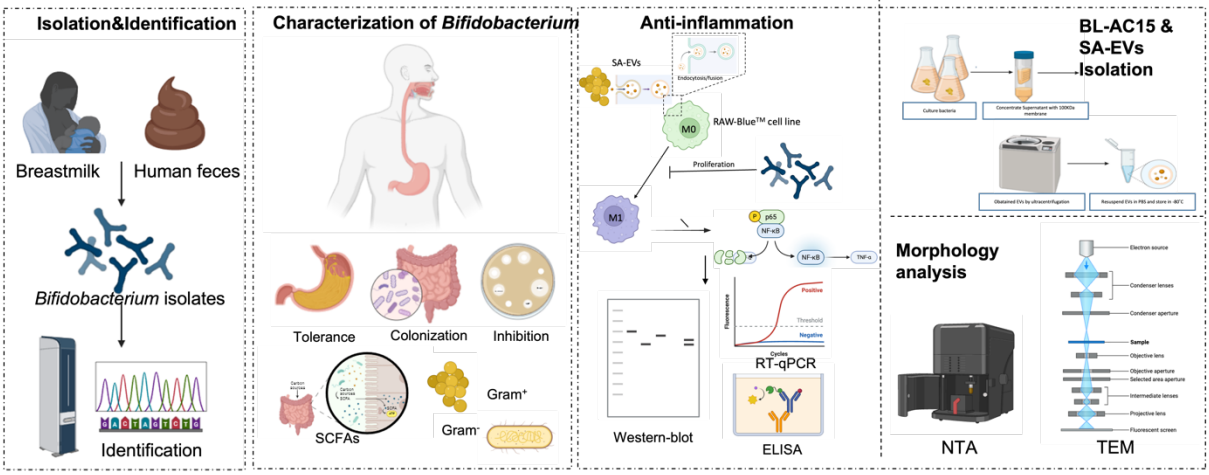

Figure 4.1: Flow chart of Bifidobacterium and EVs isolation and several in vitro experiments.

4.1 Introduction:

Bifidobacteria are Gram-positive, non-spore-forming, strictly anaerobic, pleomorphic heterofermentative bacteria that normally live in the gastrointestinal (GI) tract of humans and other animals [65]. These bacteria are constant companions throughout the human lifespan, yet their prevalence and dominant species undergo dynamic shifts with age. In early life, species such as *B. breve*, *B. bifidum*, and *B. longum* subsp. *infantis* are prevalent in the infants' GI tract due to their genetic machinery of utilizing human breastmilk oligosaccharides (HMOs), and the supporting relationship of cross-feeding [66]. As the gradual introduction of solid food, *B. longum* subsp. *longum*, *B. adolescentis* and *B. catenulatum* become predominant in the GI tract of adulthood, adapted to digesting dietary fiber [67–69]. Succession of different Bifidobacterium (sub)species is not merely a change in taxonomy but reflects a functional specialization, where different species exhibit distinct capabilities that benefit host health through diverse mechanisms.

Bifidobacteria have attracted the interest of scientists since their initial discovery due to their wide-ranging physiological benefits for the host. One key mechanism of protection is their ability to adhere to intestinal receptors, proliferate, and saturate available physical niches, thereby sterically hindering the subsequent attachment of enteropathogens like *Escherichia coli*, *Salmonella* Typhimurium, or *Listeria monocytogenes* [70]. The Caco-2 cell line is the primary *in vitro* model for studying bacterial adhesion due to its unique differentiation into a polarized monolayer, which forms tight junctions and a functional microvilli brush border, closely mimicking the structure and function of mature small intestinal enterocytes [71]. Beyond competitive exclusion, bifidobacteria actively fortify intestinal barrier integrity. Certain strains upregulate the expression of tight junction proteins, including ZO-1, occludin, and claudins, which strengthens the transepithelial electrical resistance (TEER) [19]. This enhancement

reduces paracellular permeability and helps prevent the translocation of pathogens across the monolayer.

SCFAs are not just byproducts of fermentation of bifidobacteria but are essential bioactive mediators that orchestrate host-microbiota symbiosis [72]. These key bioactive metabolites, including acetate, propionate, butyrate, valerate, iso-valerate, and iso-butyrate, serve as important signaling molecules and energy sources, exerting broad systemic effects on the host. As the primary SCFA produced by bifidobacteria, acetate enhances the defensive capabilities of the intestinal epithelial cells, shielding the host from invading pathogens [73]. Also, it lowers the luminal pH, creating a hostile environment for pH-sensitive pathogens like *Salmonella* and *E. coli* [74]. Butyrate is a typical energy source that supplies 60-70% of the energy requirement of colonocytes, although bifidobacteria is not a major producer [75]. Apart from those well-known functions, SCFAs act as signaling molecules by activating G protein-coupled receptors (GPCRs) like FFAR2 and FFAR3 to regulate hormone secretion, immune responses, and blood pressure. Moreover, they directly inhibit histone deacetylases (HDACs), leading to epigenetic modulation of gene expression involved in inflammation, cell proliferation, and metabolism [76].

Notably, bifidobacteria demonstrate anti-inflammatory potential, with a key mechanism being the direct modulation of macrophage polarization and function. Macrophages are central orchestrators of the immune response, capable of polarizing into a pro-inflammatory (M1) or an anti-inflammatory, reparative (M2) phenotype [77]. Metabolites such as lactic acid and SCFAs secreted by bifidobacteria can shift the balance toward the M2 phenotype, thereby alleviating inflammation. *S. aureus* colonization has been associated with many health-related infections, such as lower respiratory tract, blood, and peritoneal or intraabdominal infections [78]. Moreover, *S. aureus* is frequently implicated in mild to moderate skin infections in the community [79]. It secretes a variety of enterotoxins and other toxins in an extracellular vesicle form (SA-EVs), which causes inflammatory responses and activates pro-inflammatory cells like macrophages [80]. EVs are recognized as nanocarriers that could transport virulence factors to the host tissues and play a significant role in the interactions between bacteria and hosts [81]. SA-EVs are strongly associated with the development of many inflammatory diseases, particularly atopic dermatitis [82].

Given the distinct functional attributes of different bifidobacteria species and strains, targeted characterization is essential to identify strains suited for specific applications. This study aims to (1) perform an *in vitro* comparative characterization of bifidobacteria isolated from different sources, and (2) evaluate and identify potential human-sourced strains capable of surviving gastrointestinal transit and exhibiting anti-inflammatory functions. The findings will establish a preliminary basis for subsequent investigations into the capacity of *Bifidobacterium* strains to attenuate inflammation induced by SA-EVs.

4.2 Characterization of extracellular vesicles (EVs)

4.2.1 Characteristics of SA-EVs

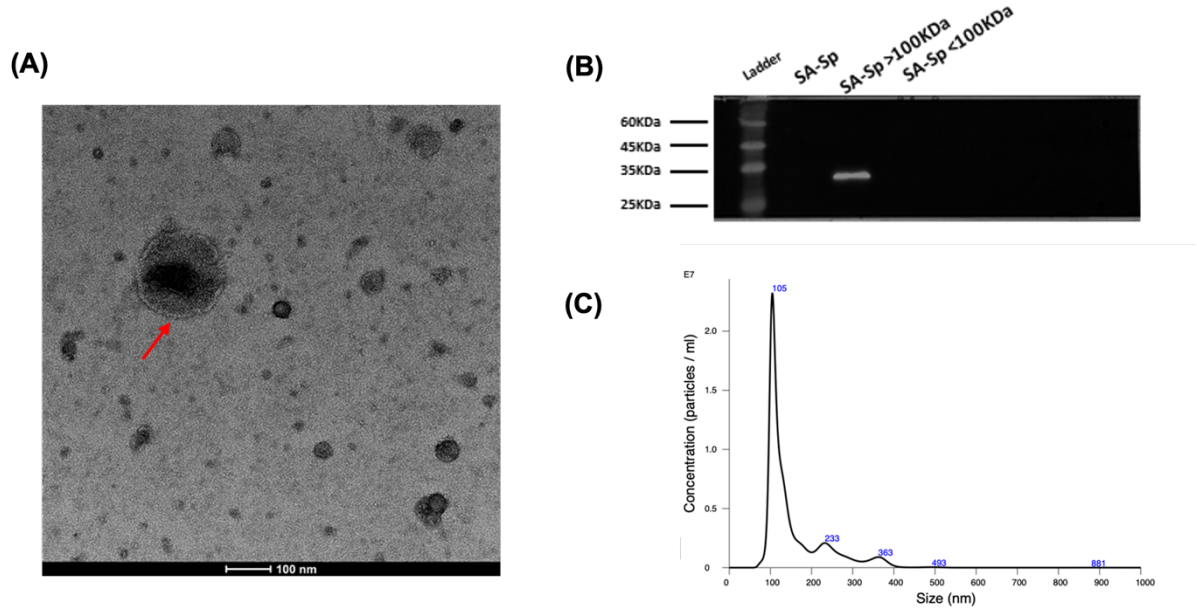

Figure 4.2: S. aureus derived extracellular vesicles (SA-EVs) Characteristics. Transmission electron microscopy demonstrated the morphology of SA-EVs, circular vesicles with a bilaminar membrane, scale bar =100 nm. Red Arrowheads identify SA-EVs (A). Western-blot analysis of the protein expression of α -hemolysin in SA-EVs (B). Nanoparticle tracking were used to analysis the particle size distribution of SA-EVs (C).

TEM is an analytical technique used to visualize structures at nanometer range. Different from microscope, it can reveal stunning details at the atomic scale by magnifying structures up to 50 million times as electrons have shorter wavelength than visible light when accelerated through a strong electromagnetic field which could increase the microscope resolution by several orders of magnitude. TEM images showed the present of *S. aureus* secreted EVs with the spherical lipid bi-layer structure (Fig 4.2 A). The *S. aureus* cultured supernatant (SA-Sp), supernatant concentrated with 100KDa Amicon and ultra-centrifuged pellet (SA-Sp >100KDa), and supernatant below 100KDa fraction (SA-Sp <100KDa) were analysed by western-blot. The results showed that the pathogenic protein, α-hemolysin, was present in the faction of SA-Sp > 100KDa rather than fraction of SA-Sp <100KDa (Fig 4.2 B). Nanosight tracking system showed the size of SA-EVs mainly distributed from 100 nm to 200 nm (Figure 4.2C). Collectively, these findings suggest that SA-EVs could be successfully isolated from the cultured supernatant of *S. aureus*, and the pathogenic protein was presented in the SA-EVs.

4.2.2 Morphology of *B. longum* AC15

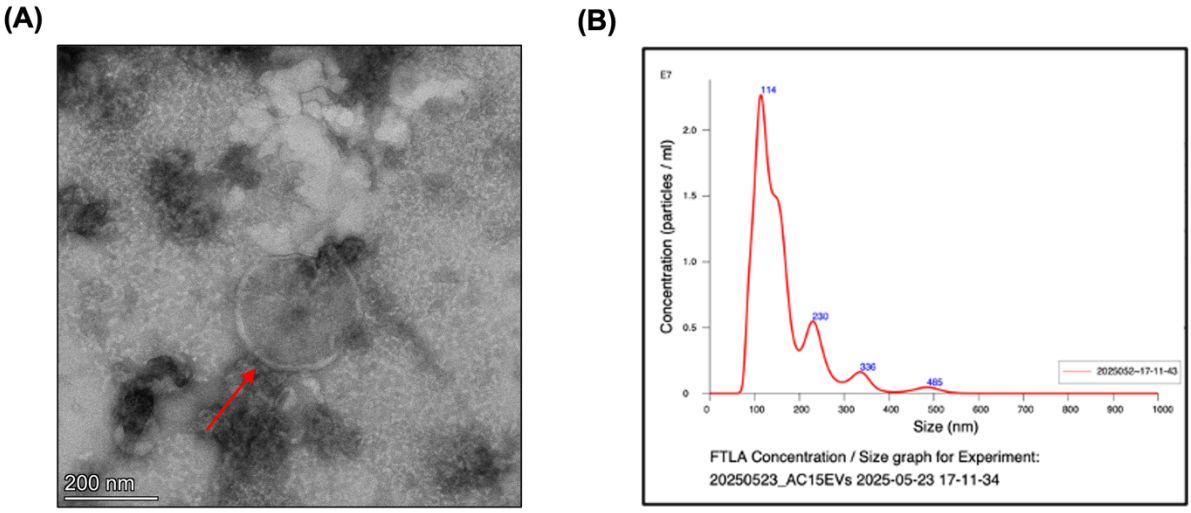

Figure 4.3: B. longum AC15 derived extracellular vesicles (BL15-EVs) Characteristics. Transmission electron microscopy demonstrated the morphology of BL15-EVs, circular vesicles with a bilaminar membrane, scale bar =200 nm. Red Arrowheads identify BL15-EVs (A). Nanoparticle tracking were used to analysis the particle size distribution of BL15-EVs (B).

As shown inFig. 4.3 A, the double lipid-layers structure of *B. longum* AC15 derived extracellular vesicles (BL15-EVs) can be clearly seen via TEM, indicating the EVs-derived from *B. longum* AC15 were successfully isolated by the aforementioned method. Through the analysis of NTA, the size of BL15-EVs ranged from 100nm to 350nm, which were mainly distributed within 134 nm to 220 nm.

4.2.3 Analysis the protein composition of SA-EVs via proteome

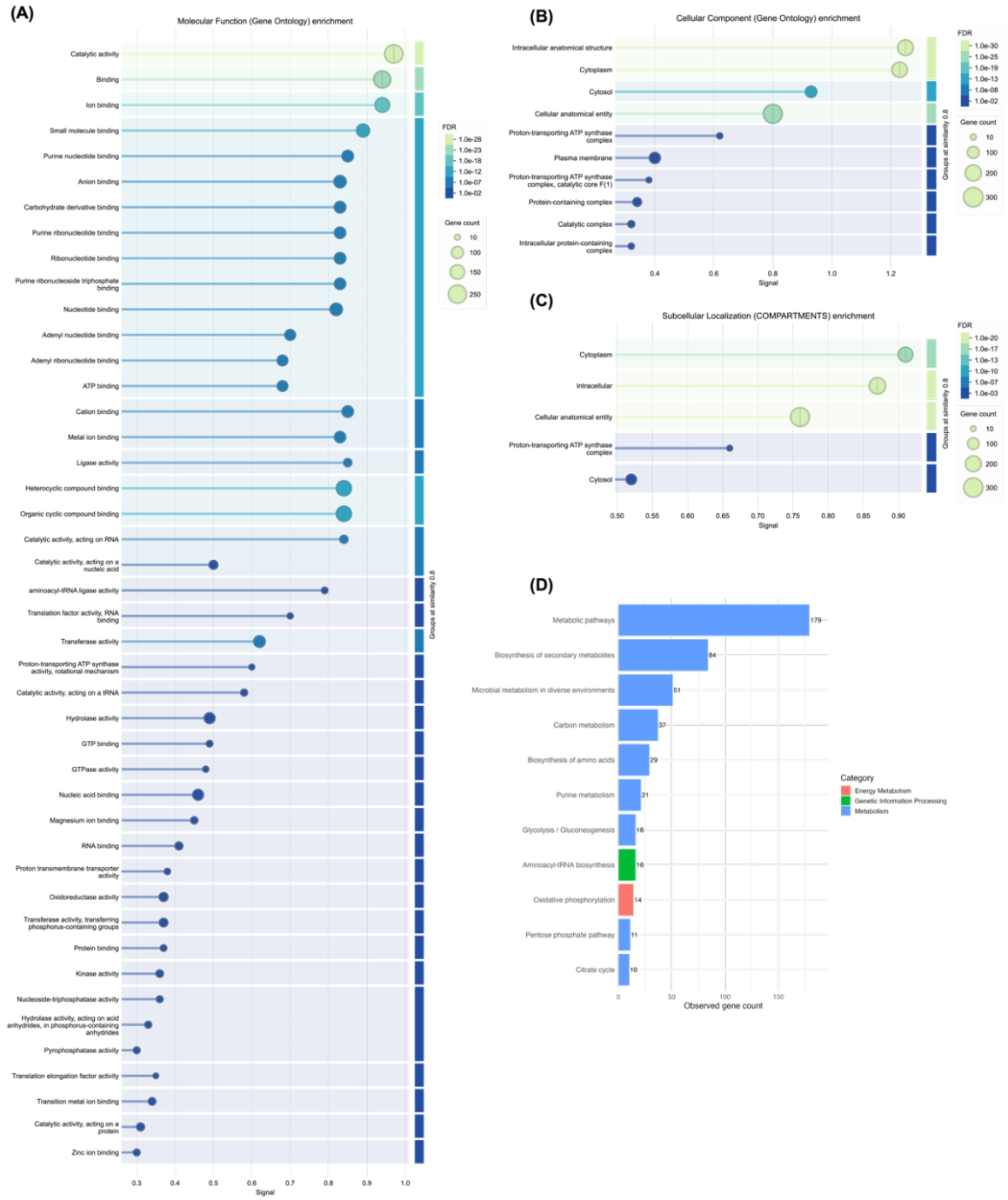

Figure 4.4: Gene Ontology (GO) analysis of SA-EVs protein components. GO analysis of the molecular function (A), cellular component (B), Subcellular component (C), and KEGG pathways (D). The graph shows the distribution of corresponding GO terms. The size of point shows the number of all proteins associated with the GO term. The length shows the FDR number.

Molecular function (MF) analysis showed that the most significant enriched proteins harbored the ability of catalytic activity. While majority of proteins have the ability of binding, such as ion binding, purine nucleotide binding, carbohydrate derivative binding, and purine ribonucleotide binding, etc. Cellular component (CC) analysis pointed out that the biggest group of proteins were from intracellular anatomical structure followed by cytoplasm and cytosol. KEGG pathway analysis revealed that detected SA-EVs proteins were involved in 11 pathways. The top three pathways based on the number of proteins involvement in SA-EVs were the metabolic pathways, the biosynthesis of secondary metabolites, and the microbial metabolism in diverse environment.

4.2.4 Analysis the protein composition of BL15-EVs via proteome

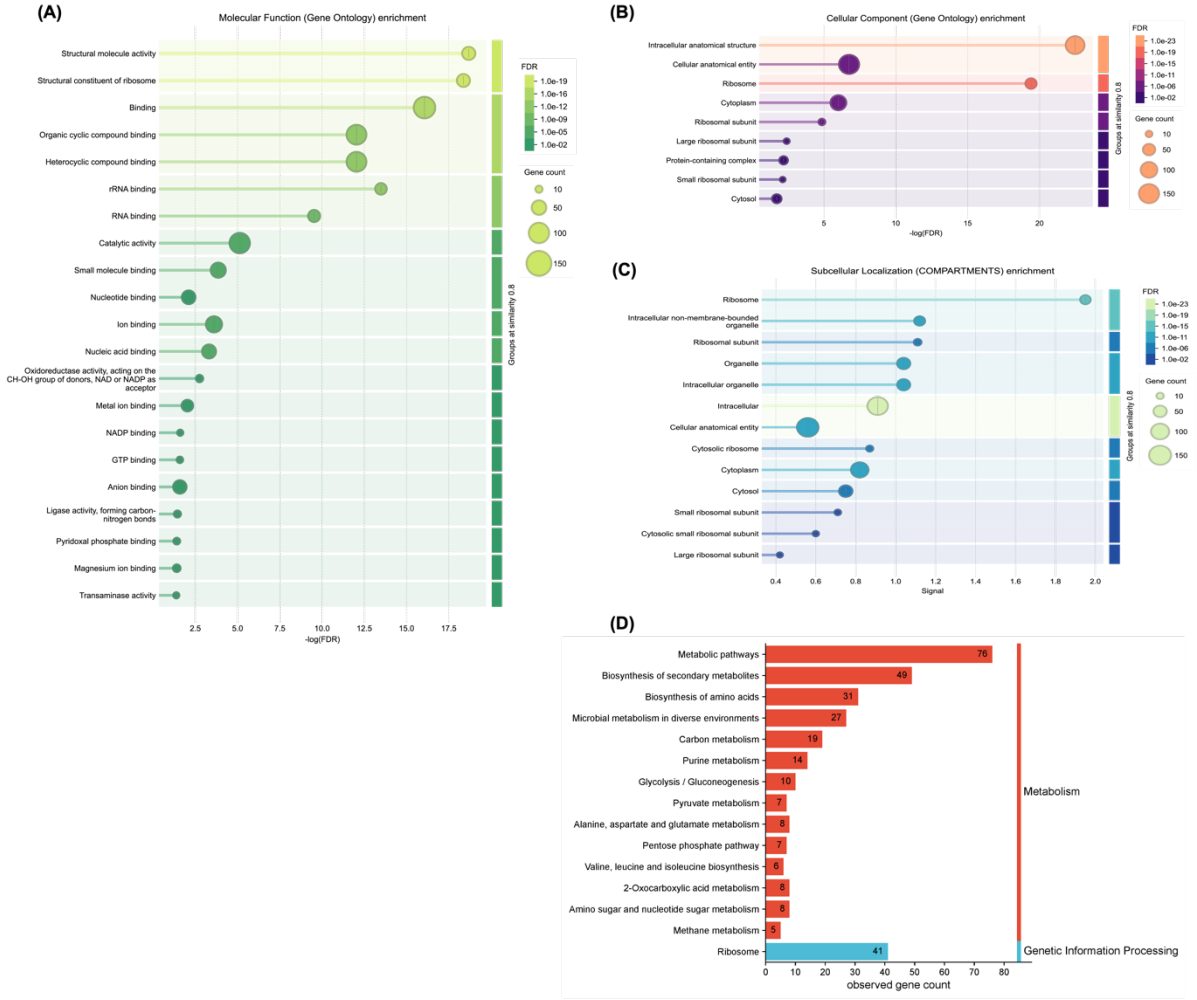

Figure 4.5: Gene Ontology (GO) analysis of BL15-EVs protein components. GO analysis of the molecular function (A), cellular component (B), Subcellular component (C), and KEGG pathways (D). The graph shows the distribution of corresponding GO terms. The size of point shows the number of all proteins associated with the GO term. The length shows the FDR number.

Similarly, GO analysis of BL15-EVs was also conducted. Different from SA-EVs, the most enriched function of BL15-EVs' protein were structural molecule activity. They also contained proteins having the ability of binding, including organic cyclic compound binding, heterocyclic compound binding, and rRNA binding, etc. CC analysis of BL15-EVs indicated that the most enriched source of those proteins was from the intracellular anatomical structure, which was the same as SA-EVs. The second source was cellular anatomical entity, followed by ribosomes. KEGG analysis revealed the detected proteins were involved in 15 pathways, which were categorized into metabolism and genetic information processing. The top three pathways based on the number of proteins involved in BL15-EVs were the metabolic pathways, the biosynthesis of secondary metabolites, and the biosynthesis of amino acids.

4.2.5 Significant findings

SA-EVs are increasingly recognized as significant contributors to the pathogenesis of AD, rather than simply the colonization of *S. aureus* on the skin [83] . The secretory products from *S. aureus* can significantly exacerbate the symptoms of AD. As a result, SA-EVs was chosen as the AD inducer in the following both *in vitro* and *in vivo* experiments. Regarding the EVs derived from probiotics, few research has been done in the field of its application on attenuating AD. This study aimed to investigate the potential beneficial effects of BL15-EVs on AD.

Beforehand, several characterizations of SA-EVs and BL15-EVs were analysed. With the advantages of small size (100 nm to 300 nm) and lipid bi-layers structure, they can easily get into cells via fusion or internalization and escape the challenges of the outside environment [84,85]. Toxic protein, α-hemolysin, as one of the pathogenetic factors can be only detected in the fraction of SA-Sp>100KDa, which were used for the following inflammation induction [83]. Also, benefiting from its structure, BL15-EVs can easily transfer the functional metabolites and proteins into hosts, which can modulate the immune system, reduce inflammation, and restore gut barrier integrity [86–88].

For the GO analysis of protein composition within the SA-EVs and BL15-EVs, most of the proteins had the ability of binding to various targets, including ion, purine, mRNA, and nucleotide, etc. This result indicated that EVs are special cargo that can deliver binding proteins to their associated ligands. Besides, EVs containing most proteins of SA-EVs and BL15-EVs were both from the intracellular anatomical structure, cellular anatomical entity, and Ribosome, indicating they were likely produced by the cell cytosol and organelles. Moreover, almost all of these proteins involved in metabolism pathway, indicating they are likely functioning as metabolic nano compartments or transcellular metabolic mediators.

4.3 Characteristics of *Bifidobacterium* isolates

4.3.1 Monitor the growth curve

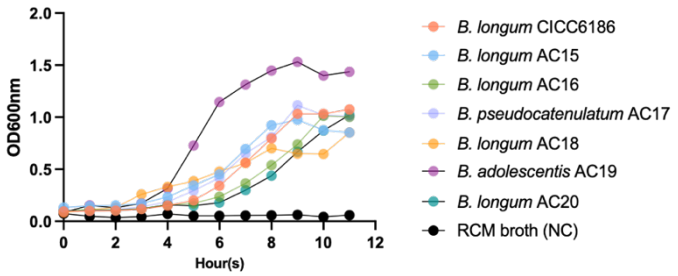

Bacteria Name	Generation Time (Min)
B. longum CICC6186	112.27
B. longum AC15	126.78
B. longum AC16	122.02
B. pseudocatenulatum AC17	126.97
B. longum AC18	208.20
B. adolescentis AC19	64.56
B. longum AC20	135.24

Figure 4.6 Growth Curve and generation time of seven Bifidobacterium isolates cultured in RCM broth.

As shown in Figure 4.6, the growth rate of *B. adolescentis* AC19 was the highest with the generation time 64.56 min among seven isolates under optimal condition. On the contrary, *B. longum* AC18 has the longest doubling time of 208.20 min among all. The rest isolates, *B. longum* CICC6186, *B. longum* AC15, AC16, and AC20, and *B. pseudocatenulatum* AC17 had similar generation time ranging from 112.27 to 135.24 min.

4.3.2 Tolerance towards Gastric Juice and Intestinal Juice

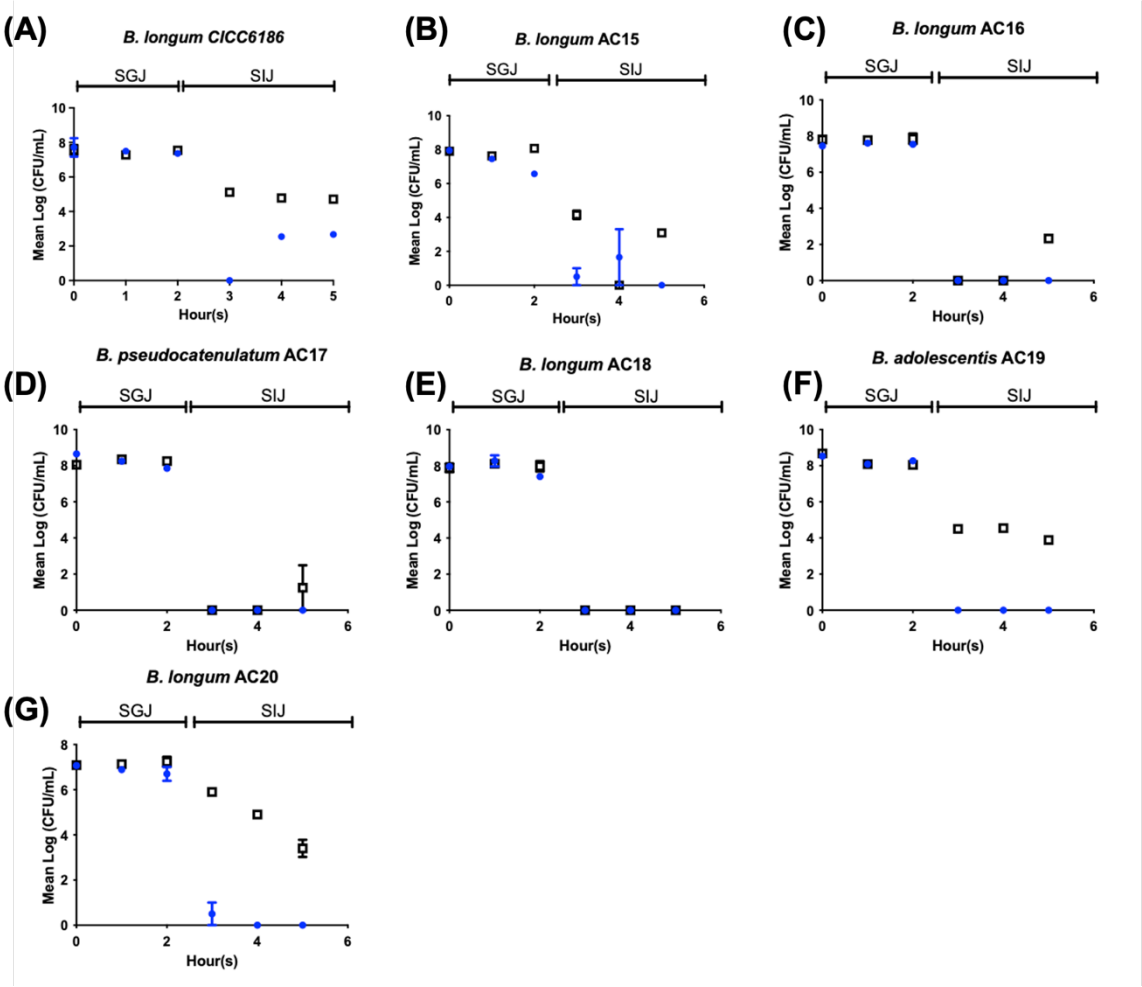

Figure 4.7:The effects of simulated gastric juice(SGJ) and simulated intestinal juice (SIJ) on the survival rate of Bifidobacterium isolates. Tolerance of seven Bifidobacterium isolates (A) B. longum CICC6186 (B) B. longum AC15 (C) B. longum AC16 (D) B. psedocatenulatum AC17 (E) B. longum AC18 (F) B. adolescentis AC19 (G) B. longum AC20 towards SGJ and SIJ. Each point was done in duplicate.

The tolerance to gastric juice and intestinal juice is crucial for probiotics as it allows them to survive and thrive in harsh environment of human GI tract. *Bifidobacterium* isolates have varying levels of tolerance to simulated GI conditions. This *in vitro* study showed in Fig. 4.7 that the seven isolates withstood the challenge of simulated gastric juice for 2 hr, while some of them struggled to survive in the simulated gastric juice for 3 hr with the log (CFU/mL) number almost reaching to zero. A certain amount of resistance to simulated intestinal juice was exhibited in *B. longum* CICC6186*, B. longum* AC15. The log (CFU/mL) number of them dropped 4 to 5 log (CFU/mL) after 3 hr incubation in the simulated intestinal juice. The rest

isolates cannot stand the challenge of SIJ for 1 hr with the log (CFU/mL) number equals to zero.

4.3.3 Adhesion and Competitive Adhesion Ability on colon epithelium cells

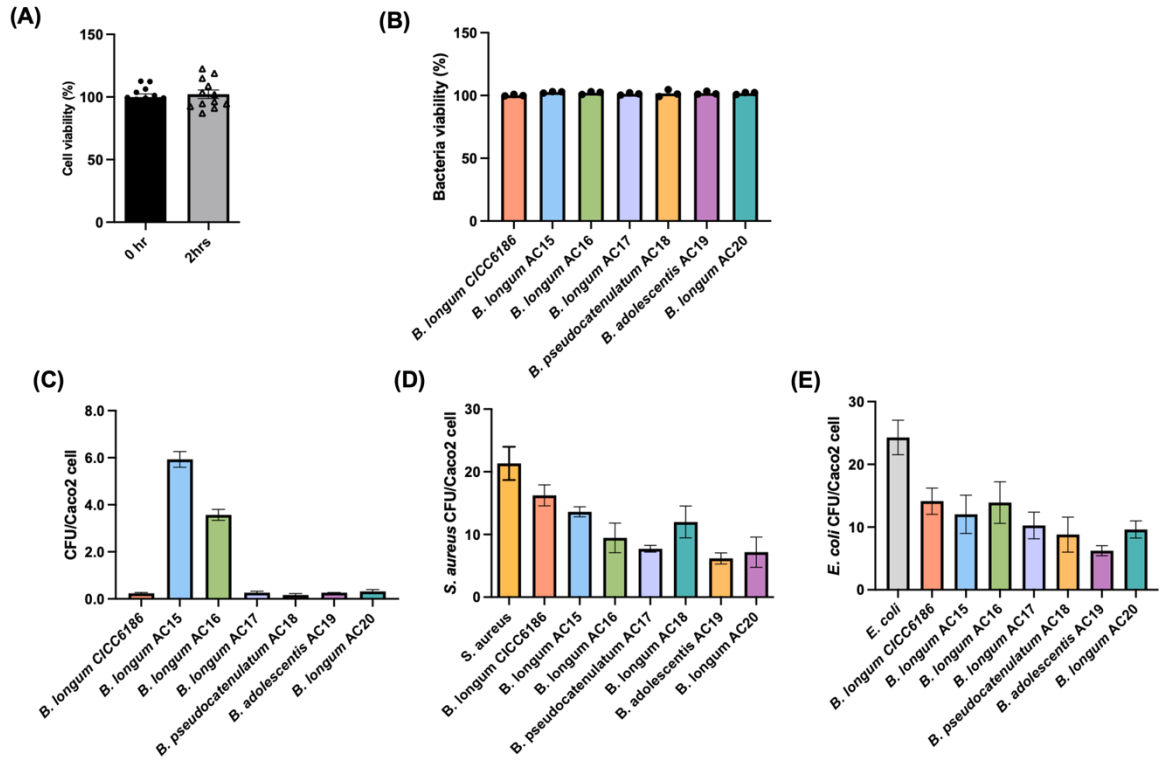

Figure 4.8: Adhesion and Competitive Adhesion Ability of Bifidobacterium isolates on colon epithelium cells (Caco-2 cells). Viability of Caco-2 cells under anaerobic condition for 2 hr (A). Viability of S. aureus ATCC6538, E. coli ATCC8739, and Bifidobacterium isolates in lysis buffer (0.5% Saponin) (B). Adhesion ability of Bifidobacterium isolates cultured in RCM broth Caco-2 (C), and Competitive adhesion ability of Bifidobacterium isolates against S. aureus (D) and E. coli (E).

The adhesion and competitive adhesion abilities to human epithelial cell of the *Bifidobacterium* isolates were tested. Those abilities are crucial for their probiotic functionality and potential health benefits by preventing the invasion and colonization of gut pathogens. As shown in Figure 4.8C, *B. longum* AC15 and *B. longum* AC16, isolated from human milk, had the outstanding adhesion ability of all with 6.0±1.1 and 3.6±0.6 bacteria per Caco-2 cell, respectively, while the rest of isolates barely adhered to the Caco-2 cells (less than one bacterium/Caco-2 cell).

The competitive adhesion properties against *S. aureus* and *E coli* amongst the seven isolates varied. *B. adolescentis* AC19 showed the distinguished ability to competitively exclude the colonization of both Gram-positive *S. aureus* and Gram-negative *E. coli* from Caco-2 cells. It

successfully reduced the number of *S. aureus* and *E. coli* per Caco-2 cell from 21.3±4.6 and 24.2±5.5 to 6.2±1.5 and 6.2±2.4, respectively (Figure 4.8D-E). The competitive adhesion ability of *B. longum* AC15 is higher on *E. coli*, as shown with reduction of 50.4% compared to adhesion of *E. coli* alone, than *S. aureus* (36.2% reduction) on Caco-2 cells

4.3.4 Determination of Short chain fatty acids

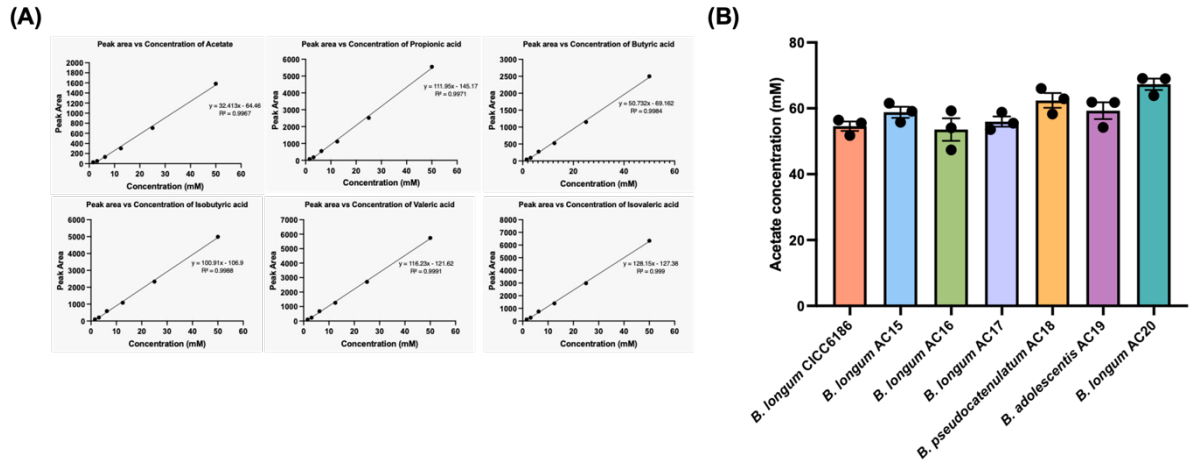

Figure 4.9: Comparison SCFAs production ability among seven Bifidobacterium isolates. Standard curve of six SCFAs, acetate, propionic acid, butyric acid, isobutyric acid, valeric acid and isovaleric acid (A). Comparison the amount of acetate produced by seven Bifidobacterium isolates (B).

SCFAs are the fermentation products of dietary fibers by certain gut microbiota, which have a variety of impacts on host metabolism and can be utilized as an energy source supporting the intestinal barrier system. Bifidobacteria, as GI tract's ubiquitous inhabitants, serve to increase the production of SCFAs in the gut and regulate host energy metabolism. The amount of six SCFAs produced by *Bifidobacterium* were analysed via GC-FID (Figure 4.9). The acetate production ranged between 53.56 mM to 67.31 mM, with no statistical differences among the tested isolates. The rest of five SCFAs were below the limit of detection.

4.3.5 Antimicrobial Assessment

Table 4.1 Antimicrobial activity towards S. aureus ATCC6538 and E. coli ATCC8739 of Bifidobacterium isolates.

Strain Name	Against *S. aureus* ATCC6538 w/o Glucose+Starch	Against *S. aureus* ATCC6538 w Glucose+Starch	Against *E. coli* ATCC8739 w/o Glucose+Starch	Against *E. coli* ATCC8739 w Glucose+Starch
B. longum CICC6186	0.57±0.06	0.77±0.12	0.47±0.06***	1.07±0.12
B. longum AC15	0.43±0.06	0.53±0.06	0.27±0.06***	0.63±0.06

B. longum AC16	0.47±0.06**	0.80±0.10	0.53±0.06*	0.67±0.06
B. longum AC17	0.53±0.06*	0.66±0.06	0.30±0.01*	0.43±0.06
B. pseudocatenulatum AC18	0.70±0.01*	0.90±0.10	0.27±0.06*	0.43±0.06
B. adolescentis AC19	0.43±0.06**	0.80±0.10	0.23±0.06*	0.43±0.06
B. longum AC20	0.66±0.06	0.86±0.15	0.30±0.01***	0.77±0.06

*Antimicrobial activity towards S. aureus ATCC6538 and E. coli ATCC8739 of Bifidobacterium isolates. Summary of inhibition radius of each Bifidobacterium isolate on the RCM agar plate in the presence or absence of starch and glucose and illustration the radius of inhibition zone. All the experiments were repeated at least three times and the data were shown as mean ± SEM values. ***P < 0.001, **P <0.01, *P <0.05.*

As shown in Table 4.1, all tested isolates displayed different levels of inhibition zone against the two typical Gram-positive and Gram-negative pathogens, with the inhibition radius ranging from 0.53 cm to 0.90 cm and 0.43 cm to 1.07 cm against *S. aureus* ATCC6538 and *E. coli* ATCC8739, respectively, in the presence of carbohydrates. Amongst all analysed *Bifidobacterium*, *B. longum* AC20 had the biggest inhibitory zone against *S. aureus* with the number of 0.86±0.15cm, while *B. longum* CICC6186 was the best one against *E. coli* with the inhibition radius of 1.07±0.12 cm. Moreover, *Bifidobacterium* strains AC16, and AC19 showed significant wider inhibition zone against *S. aureus* when they were cultured in the RCM plates with carbon sources (1 g/L starch and 5 g/L glucose) than that without it, indicating the acid production is the major factor contributing to their antimicrobial ability. In test of inhibiting *E. coli*, all the isolates presented distinct inhibition ability in RCM plates with carbon sources. Interestingly, all isolates showed inhibition zone against both pathogens in the absence of carbon source, suggesting that they produce other antimicrobial substances other than acid, such as bacteriocins.

4.4 Investigation the functional properties of *Bifidobacterium* and EVs *in vitro*

4.4.1 Differentiation of HaCaT cells

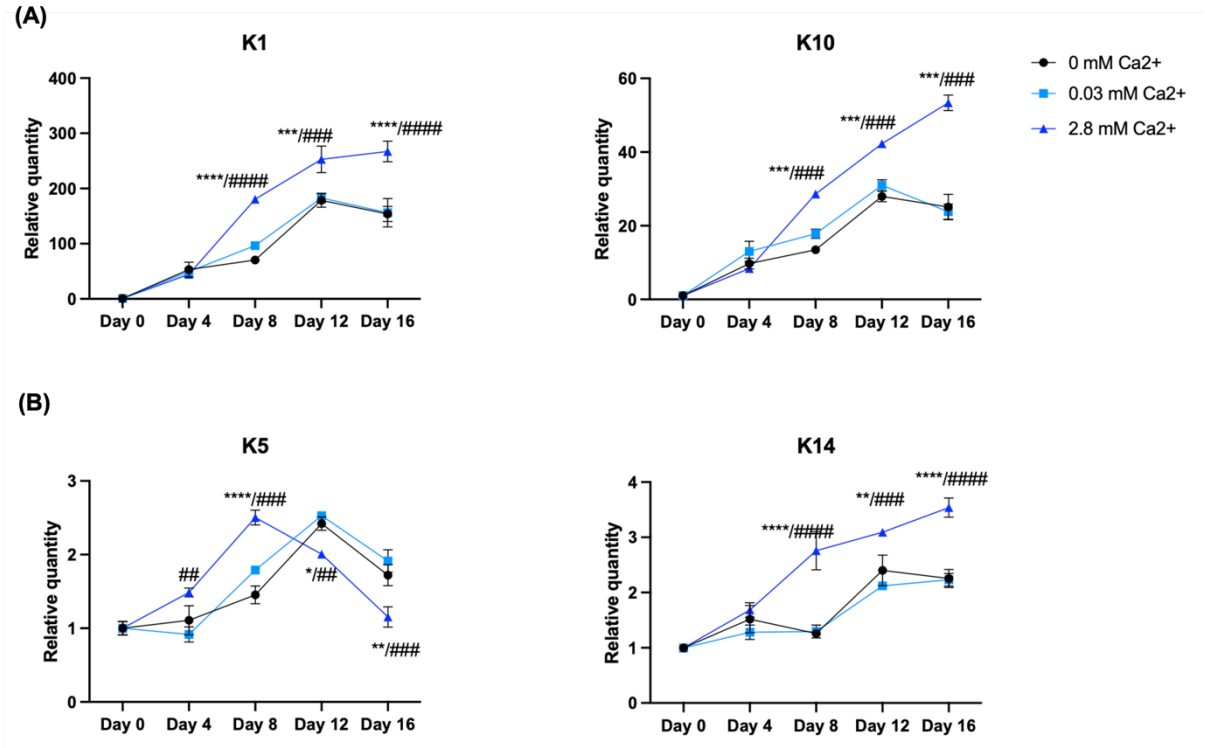

Figure 4.10: Calcium level influenced the proliferation of HaCaT cells. Detection the markers of suprabasal layer (A), and basal layer (B) of skin keratinocytes.

In order to study the mechanism of AD, HaCaT cells were induced to differentiate into multiple layers to mimic the structure and function of skin. In the skin, K1 and K10 are markers for differentiated keratinocytes in the suprabasal layer, while K5 and K14 are restricted to the basal keratinocytes. K1 and K10 are expressed in the upper layers as keratinocytes mature and move away from the basal layer. K5 and K14 are found in the basal layer, where new skin cells are produced and where epidermal stem cells reside.

As shown in Figure 4.10, HaCaT cells cultured in 2.8 mM Ca^{2}+ medium expressed higher level of K1, K10, and K14 than those in 0.03 mM Ca^{2+} medium. This difference grew steadily after Day 4 and started to distinguish it from the other two groups. In contrast, the level of K5 in the 2.8 mM Ca^{2+} group initially rose to twice the level of the other two groups before Day 8, followed by a rapid decline in Day 12 to the lowest level amongst all until Day 16. These results suggested that incubating with high concentration of Ca^{2+} (2.8 mM) for at least 8 days can lead to keratinocytes starting to transform from basal to suprabasal layer of skin, while at least 12 days can successfully differentiate into suprabasal layer of skin.

4.4.2 SA-EVs dosages titration on HaCaT cells

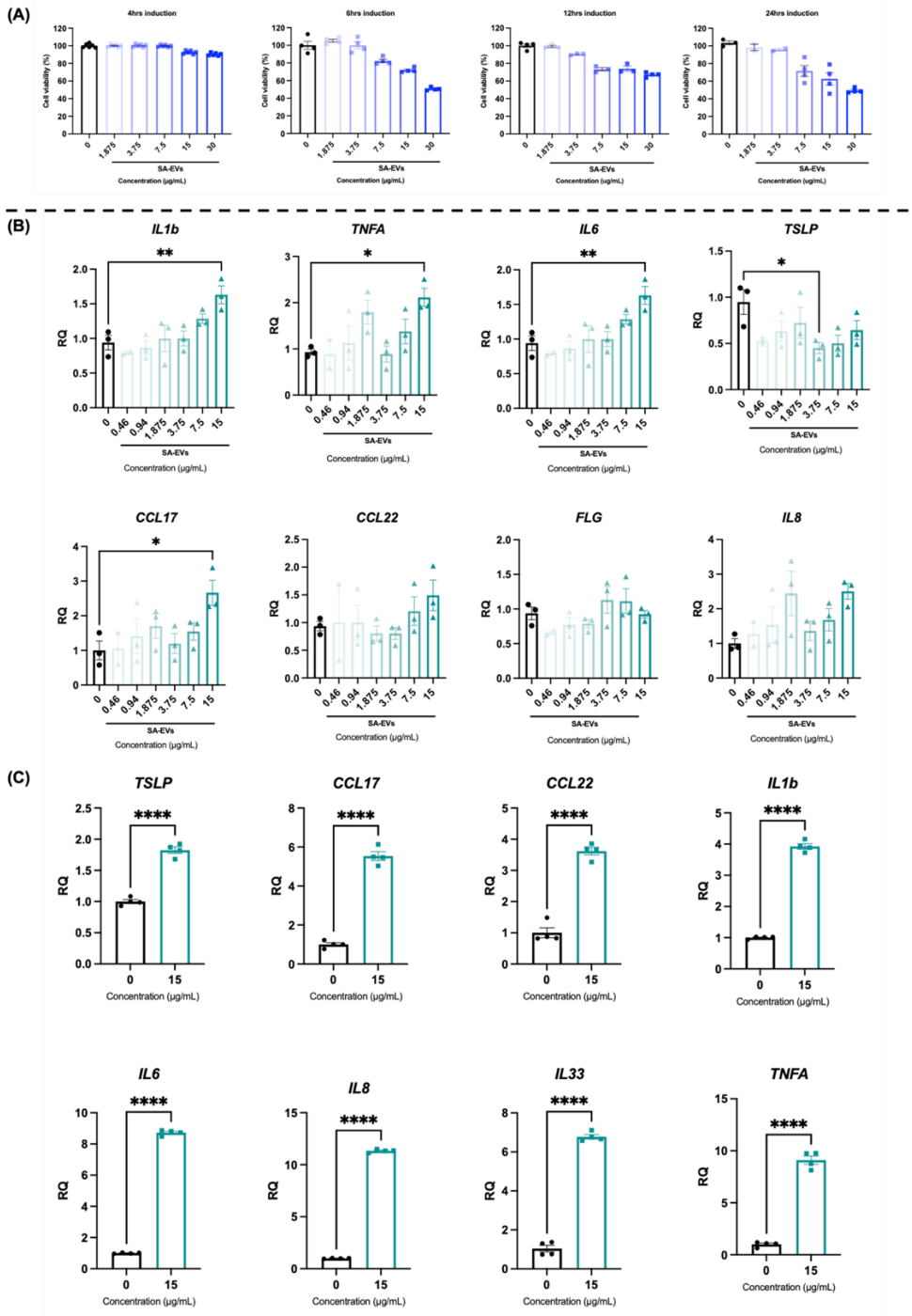

*Figure 4.11: Investigation of toxicology and inflammatory effects of SA-EVs on HaCaT cells. Viability of HaCaT cells after 4 hr, 6 hr, 12hr, and 24 hr induction of SA-EVs (A). in vitro effects of SA-EVs on the mRNA expression level of IL1b, TNFA, IL6, TSLP, IL8, IL33, CCL17 and CCL22 of HaCaT cells after 6 hr induction (B) and 4 hr induction (C). Statistically analysis was used ONE-ANOVA in Prism 9, *p<0.05, **p<0.01, ***p<0.005, ****p<0.001.*

The SA-EVs were assumed having pathogenic effects on human skin. To evaluate it toxicological impacts, spontaneously immortalized human skin epidermis cells (HaCaT) was recruited in this study. Cell viability was assessed using MTT Assay after inducing with SA-EVs dosages from 1.875 μg to 30 μg through a two-fold serial dilution. Data from Figure 4.11 (A) showed that no noticeable cytotoxicity was observed on HaCaT cells after incubating with SA-EVs with concentration up to 3.75 μg/mL for long periods (6 hr, 12 hr and 24 hr) or 15 μg SA-EVs for 6 hr. However, HaCaT cells incubated with SA-EVs with concentration over 15 μg/mL for longer than 12 hr caused significant reduction of cell viability (dropping down to less than 50%). This result indicated that both short-time incubation with high dosage SA-EVs or long-time incubation with low dosage SA-EVs might be the suitable condition of the following experiments.

However, determining the induction condition also heavily relies on the inflammatory response presented in Figure 4.11B, low dosages of SA-EVs did not result in significant cell death, but they were unable to raise the expression of inflammatory cytokines and chemokines on HaCaT cells. 15 μg/mL of SA-EVs triggered robust inflammatory reactions without causing significant cell death, with a significant upregulation of markers linked to AD and allergic reaction, including *IL1b, IL6, IL8, IL33, CCL17, CCl22*, and *TSLP*, etc (Figure 4.11C). *IL1b* and *TNFA* are two of the proinflammatory cytokines that contribute to the early stages of allergic responses. *IL-33* plays a crucial role in the pathogenesis of AD by reducing the expression of filaggrin and claudin-1, leading to a decrease in skin barrier function. *TSLP* and *IL8*, mainly produced in keratinocytes, can initiate Th2 and Th22 immune responses and leads to the progression of immune reactions in AD while *CCL22* and *CCL17* are the important Th2-related chemokines and the markers of severity in AD. In conclusion, those results suggested that induction with 15 μg/mL of SA-EVs for 4 hr is the ideal condition for triggering the inflammatory responses on HaCaT cells, which were used to test the further biological activity.

4.4.3 Toxicity and proinflammatory effects of SA-EVs on RAW-BLUE™

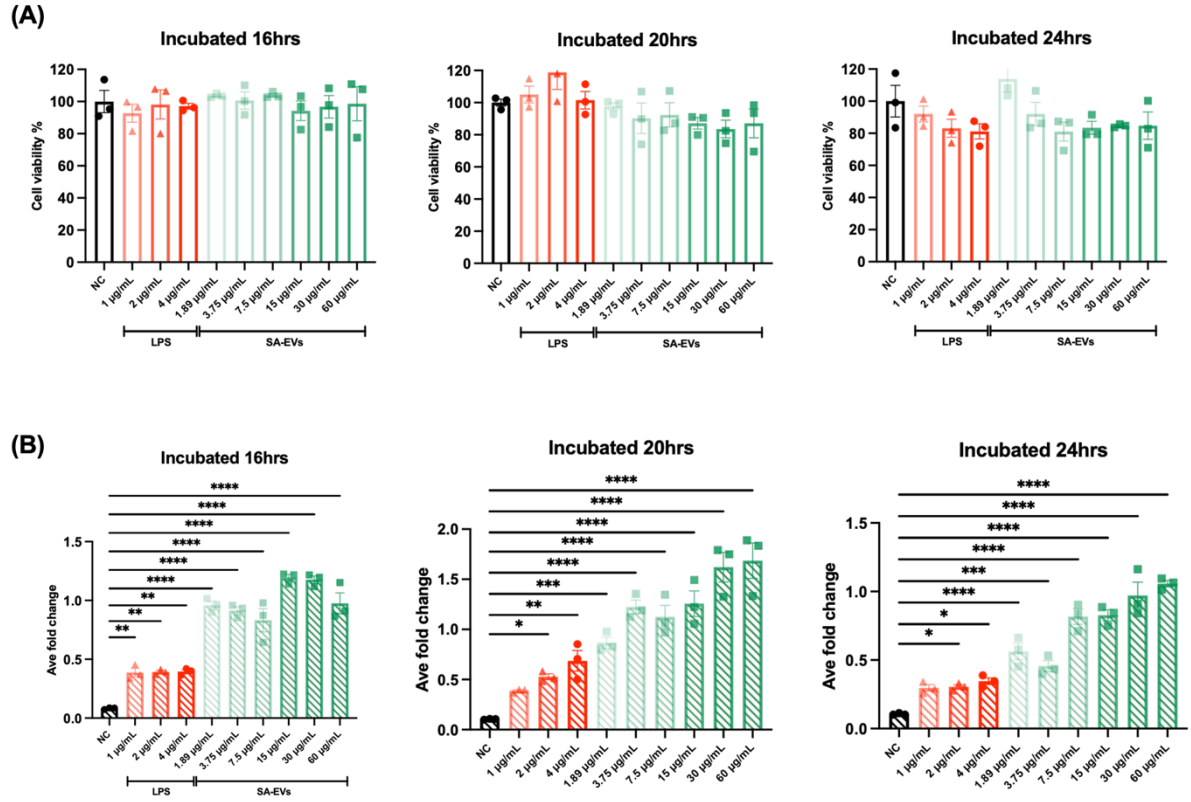

*Figure 4.12: The impact of various dosages of SA-EVs on RAW-BLUE™ cells at three different time points, using LPS as a positive control. MTT Assay was used to determine the cell viability of RAW-BLUE™ cells after induction by SA-EVs (A). SA-EVs stimulation was assessed by measuring the level of SEAP using QUANTI-BLUE™TM. Data are shown as average Fold change of QUANTI-BLUE™TM absorbance which were normalized by cells total protein (mean± SEM) (B). Statistically analysis was used ONE-ANOVA in Prism 9, *p<0.05, **p<0.01, ***p<0.005, ****p<0.001.*

The impact of SA-EVs on the macrophage was studied using RAW-BLUE™ cells. The stimulation with three dosages of LPS, which is broadly used in the establishment of AD cell modes, was applied as a positive control. The cytotoxicity of various dosages of LPS and SA-EVs was assessed on RAW-BLUE™ cells across three different induction time points. Results showed that induction with SA-EVs dosages ranging from 1.89 μg/mL to 30 μg/mL for 16 hr did not cause significant cell death. However, as the induction time increased from 16 hr to 24 hr, the viability of RAW-BLUE™ cells decreased in a time-dependent manner, with the final number less than 80% in the highest dosage group. Overall, under the condition of causing no significant cell death, the simulation capability of SA-EVs peaked at a concentration of 15 μg/mL after 16 hr incubation, suggesting that this condition was optimal for eliciting strong inflammatory responses for the following experiment.

4.4.4 Toxicity and anti-inflammation capacity of HI *Bifidobacterium* on RAW-BLUE™

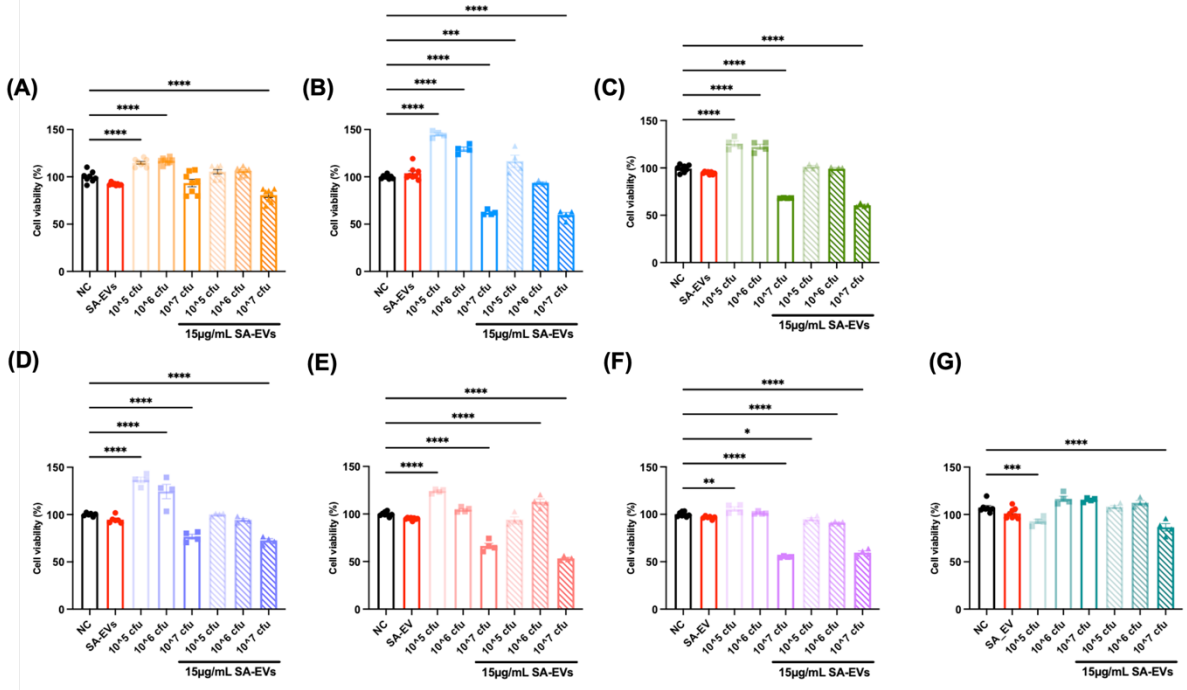

*Figure 4.13: Toxicity effects of Heat-inactivated Bifidobacterium on the cell viability of RAW-BLUE™ cells. Dose-depended effect of HI Bifidobacterium isolates (A) B. longum CICC6186, (B) B. longum AC15, (C) B. longum AC16, (D) B. longum AC17, (E) B. pseudocatenulatum AC18, (F) B. adolescentis AC19, and (G) B. longum AC20 on RAW-BLUE™ cells. All the experiments were repeated in triplicates, and the data are shown as mean ± SEM values. **** P < 0.0001, ***P < 0.001, **P <0.01, *P <0.05 versus SA-EVs treatment alone.*

Before investigating the possible beneficial effects of seven isolates, their toxicity on RAW-BLUE™ was assessed via MTT Assay. Cell viability after pretreatment of three dosages of seven HI *Bifidobacterium*, ranging alone from 10^5 CFU/mL to 10^7 CFU/mL for 24 hr, with or without the addition induction of 15 μg/mL SA-EVs for 16 hr were both evaluated. Data suggested that pretreatment with HI *Bifidobacterium* alone at dosage lower than 10^6 CFU/mL did not cause significant cell death, while as the concentration increased to 10^7 CFU/mL, the toxicity effects started to show up and the cell viability decreased to less than 60% even without the present of inflammatory inducer. After applying the inflammatory inducer to the aforementioned cells, the toxicity effects were not affected dramatically. To sum up, those results suggested that the suitable dosage of HI *Bifidobacterium* is equal or less than 10^6 CFU/mL.

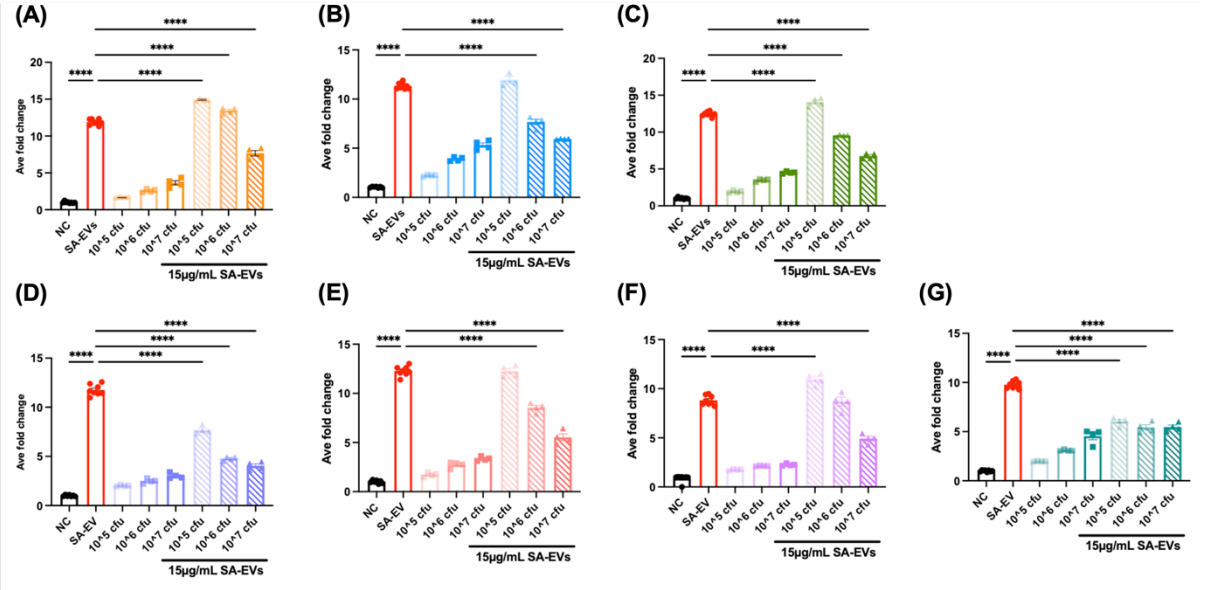

*Figure 4.14: Quantification the expression of anti-inflammatory cytokines on Raw Blue™ cell via reaction with QUANTI-BLUE. Dose-depended effect of HI Bifidobacterium isolates (A) B. longum CICC6186, (B) B. longum AC15, (C) B. longum AC16, (D) B. longum AC17, (E) B. pseudocatenulatum AC18, (F) B. adolescentis AC19, and (G) B. longum AC20 on RAW-BLUE™ cells. All the experiments were repeated in triplicates, and the data are shown as mean ± SEM values. **** P < 0.0001, ***P < 0.001, **P <0.01, *P <0.05 versus SA-EVs treatment alone.*

The induction of 15 μg/mL SA-EVs alone for 16 hr increased the secreted embryonic alkaline phosphatase (SEAP) release by a mean of 10-fold over the PBS treatment on RAW-BLUE™cells. To rule out the influence of cell numbers on the results, the total protein of each well was measured using BCA assay. And the absorbance of QUANTI-BLUE™ was normalized to total protein in each well correspondingly. Seven isolates tested in this experiment showed great anti-inflammatory effects against SA-EVs at all dosages. *B. longum* AC17 and *B. longum* AC20 (Figure 4.14D and 4.14G) are the two most potent strains having anti-inflammatory capabilities amongst all since they began to exhibit considerable anti-inflammatory effects at the lowest dosage of 10^5 CFU/mL. The remaining isolates only began to show significant positive effects in the middle dosage of 10^6 CFU/mL (Figure 4.14).

4.4.5 Anti-inflammatory effects of *Bifidobacterium* by inducing the polarization of M1 Macrophage via NF-κB pathway

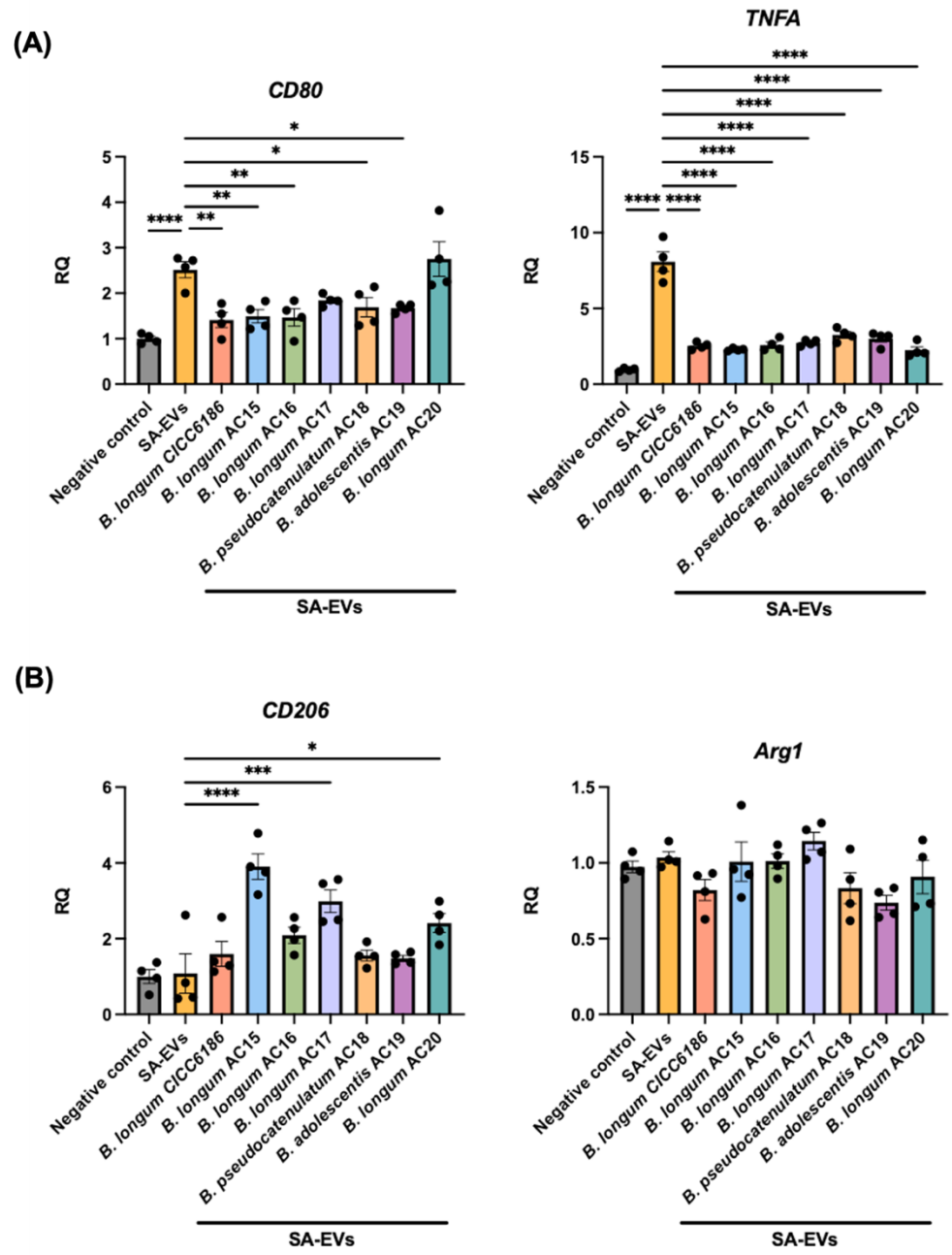

*Figure 4.15: The mRNA expression of macrophage polarization-associated genes in Raw 264.7 cells. The mRNA levels of (A) M1 markers and (B) M2 markers were analysed and compared between the SA-EVs and seven Bifidobacterium isolates. All the experiments were repeated at least three times, and the data are shown as mean ± SEM values. **** P < 0.0001, ***P < 0.001, **P <0.01, *P <0.05 versus SA-EVs treatment alone.*

The expression levels of M1 macrophage polarization-related genes, CD80 and TNFA, were significantly upregulated by SA-EVs, while pre-treatment with all tested HI *Bifidobacterium* isolates, except *B. longum* AC17 and *B. longum* AC20, could prevent this polarization. The expression of M2 macrophage polarization-related genes CD206 and Arg were not activated by SA-EVs. However, one marker of M2 macrophage, CD206, was observed significant higher in *B. longum* AC15, *B. longum* AC17 and *B. longum* AC20 than in the rest groups. The other M2 marker, Arg1, showed no significant change amongst all groups. This result indicated that some HI *Bifidobacterium* could prevent the inflammation response induced by SA-EVs via suppressing the polarization of macrophage.

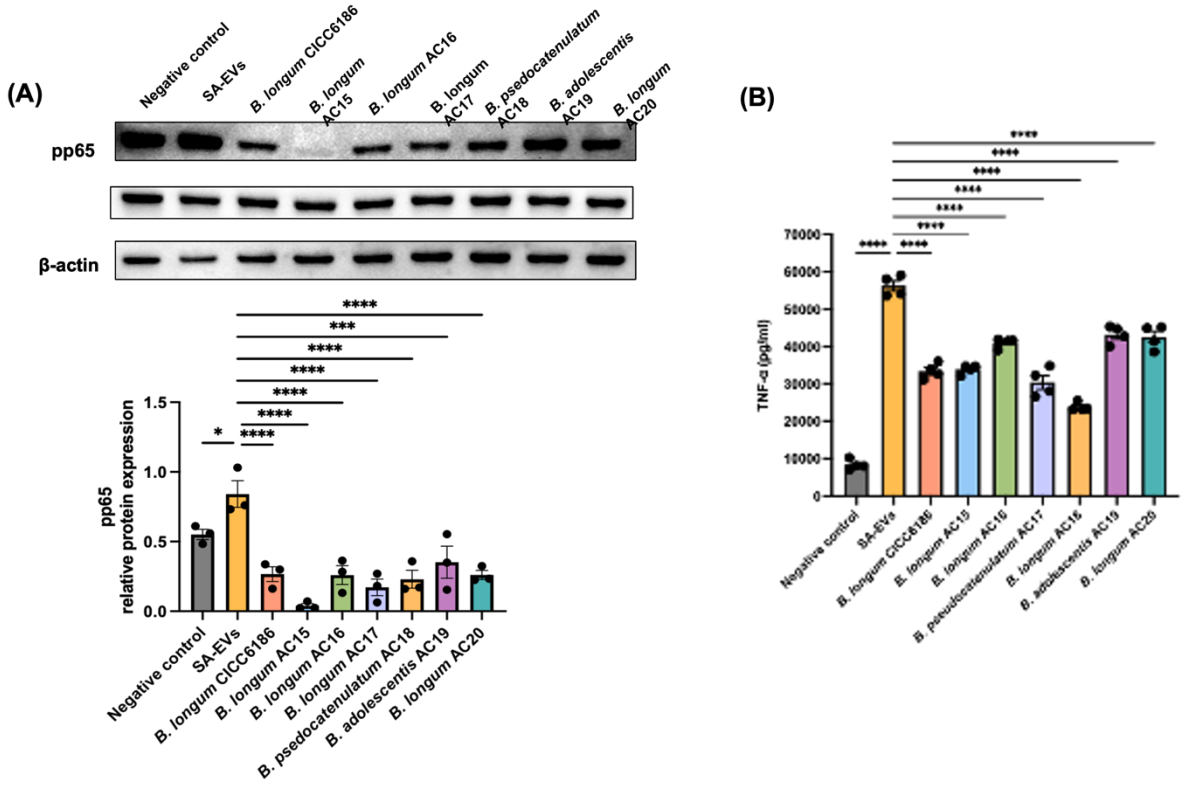

*Figure 4.16: Determination of Nuclear translocation of NF-κB sub-unit by (A) western blot and (B) TNF-α activation by ELISA. All the experiments were repeated for three times, and the data are shown as mean ± SEM values. **** P < 0.0001, ***P < 0.001, **P <0.01, *P <0.05 versus SA-EVs treatment alone.*

To further confirm which pathway was influenced by HI *Bifidobacterium* isolates to prevent the inflammation induced by SA-EVs on Raw 264.7 cells, the TNF-α, transcription factor p65 and its phosphorylates were analysed via ELISA and western blot with beta-actin as reference protein, respectively. Induction with SA-EVs alone on Raw 264.7 cells activated the phosphorylates of NK-κB signaling pathway, while pre-treatment with the HI *Bifidobacterium*

isolates, especially *B. longum* AC15 could prevent this occurrence. Besides, there was a notable decrease in the level of NK-κB-dependent genes, TNF-α, in those seven treatment groups.

4.4.6 *B. longum* AC15 prevented the internalization of SA-EVs on skin keratinocytes

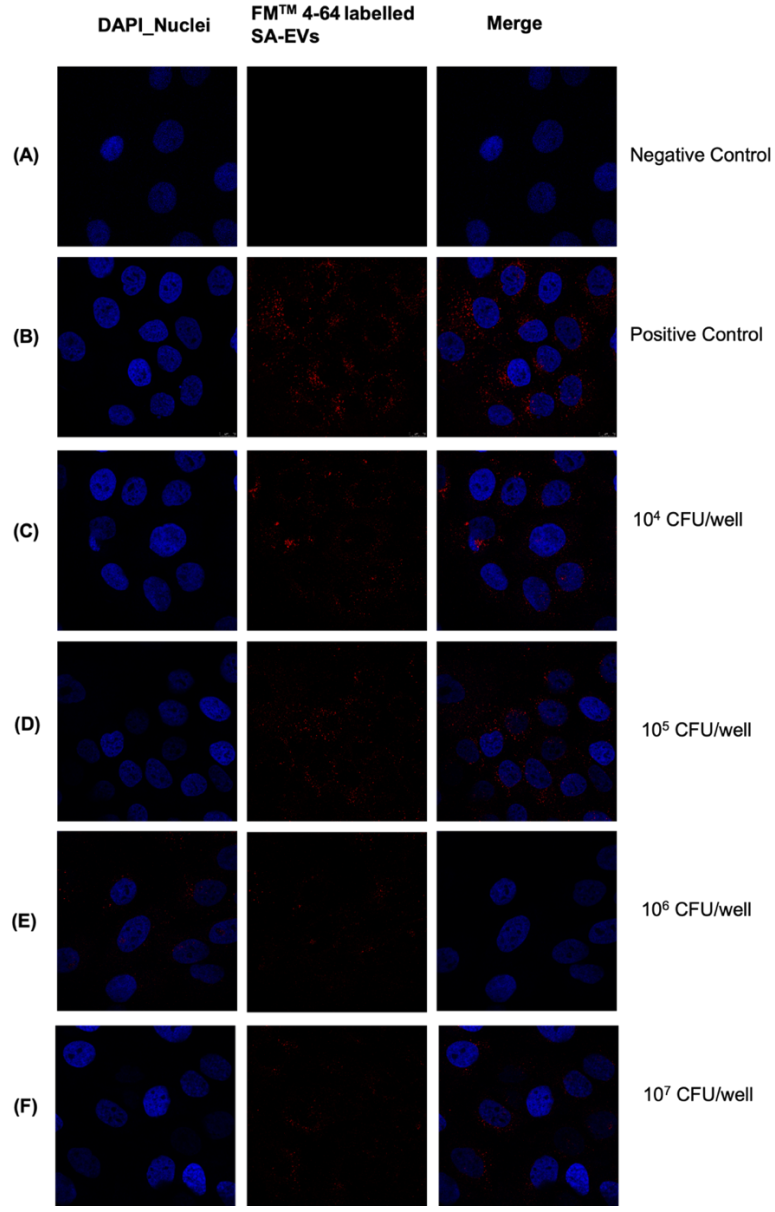

Figure 4.17: Confocal microscopy analysis of the prevention effects of B. longum AC15 on the internalization of SA-EVs on HaCaT cells. Cells pretreated with three dosages (104 CFU/mL, 105 CUF/mL, and 106 CFU/mL) HI B. longum AC15 for 24 hr and then incubated with 15 μg/mL of BL15-EVs dyed with FMTM 4-64. Nuclei was dyed with DAPI. We acquired grayscale images that were artificially colourized, using pseudo-colours, being FMTM 4-64 dye showed in red and DAPI showed in blue.

To investigate how *Bifidobacterium* prevented the inflammation induced by SA-EVs on HaCaT cells, the best anti-inflammatory candidate, *B. longum* AC15, was chosen to do further investigation. HaCaT cells were incubated with three dosages HI *B. longum* AC15 for 24 hr and then added 15 μg/mL FM™4-64 labelled-SA-EVs for 4 hr. As shown in Figure 4.17, the intensity of FM™4-64 was the highest in the positive group (Figure 4.17 B), while it was literally cannot be seen in negative group. As the treatment dosage of HI *B. longum* AC15 increasing from 10^4 to 10^7 CFU/mL, the intensity of FM™ 4-64 decreased (Figure 4.17 C-F). This result indicated that *B. longum* AC15 prevented the internalization of SA-EVs and then further decreased the inflammation of HaCaT cells.

4.5 Significant findings and implications

Based on the correlation between higher abundance of *Bifidobacterium* and lower parental-reported illness incidence in infants, we suspected that *Bifidobacterium* may have positive effects on prevention and attenuation of AD. Six *Bifidobacterium spp*. isolated from breastmilk and human feces were investigated and selected according to their *in vivo* characteristics. The goal of this chapter is to investigate and compare *Bifidobacterium* isolates from different sources in terms of their abilities to survive in the GI tract, adhesion abilities to colon and exclusion of foodborne pathogens, as well as anti-inflammation ability against SA-EVs. Obtaining *Bifidobacterium* via either daily supplements or the micronutrients in human milk, the first challenge is passing through the gastric digestion, where the bacteria are exposed to low pH (3.0 in an empty stomach) and high pepsin concentration in gastric juice. The two stresses have the potential to be bacteriostatic or bactericidal. The second challenge is the natural barrier, the duodenal loop of the small intestine, where the majority of bile salt exposure happens. This could destroy the lipids in the cell membrane, injuring the cell permeability and inhibiting many bacteria. In order to exert beneficial effects on human body, surviving the harsh environment of stomach and GI track is critical for probiotics. In our study, all selected *Bifidobacterium* isolates remain viable under the low pH environment of simulated gastric juice while almost none of them could survive after incubating with 3.0 g/L of bile salt for 3 hr. This observation is consistent with previous findings [89]. Those strains of *Bifidobacterium* who are vulnerable to bile salt probably lack the bile salt hydrolase enzyme, which helps to break down bile salts into free amino acid and bile acid. Some *Bifidobacterium* strains may harbor bile salt hydrolases, which can generate deconjugated bile salts during biotransformation and protect them from the harm of bile salt, thereby surviving in the small intestine [90]. In this study, *B. longum* AC15 and *B. longum* CICC6186 appear to harbor bile salt hydrolase as they could survive the challenge of intestinal juice.

The adhesion and competitive adhesion ability of *Bifidobacterium* spp. against pathogens also is a key aspect in relation with modulation of host immune system and the exclusion of enteric pathogens. For those *Bifidobacterium* isolates which could withstand the harsh conditions in the stomach and intestines would make it to the colon eventually, they may colonize in the

GI tract and protect it from pathogens by competing for the adhesion niches. Aligned with previous findings, the *Bifidobacterium* isolates tested in this study showed variable adhesion ability in a strain-specific manner. Amongst all tested bacteria, two isolates from human milk, namely *B. longum* AC15 and *B. longum* AC16, displayed superior adhesion ability to Caco-2 cells. There are many factors leading to these differences, such as cell surface structure, genetic differences, and receptor specificity, etc [91]. However, the specific reasons responsible for the good adhesion ability of these two isolates remains to be uncovered. Regarding the capability to compete with pathogens, the *Bifidobacterium* isolates showed excellent performance against two typical gram positive and negative pathogens, eliminating the binding of over 50% pathogens on Caco-2 cells. Notably, *B. adolescentis* AC19 and *B. longum* AC20 took the crown from the best competitive bacteria, excluding 71.0% to 60.37% of *S. aureus* ATCC6538 and 74.3% to 66.38% of *E. coli* ATCC8739 that bound to Caco-2 cells, respectively. In the assessment of antimicrobial ability, the *Bifidobacterium* isolates showed great inhibition zone towards two pathogens, *S. aureus* ATCC6538 and *E. coli* ATCC8739, in RCM plates with carbon sources. Besides, they produced comparable amounts of short chain fatty acids, with acetate being the most abundant which ranged between 53.56 to 67.31 mM. Taken together, those results suggested that with the support of glucose and starch, *Bifidobacterium* may generate and secrete high amount of acid during growth, leading to the pH drop dramatically and killed those pathogens [92]. Moreover, in the RCM agar plate without carbon source, the level of inhibition zone of several stains of *Bifidobacterium* against *S. aureus* ATCC6538, such as *B. longum* CICC6186, *B. longum* AC15, was not significantly influenced. These results suggested another possibility that *Bifidobacterium* may form the inhibition zone through a different mechanism. Acid production is considered as major reason for the antimicrobial ability of bacteria, as people neglected the effects of another group of curial compounds called bacteriocin. Tracing back to 1980, scientists had reported bacteriocin, a brunch of diverse ribosomal-synthesized antibacterial peptides associated with *Bifidobacterium,* harbored the ability to suppress the growth of foodborne pathogens [15,93]. As the tested *Bifidobacterium* isolates all showed excellent inhibition ability against both *E. coli* and *S. aureus*, it is highly possible that they can produce bacteriocins such as *B. bifidum*, which is known to harbor a broad activity spectrum towards Gram-positive bacteria such as *Streptococcus*, *Staphylococcus* and *Clostridium*, and Gram-negative ones such as *Salmonella*, *Shigella* and *E. coli* [94].

Another crucial feature of *Bifidobacterium* isolates is the anti-inflammatory ability. In this study, the reporter cell line, RAW-BLUE™ derived from murine RAW 264.7 macrophages, was used to monitor the NF-κB and AP-1 responses upon PRR (pattern recognition receptor) stimulation. Instead of the conventional inflammation inducer LPS, SA-EVs was used to induce inflammation in this study as it highly correlates with many inflammatory diseases, such as atopic dermatitis [95,96]. As shown in our results, SA-EVs activated the macrophages polarization from M0 into M1, which triggered proinflammatory reactions and generated pro-inflammatory cytokines such TNF-α. Pre-treatment with the HI *Bifidobacterium* isolates

effectively inhibited the proliferation of macrophage and supressed inflammatory responses induced by SA-EVs, most likely by preventing p65 phosphorylation and subsequently blocking the activation of the NF-κB signaling pathway.

In summary, the assessment of all selected *Bifidobacterium* isolates in this study reveals that each strain possesses unique characteristics. Amongst all tested isolates, *B. longum* AC15 displayed a relatively good quality, demonstrating a strong SGJ and SIJ tolerance, as well as abilities in adhesion and competitive adhesion towards pathogens on enterocytes, SCFAs production and anti-inflammatory responses. These evidence suggest that *B. longum* AC15 might be a potential candidate in modulating immune responses and potentially serve as a therapeutic strategy to mitigate inflammation associated with various diseases. The current work, which marks a first step in this direction, has demonstrated the significance of utilizing strain-specific features in probiotic selection.

Chapter 5 Challenge standard model induced via DNCB with SA-EVs

5.1 Introduction

AD is one of the most prevalent inflammatory skin disorders of recent decades, affecting up to 10% adults and 15-30% children [97]. It is clinically characterized as pruritus, erythema, swelling, dryness, and fissures. Besides, histological findings reveal spongiosis and infiltration of inflammatory cells residing in the epidermis and dermis layers of patients' skin [98]. Normally, the high-risk patients of AD are infants within the first six months of life are at highest risk for AD, accounting for 45% of all cases [99]. It has been reported that about 1 in 2 children may develop secondary allergic reactions such as allergic rhinitis, asthma, and food allergies in the future. Persistent AD exacerbations not only reduce the quality of life, leading to depression, anxiety and even suicide, but also affect the economy as people seek regular medical attention and prevent them from working.

The pathophysiology of AD is complex and multifactorial. The variability in influencing factors contributes to the diversity of AD phenotypes and endotypes, which remain challenging to fully characterize. Genetic disorders, deficient epidermal barriers, altered immune system, and environmental exposure are all acknowledged to significantly influence the development of AD [100]. In addition, dysbiosis of skin microbiome represents another vital factor in the pathogenesis of AD. Frequent colonization of *S. aureus* is particularly significant since it is strongly correlated with the severity of the disease and could be found on the skin of over 70% of AD patients with skin lesions [101,102]. This bacterium promotes and aggravates AD symptoms through secreting numerous virulence factors, such as toxins, enzymes, and other proteins that cause skin barrier dysfunction. During the growth, *S. aureus* secretes those pathogenic molecules in the form of EVs which process nanoscale bilayer lipid vesicle structures. This structure shields them from the attack of antimicrobial fatty acids produced by the host and evades the activation of innate immune response [103]. Taken advantages of their special structure and small size (20-100nm), those nanocarriers efficiently facilitate communication between host and bacteria. AD-associated pathogenic factors, such as cysteine and α-hemolysin, can be easily transported to the host and further trigger severe inflammatory reactions on the skin [104,105]. Those superantigens also trigger acute toxin shock by binding to MHC class II molecules on antigen presenting cells (APC) and stimulating the activation of large population of T cells [106]. When they persist, these secreted virulence factors enhance bacterial survival through host invasion and evasion mechanisms. In response, epithelial cells can release damage-associated molecular patterns (DAMPs) or alarmins, such as TSLP, IL-25, IL-33, and chemokines to recruit innate and adaptive immune cells to cause inflammation [107]. These findings imply that SA-EVs is a potent initiator for the establishment of AD model.

However, contradicted to the real scenario, most of AD animal models used in the research fields were established by employing a synthetic chemical substance named 2,4-dinitrochlorobenzene (DNCB) rather than the pathogenetic factors diagnosed in clinical cases [108–110]. It induces AD-like symptoms through a combination of skin barrier disruption, immune

dysregulation, and inflammation signaling pathways. After application, DNCB binds to extracellular and intracellular proteins in the skin and forms hapten-protein complexes [111]. Those complexes are recognized as immunogens by local antigen-presenting cells (APCs), such as skin Langerhans cells, dermal dendritic cells and macrophages, processed and presented to T cells for activation, leading to the differentiation of Th2 cells and memory T cells. Besides, it disrupts keratinocyte differentiation, leading to thickening of the stratum corneum and compromising skin barrier integrity [112]. Moreover, it triggers the phosphorylation of MAPK/NF-KB signaling pathways, driving the release of several pro-inflammatory cytokines and chemokines [109,113]. In scientific studies, inducing AD-like skin with DNCB is known as a standard method as it has short experiment period and easily creates many disease characteristics linked to AD, such as high level of serum IgE and inflammatory status in skin [114].

However, many reports reported difficulties in the reproducibility of AD model by DNCB. Besides, it is unclear whether those presented phenotypes induced by DNCB shared similar pathways as the formation of AD in the real-world. The differences between research methods and real-world pathogenic factors raises the question whether medications showed promising results in research will also function well in actual situations. Therefore, establishment of a disease model based on actual pathogenic factors is desperately needed to support further investigation and validation of the effectiveness of prospective treatments for AD.

Although there are several studies mentioned and studied, a comprehensive comparison remains lacking in varies aspects between these two disease models, including phenotype, skin microbiome composition, differential gene and protein expression of skin and the underlying pathogenetic pathways [105,115]. This study aims to fill the research gap by employing the toxin complex secreted from *S. aureus* ATCC6538 (SA-EVs), one of the clinically identified factors, for the establishment of AD-like skin model.

5.2 Establishment of AD model via SA-EVs

5.2.1 Dosage optimization of SA-EVs-induced AD disease model

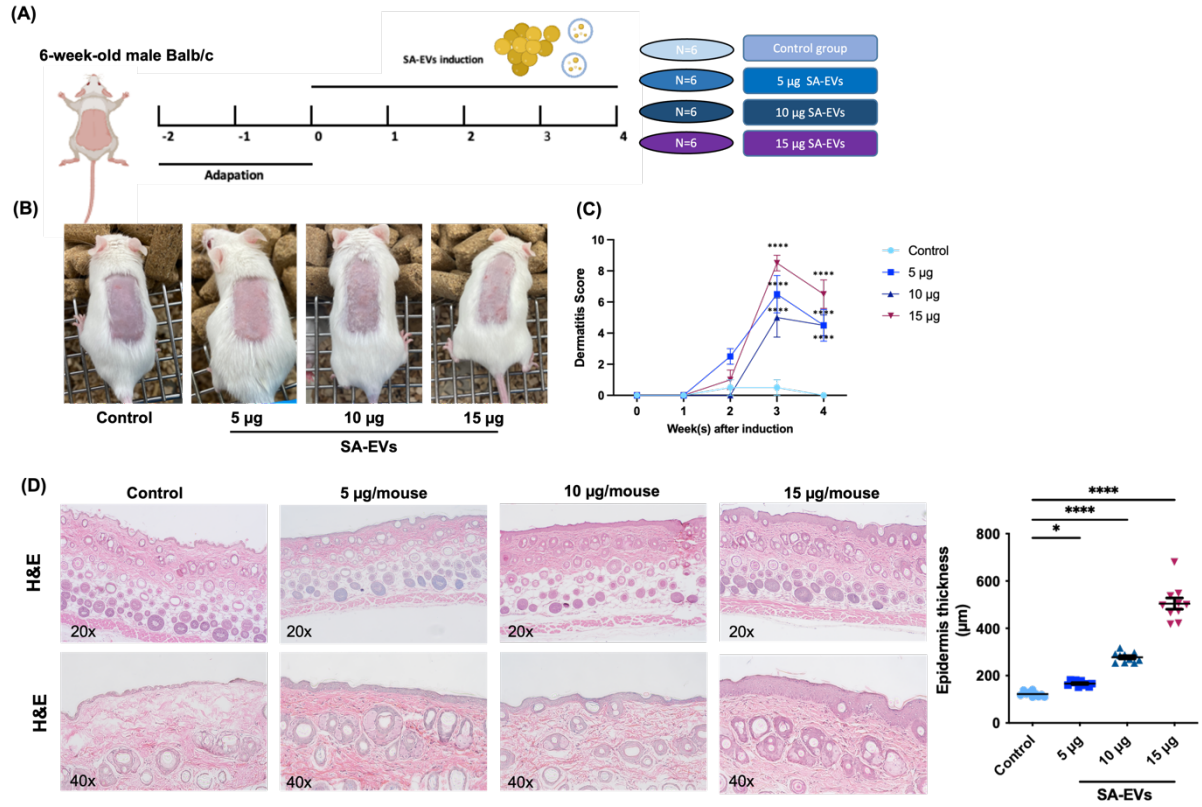

*Figure 5.1: Phenotype of SA-EVs-induced AD mice. The in vivo effects of three dosages (5 μg, 10 μg, and 15 μg) of SA-EVs on the development of AD-like skin animal model. Experiment design of AD disease model establishment (A). Images of phenotype (B). Dermatitis score of AD (C). The dermatitis score of all groups was compared to control group. Histology analysis of epidermal thickness, magnification 200x and 400x (D). Data was shown in AVE ± SEM. All compared to control group. Statistically analysis was used One-way ANOVA in Prism 9, *p<0.05, **p<0.01, ***p<0.005, ****p<0.001.*

To assess the effects of SA-EVs on the establishment the AD-like symptoms on Balb/c mice, three dosages of EVs generated from AD disease pathogenesis, *S. aureus*, were used as the induction. According to observation data shown in Figure 5.1C, after treated with SA-EVs for 2 weeks, some reddish spots started to appear on the back of Balb/c mice in the two high-dosage groups (10 μg and 15 μg), although the statistical analysis showed no difference between them and control group. In week 3, the distinction between disease and control groups started to show, even the lowest dosage could cause remarkable AD-like symptoms. However, in the following extension week, the AD dermatitis score dropped to a relatively lower level than Week 3 but remained at a relatively higher level than the control group.

The epidermis thickness was visualized by H&E staining. After SA-EVs induction, there was a dose-dependent increasement in the thickness of the mouse epidermis. As shown in Figure

5.1D, the epidermis thickness was slightly but significantly increased by 5 μg of SA-EVs, and this symptom was further aggravated in higher dosage groups, indicating SA-EVs successfully influenced the epidermis thickness and created the AD-like skin on Balb/c mice.

5.2.2 Determination of allergic response level in serum

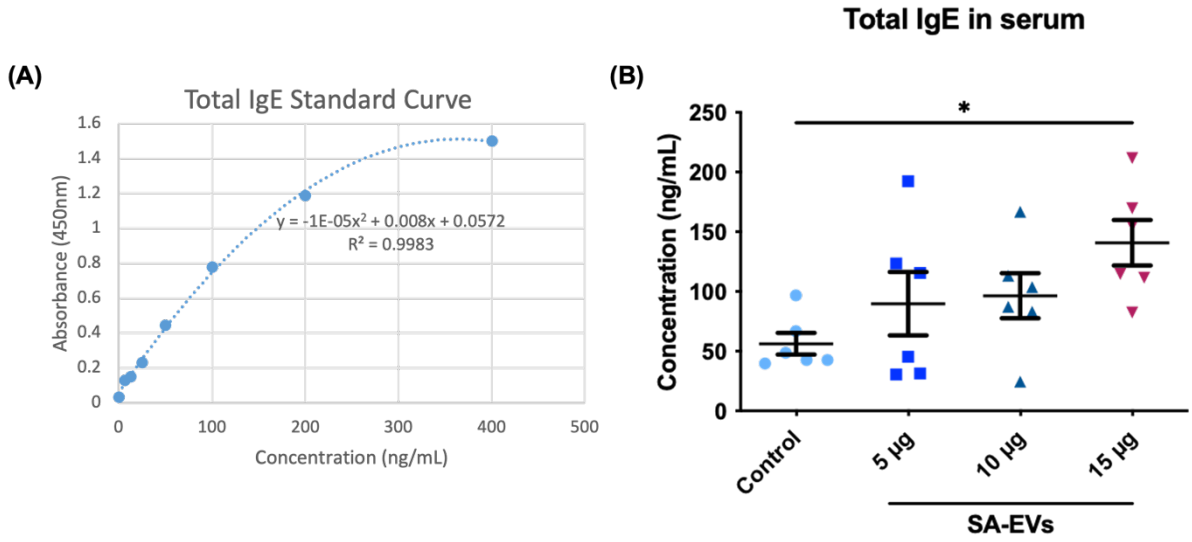

*Figure 5.2: Determination of total IgE in serum. Serum samples were prepared from Balb/c mice blood for total IgE analysis by ELISA. The standard curve of total IgE (A). The level of total IgE in serum (B). All groups were compared to control group. Statistically analysis was used One-way ANOVA in Prism 9, *p<0.05, **p<0.01, ***p<0.005, ****p<0.001.*

Total IgE is one of the typical markers for allergic reactions. In our experiment, the level of IgE in mouse serum was increased by SA-EVs in a dose-dependent manner, while only the dosage of 15 μg statistically significant increased it. This may owe to the big individual differences presented in the two relevantly lower dosage groups. Taken together, only 15 μg of SA-EVs successfully significant triggered the allergic reaction in Balb/c mice.

5.2.3 T cells proliferation in spleen

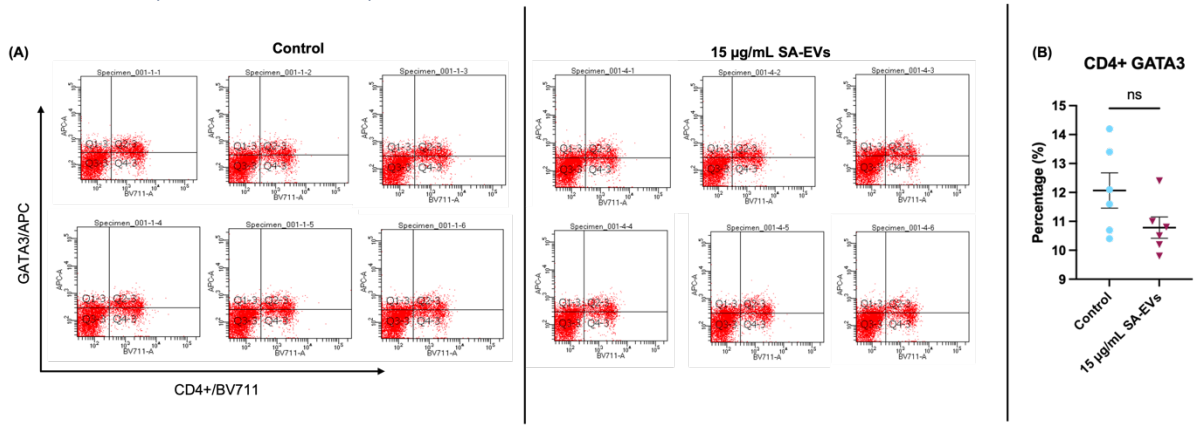

*Figure 5.3: Analysis of T cells proliferation in spleen. Identification of Th2 proliferation after 15 μg/mL SA-EVs induction. Flow cytometry assay were performed on CD4+ cells population isolated from spleen (A). Statical analysis of Th2 population in spleen (B). CD4+ were labeled with APC. GATA3 were labeled with BV711. Statistical analysis was done by Student T-test. *Compared with control. Statistical significance is indicated as follows: *p<0.05, **p<0.01, ***p<0.005 and ****p<0.0001.*

To investigate the effects of SA-EVs on Th2 proliferation, the population of CD4+ GATA3+ cells from the spleens of mice was evaluated via flow cytometry. Data in Figure 5.3 presented that the percentage of CD4+GATA3+ cells decreased from an average of 12% to less than 11% after induction with 15 μg/mL of SA-EVs. However, statistical analysis showed that there was no significant difference between the control group and the disease group, indicating Th2 may not be the major factor leading to the AD development via SA-EVs. These results suggested a future direction for our study: the impact of SA-EVs may impact the immune system through rising the proliferation of other CD4+ T cells, such as Treg, Th1, and Th17, rather than the often-reported Th2.

5.2.4 Quantification of inflammatory cytokines, chemokines, and T cell proliferation markers

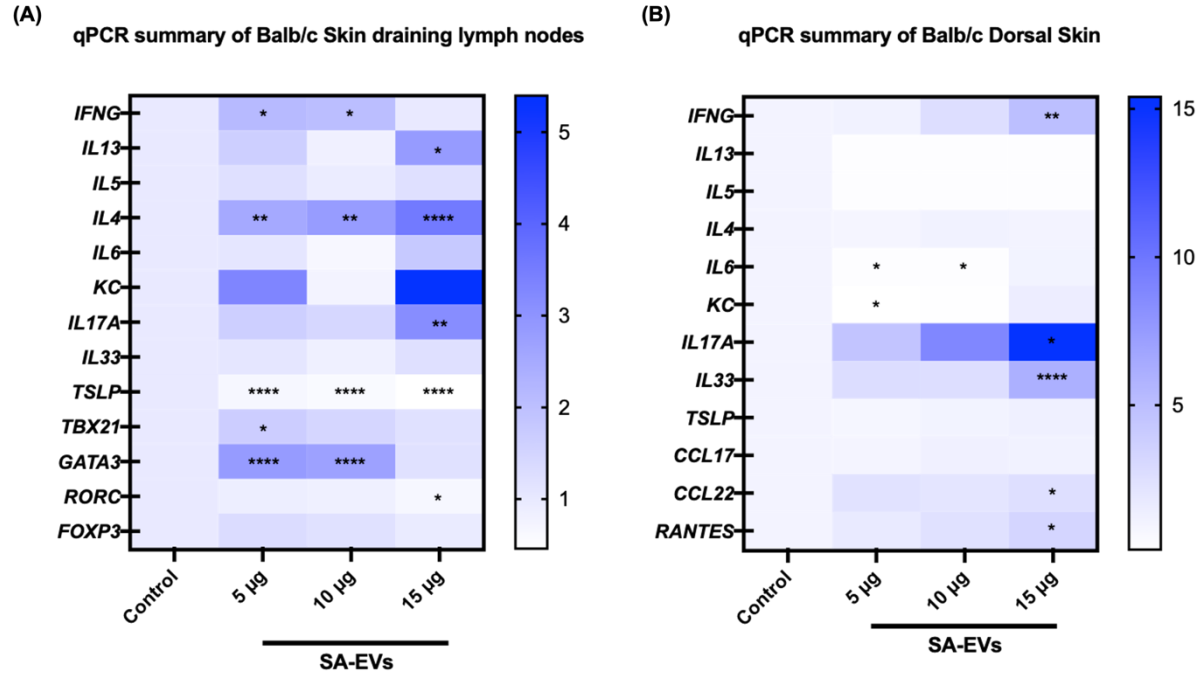

*Figure 5.4 Analysis of the expression of proinflammatory cytokines in skin draining lymph nodes and dorsal skin of mice.Four weeks exposure of tape-stripped mouse skin to SA-EVs induced a mix Th1/Th2/Th17-type inflammatory response in skin (A) and SDLN (B). All induction groups were compared to control group. Statistically analysis was used One-way ANOVA in Prism 9, *p<0.05, **p<0.01, ***p<0.005, ****p<0.001.*

Apart from the phenotypes of AD, the cytokine and chemokine markers related to AD in skin and skin draining lymph nodes were also quantified by RT-qPCR. The inflammatory profiles in SDLNs between the highest dosage group and two lower groups were quite different. Cytokines related to Th1 (*IFNG* or *Treg*) and Th2 (*IL4*) were increased remarkably in 5 μg and 10 μg groups, while the one Th17-related (*IL17A*) and Th2 (*IL13*) were only significantly changed in the highest group. The situation was similar in the dorsal skin. In the tested targets, there were not many changes in two lower-dosage groups, while only the highest groups showed significant increasement, such as *IFNG*, *IL17A*, *CCL22* and *RANTES* (*CCL5*). This result indicated that different dosages of SA-EVs trigger different immune responses in mice. Infection with relatively lower dosages of SA-EVs triggered the Th1- and Th2- dominated immune response, while highest dosage of SA-EVs triggered Th2- and Th17- dominated immune responses.

5. 3 Comparison AD disease models induced by SA-EVs and DNCB

5.3.1 AD phenotype comparison

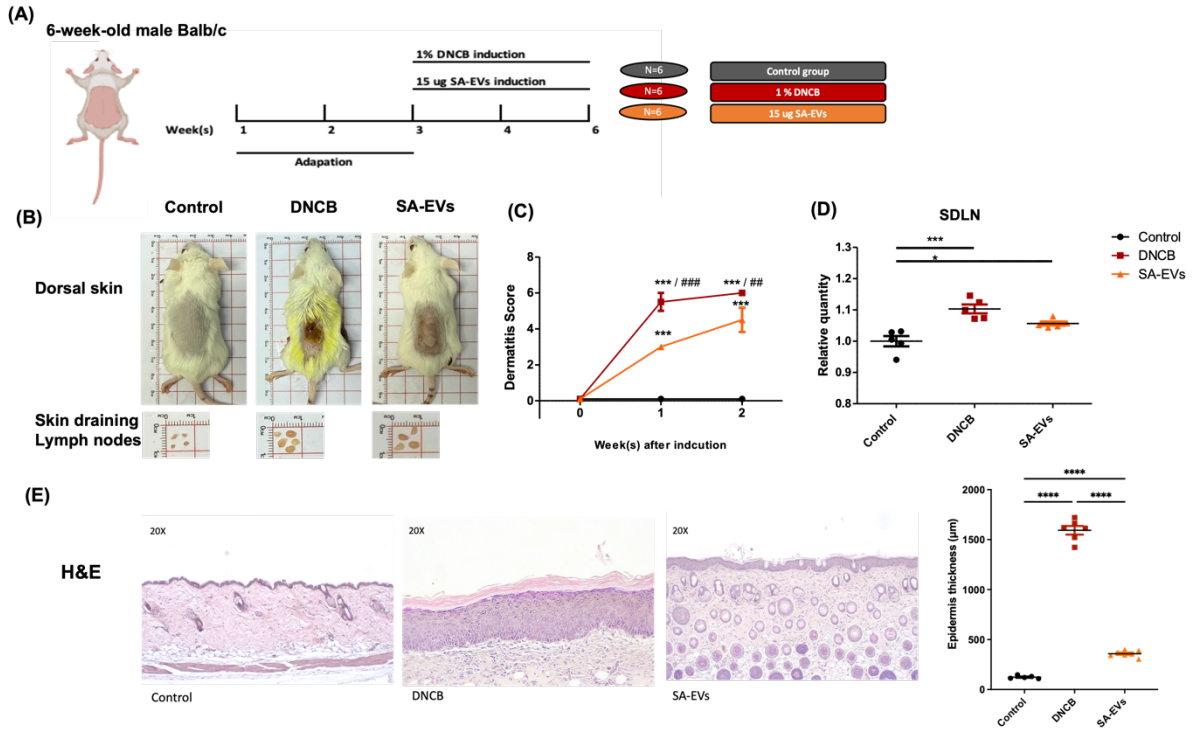

*Figure 5.5 Comparison of phenotypes of DNCB- and SA-EVs-induced Atopic dermatitis (AD). Experiment design of AD disease model establishment (A). Phenotype of AD after induction with 1% DNCB and 15 μg of SA-EVs (B). Dermatitis score of AD (C). Relative quantity of SDLN measures by ImageJ (D). DNCB and SA-EVs groups were compared to AD group. Effects of DNCB and SA-EVs on Balb/c mice dorsal skin. Magnification, ×200 (E). Data was shown in AVE±SEM. Statistical analysis was done by Two-way ANOVA or One-way ANOVA; *compared with control, #compared with DNCB. */#p<0.05, **/##p<0.01, ***/### p<0.005, and ****/#### p<0.0001.*

To evaluate the efficiency of AD-like symptoms developed by SA-EVs, DNCB, a golden method for AD-like skin model establishment, was included as a positive control in the following experiment. After adaptation for two weeks, 15 μg of SA-EVs and 1% of DNCB were applied on the shaved dorsal skin of mice for another 2 weeks. According to Figure 5.5B and Figure 5.5C, both inducers created AD-like symptoms on mice within two weeks, however the DNCB group formed a considerably more severe reddishness than SA-EVs and only this group's mice had a thick scar on the back. Additionally, two disease groups had dramatically larger SDLNs than the control group determined by ImageJ, indicating the extensive immune cell infiltration. Same as the phenotype, H&E staining results clearly demonstrated the thickness of the skin. The epidermis level of both disease groups was noticeably thicker than that of the control group, and the level in the DNCB group was even higher than those of the SA-EVs group.

5.3.2 Determination of total IgE level in serum by ELISA

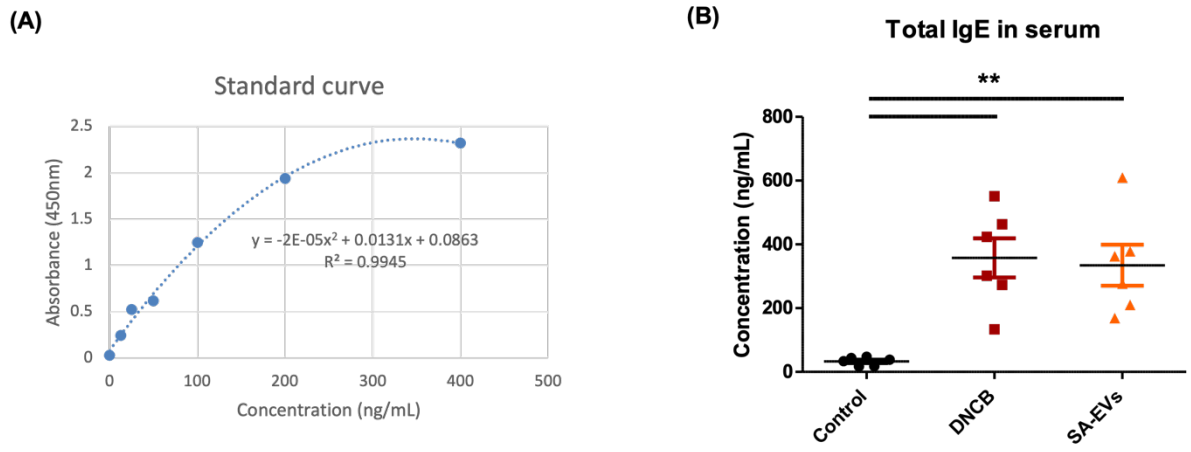

*Figure 5.6 Determination of total IgE in serum. Serum samples were prepared from Balb/c mice blood for total IgE analysis by ELISA. The standard curve of total IgE (A). The level of total IgE in serum (B). Data was shown in AVE±SEM. Statistical analysis was done by Two-way ANOVA or One-way ANOVA; *compared with control, #compared with DNCB. */#p<0.05, **/##p<0.01, ***/### p<0.005, and ****/#### p<0.0001.*

In the allergic reaction aspect, the total IgE was determined by ELISA. Although the levels in the two illness groups were comparable, they were both noticeably greater than those in the control group. According to the level of the allergy marker shown in Figure 5.6B, application 15 µg of SA-EVs topically for two weeks was effective in causing a hypersensitive reaction throughout the body, and its efficacy was comparable to that of the chemical 1% DNCB.

5.3.3 T cells proliferation profiles in skin draining lymph nodes

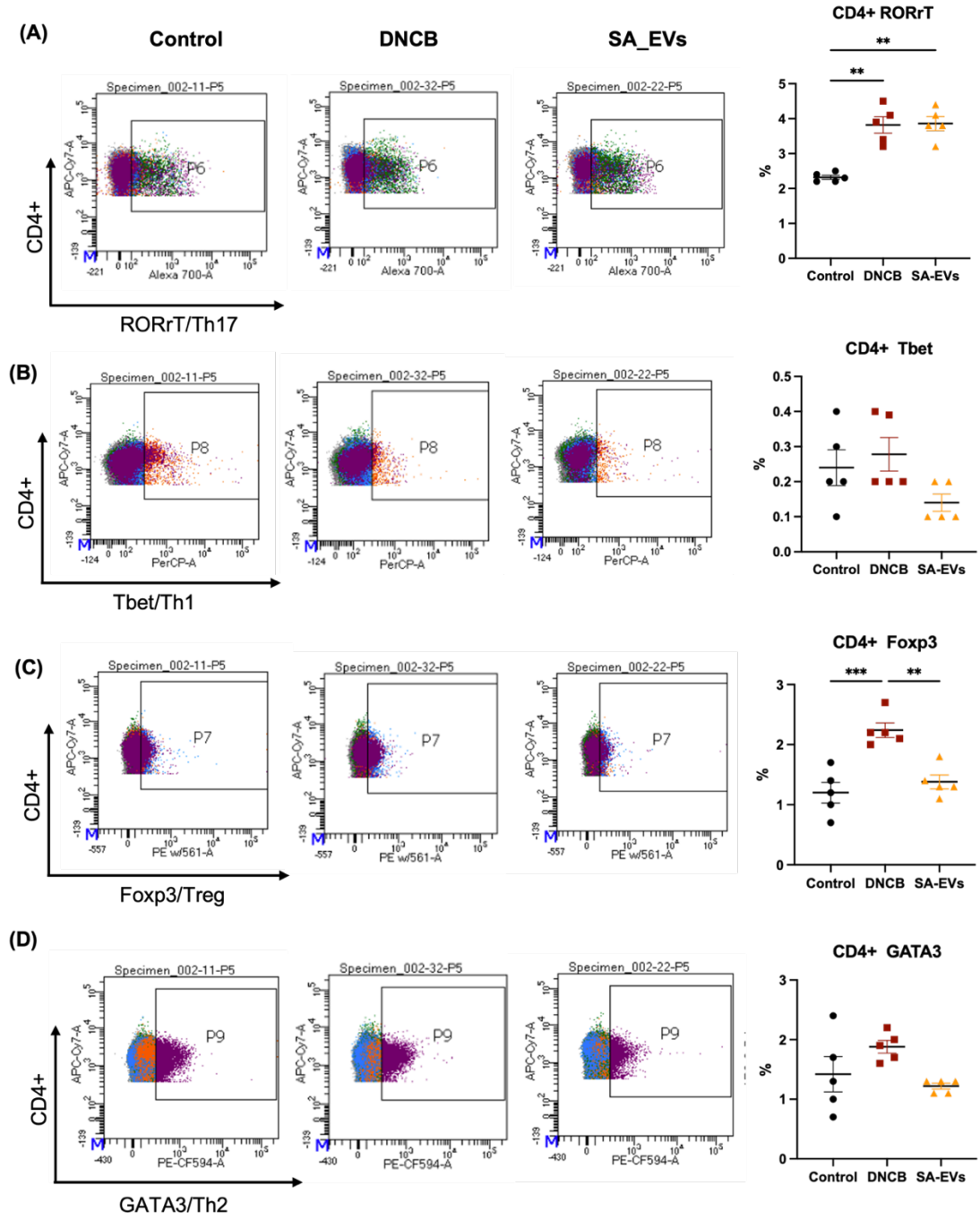

*Figure 5.7 Identification of Th1/Th2/Th17 and Treg in atopic dermatitis with flow cytometry. Flow cytometry assay were performed on CD4+ cells population isolated from skin draining lymph nodes. CD4+ were labeled with APC. RORγT were labeled with Alexa 700 (A). Tet were labeled with PerCP (B). FoxP3 were label with PE (C). GATA3 were labeled with PE-CF594 (D). Data was shown in AVE±SEM. Statistical analysis was done by Two-way ANOVA or One-way ANOVA; *compared with control, #compared with DNCB. */#p<0.05, **/##p<0.01, ***/### p<0.005, and ****/##### p<0.0001.*

The gating strategy for Treg/ Th1/Th2/Th17 was shown in Supplementary Figure 1. The frequency of these cells was evaluated after stimulation of SA-EVs and DNCB. As shown in Figure 5.7A and 5.7C, the frequency of $CD4^+RORγT^+$ was significantly increased in two disease groups when compared with the control group, while the frequency of $CD4^+Foxp3^+$ was only remarkably increased in the DNCB group. Moreover, no changes in the frequencies of $CD4^+Tbet^+$ and $CD4^+GATA3^+$ were observed under SA-EVs and DNCB stimulation as presented in Figure 5.7B and 5.7D. In our investigation, neither of the AD inducers significantly affected Th2 proliferation, despite many studies found that the occurrence of AD was strongly associated with Th2. On the contrary, in our case, two inducers had great impacts on the proliferation of Th17, which indicated that SA-EVs and DNCB may share similar pathogenetic effects of AD by affecting the differentiation of Th17.

5.3.4 Different expression of AD-related genes in dorsal skin of AD mouse

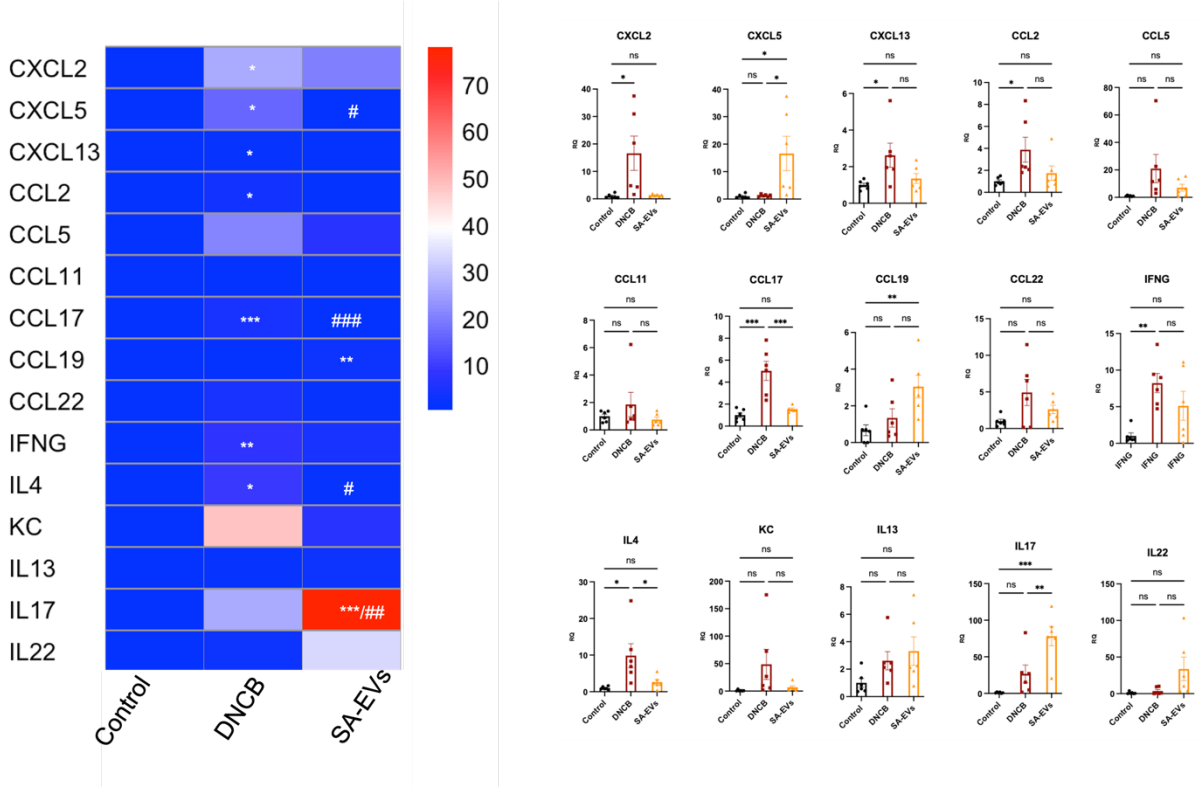

*Figure 5.8 Evaluation of key markers of AD in the dorsal skin of mice. All groups were compared with *control group and # DNCB group. Data was shown in AVE±SEM. Statistical analysis was done by One-way ANOVA; * p<0.05, ** p<0.01, *** p<0.005, and **** p<0.0001.*

RT-qPCR was used to assess the expression of AD-related chemokines and cytokines, and the results were reported in the heatmap on the left side of Figure 5.8. In general, two inducers

both have great impacts but through different chemokines to traffic neutrophil. As shown in Figure 5.8, the expressions of *CXCL2* and *CXCL5* were significantly increased in DNCB and SA-EVs groups, respectively. Both chemokines could attract the collection of neutrophils to the dorsal skin and cause inflammatory responses. Besides, there was an abnormal increasement of *CCL17 and CCL19* in DNCB and SA-EVs groups, respectively, which attracted T cells or DC cells to the skin and activated immune responses.

Apart from the chemokines, the cytokines overexpression profiles were also different in two disease groups. DNCB group had significant higher amounts of *IL4* and *IFNG* than the control group, while SA-EVs group had considerably higher amount of *IL17* than the control and DNCB groups. This finding suggested that the two inducers affected distinct cells in the skin, resulting in inflammatory reactions.

5.3.5 Comparison Skin microbiome composition between two AD models by 16S sequencing

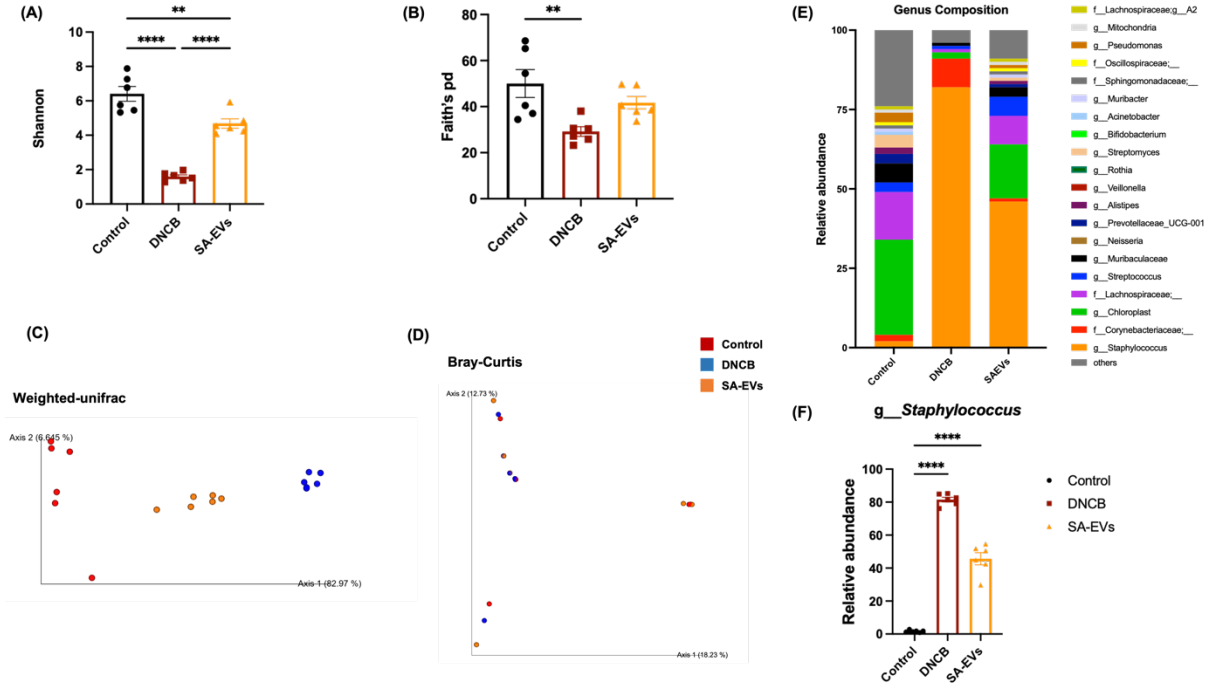

*Figure 5.9 Comparison of Alpha diversity and Beta diversity of skin microbiota in three groups, Control, DNCB, and SA-EVs. Shannon diversity index (A). Faith's phylogenetic diversity (B). Weighted UniFrac (C). Bray-Curtis (D). Taxonomy Comparison of the skin microbiota at genus level (E). Relative abundance of Staphylococcus (F). Data was shown in AVE±SEM. Statistical analysis was done by One-way ANOVA; * p<0.05, ** p<0.01, *** p<0.005, and **** p<0.0001.*

Figure 5.9A and 5.9B showed alpha diversity of skin microbiome of three groups, measured by Shannon and Faith's pd. After induction with DNCB and SA-EVs, Shannon index of two disease groups dropped remarkably and DNCB had the lowest number among three groups,

indicating both inducers significantly reduced the richness and evenness of skin microbiome species, especially by DNCB. For the Faith's phylogenetic diversity measurement, the biodiversity of skin microbiome only significantly decreased in DNCB group but not SA-EVs compared to the control group. Regarding beta-diversity assessed through weighted UniFrac in Figure 5.9C, three groups exhibited distinct separation and were categorized into separate clusters, indicating that the phylogenetic diversity of the skin microbiome among them was significantly different from one another, while the abundance of skin microbiomes that shared among three groups were similar as the Bray-Curtis was clustered together as shown in Figure 5.9D. The relative abundance of skin microbiome was analysed at genus level, as illustrated in Figure 5.9E and 5.9F. The composition of skin microbiomes changed remarkably after induction of DNCB and SA-EVs compared to the control group. The most significant one is *Staphylococcus*. As one of the key factors leading to AD development, it increased dramatically and then became the major skin microbiome in two disease groups, with the proportion rising from 1.71% to 81.52% and 45.66%, respectively.

5.3.6 Transcriptome and proteome profiling reveal signatures genes, proteins and pathways in the dorsal skin of two disease models.

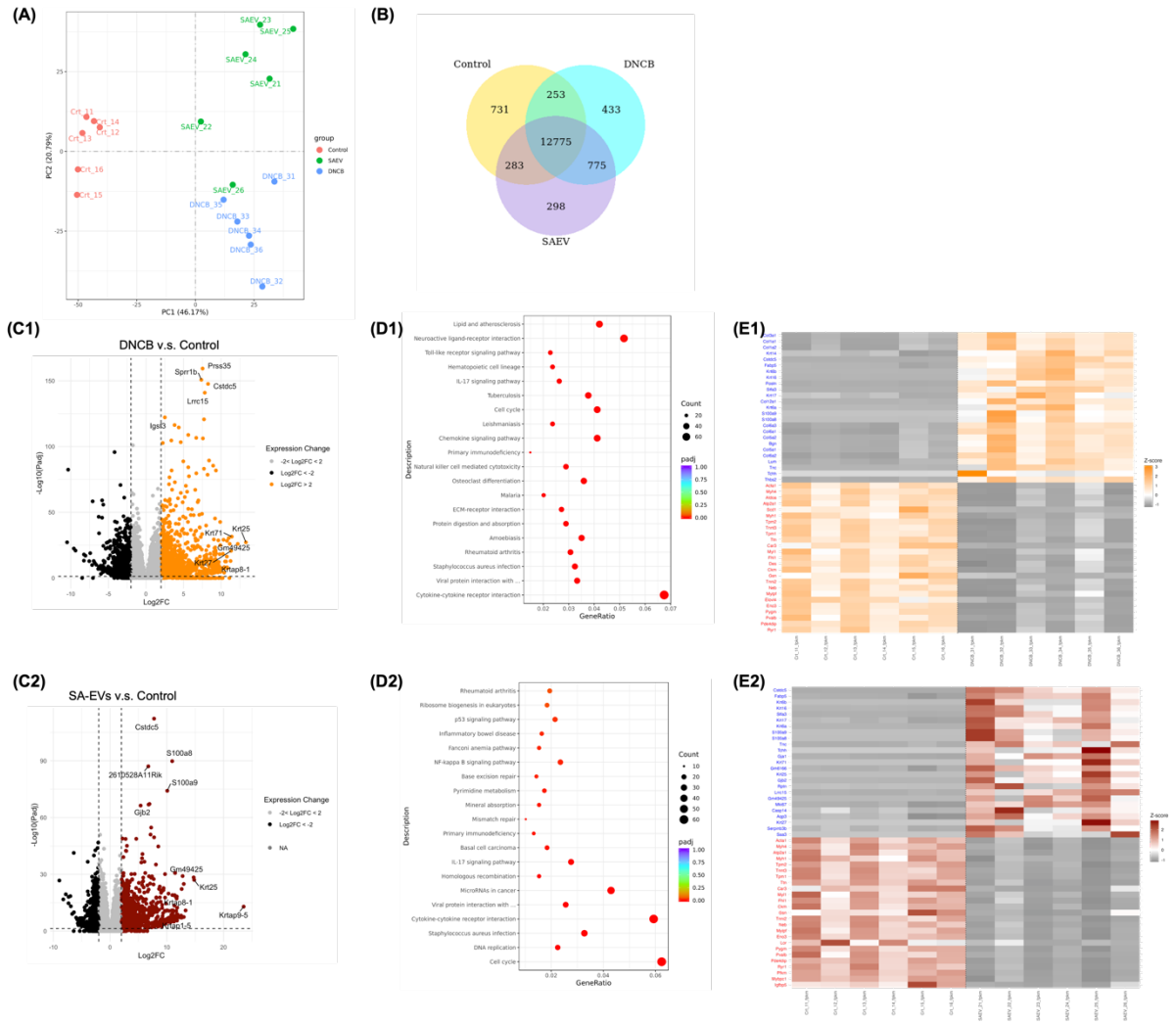

Figure 5.10 Comparison of impacts of DNCB and SA-EVs on mice dorsal skin at gene level. RNAseq analysis was performed using dorsal skin of Balb/c mice (n=6). PCA based on the FPKM value of all detected genes (A). Venn diagram depicting the shared or unique genes numbers in Control, DNCB and SA-EVs groups (B). Volcano plot presenting all DEGs in the DNCB v.s. Control, and SA-EVs v.s. Control comparison groups. Absolute Log2FC >2 and Padj <0.05. Orange indicated unregulated genes in DNCB (C1) and red indicated upregulated genes in SA-EVs (C2) compared to controls indicated in Black. Dot plot of KEGG pathway enrichment analysis. The color of the dots represents the Padj; the size of the dots represents the number of DEGs in the pathway. Top 20 significant pathways in DNCB v.s. Control (D1) and SA-EVs v.s. Control (D2) were presented. Heatmap showing the top 50 genes with absolute Log2FC >2 and Padj <0.01 in the DNCB v.s. Control (E1), and SA-EVs v.s. Control (E2) comparison groups.

To gain a comprehensive understanding of the differential expression genes between SA-EVs v.s. Control and DNCB v.s. Control comparison groups, transcriptome sequencing analysis were performed. In Figure 5.10A, principal component analysis (PCoA) was conducted to

visualize variation of genes in three groups with PC1 accounted for 20.79% and PC2 accounted for 46.17%. Samples from each group clustered together to form three separate clusters, proving that the gene expression among them varied greatly from one another.

As shown in the volcano plots of Figure 5.10C1 and 5.10C2, upregulated genes with absolute Log2FC over 2 and Padj <0.01 were highlighted in orange or red in the comparison of DNCB or SA-EVs over control group. The most significant genes identified in the comparisons between the DNCB v.s. control group, as well as the SA-EVs v.s. control group, were notably different. The only gene they shared was *Cstdc5*. In the DNCB group, *Prss35*, *Sprr1b*, and *Lrrc15* were the top three significant genes, whereas *S100a8*, *S100a9*, and *2610528A11Rik* were the most noteworthy genes in SA-EVs group. The comparative analysis of the DNCB and SA-EVs groups reveals a fascinating landscape of genetic diversity, underscoring the unique biological pathways influenced by each condition. These distinct gene signatures highlighted their divergent mechanisms.

Apart from gene expression comparison, the top 20 most significantly influenced pathways of each disease group were also listed and presented in KEGG dot plots as shown in Figure 5.10D1 and 5.10D2. The influenced pathways between two disease models were analogous and distinct. Two inducers of AD impacted several overlapping pathways, including the IL-17 signaling pathway, rheumatoid arthritis, *Staphylococcus aureus* infection, primary immunodeficiency, and cytokine-cytokine receptor interactions, while most of the significantly affected signaling pathways were distinct from one another. For instance, three pathways related to parasites in the DNCB group, leishmaniasis, malaria, and amoebiasis, were barely seen in the SA-EVs group. On the contrary, typical inflammatory-related pathways, including the P53 signaling pathway, inflammatory bowel disease, the NF-Kappa B signaling pathway, and homologous recombination, were only presented in the SA-EVs group. Those results indicated AD development by DNCB and SA-EVs through several shared pathways while most of the influenced pathways were distinct. This exploration not only enhances our comprehension of these two groups but also opens avenues for future research aimed at unravelling the complexities of their respective roles in disease processes.

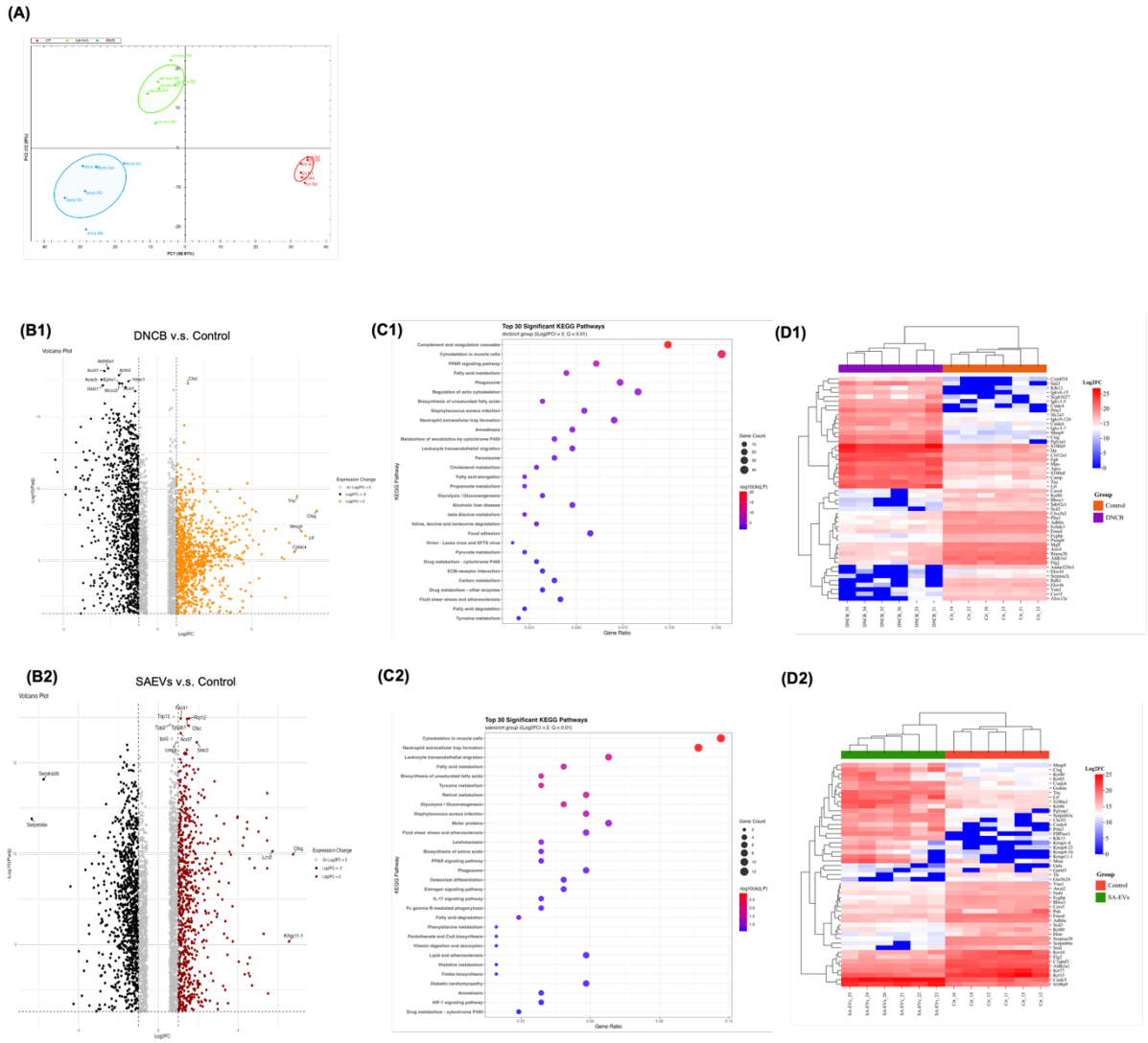

Figure 5.11 Comparison of impacts of DNCB and SA-EVs on mice dorsal skin at protein level. Proteomics analysis the differential protein expression in dorsal skin of Balb/c mice. PcoA analysis of DNCB, SA-EVs and control groups (A). Volcano plot with significantly differentially expressed protein |Log2FC| >2 and Padj <0.05 in skin highlighted in orange (unregulated genes in DNCB) (B1) and red (upregulated genes in SA-EVs) (B2) compared to controls. Dot plot of KEGG pathway enrichment analysis. The color of the dots represents the Padj; the size of the dots represents the number of proteins in the pathway. Top 30 significant pathways in DNCB v.s. Control (C1) and SA-EVs v.s. Control (C2) were presented. Heatmap showing the top 50 genes with absolute Log2Fold Change >2 and Padj <0.01 between DCNB v.s. Control (D1), and SA-EVs v.s. Control (D2) comparison groups.

In addition to the gene expression analysis, another omics approach was conducted to examine and compare the differential protein expression and pathways impacted by DNCB and SA-EVs at the protein level. The results of the PCA analysis were comparable to that of

transcriptomics. Similarly, three groups formed distinct groups, suggesting that their dorsal skin profile at protein-level was also unique. In Figure 5.11B1 and 5.11B2, volcano plots of two comparison groups were depicted with proteins with absolute Log2FC > 0.585, Padj < 0.05. Top 10 proteins with lowest Padj value and biggest absolute Log2FC among all proteins were pointed out. In the DNCB v.s. Control comparison group, Ctsc was the only standout upregulated protein in the top 10 proteins, wherever SA-EVs v.s. Control comparison group had 5 distinct upregulated proteins, including Tpsab1, Fscn1, Rrp12, Acot7 and Smc2. In the pathway analysis, proteins with absolute Log2FC > 2, Padj < 0.01 were recruited for pathway analysis. Top 30 most significant pathways of two comparison groups were listed as shown in Figure 5.11C1 and 5.11C2. 17 out of 30 different signaling pathways were present at the protein level in those two disease models, suggesting that the fundamental mechanisms causing AD disease progression were highly distinct.

To further narrow down the signaling pathway scope, the results of transcriptome and proteome were combined for further investigation. In the comparison group of DNCB v.s. Control, there were only two overlapped signaling pathways of transcriptome and proteome, which were Amoebiasis and *Staphylococcus aureus* infection. On the contrary, in the SA-EVs v.s. Control group, they were IL-17 signaling pathway and *Staphylococcus aureus* infection.

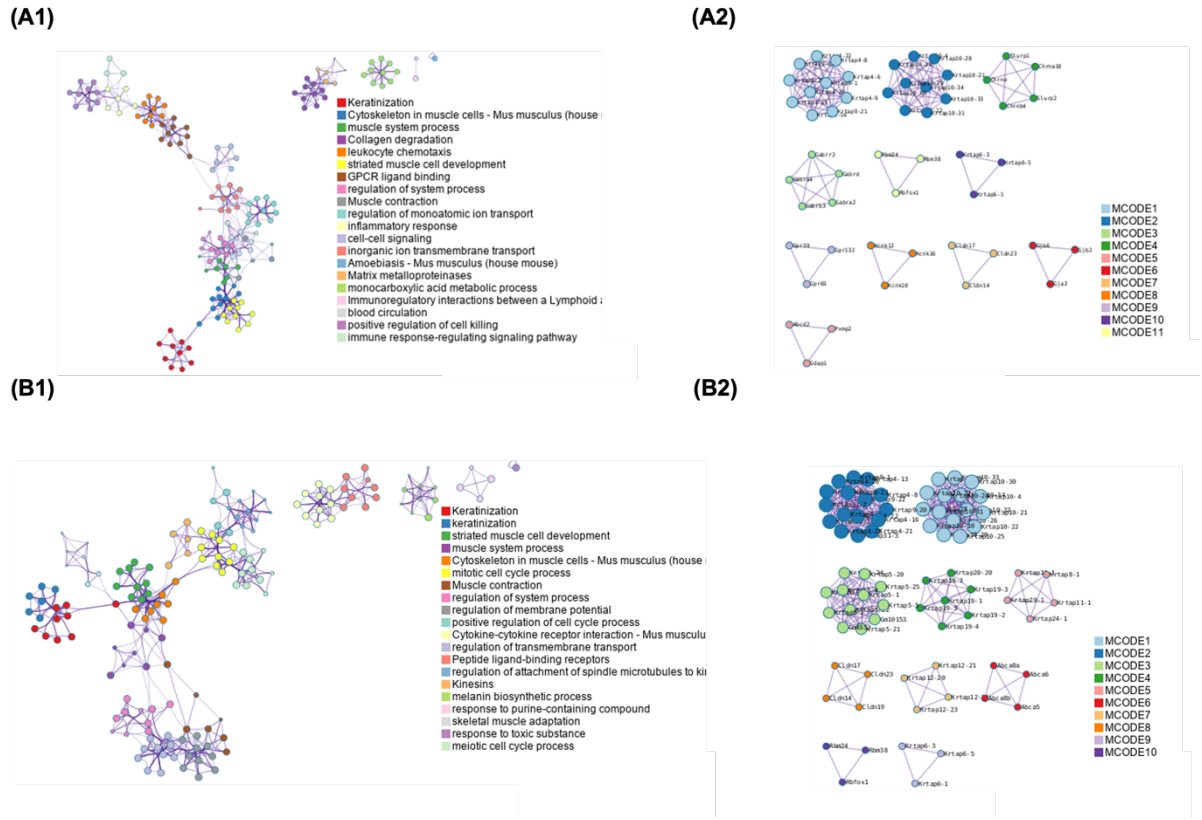

Figure 5.12 STRING protein-protein interaction (PPI) Netwrok analysis of the identified differential proteins expressed in the dorsal skin of mice. DNCB v.s. Control (A), SA-EVs v.s. Control (B).

Figure 5.12A illustrates that most of the differential proteins between the control and DNCB groups were categorized into keratinization, the gamma-aminobutyric acid (GABA) signaling pathway, and neuroactive ligand-receptor (NLR) interactions. The chemical DNCB impaired the GABA signaling in the skin, which can lead to hyperexcitability of sensory nerves, make the skin overly sensitive, finally lead to chronic itch and pain [116].

While major differential proteins between the control and SA-EVs groups were keratinization, ABC transporters, and calcium-independent cell-cell adhesion mediated by plasma membrane cell-adhesion molecules as shown in Figure 5.12B, the metabolites SA-EVs compromising the skin's physical barrier integrity through the dysregulation of critical lipid transport systems [117]. This is a fundamental mechanism in AD pathogenesis, which is distinct from the nerve-focused pathway activated by DNCB.

5.4 Significant findings and implications

EVs have long been recognized as a promising biological drug delivery vehicle and have been extensively investigated for decades, while bacterial EVs released by both Gram-positive and Gram-negative bacteria just started to capture scientific attention in recent years. In this study, EVs derived from *S. aureus* ATCC6538 were successfully extracted and applied as an inducer of AD disease in both *in vivo* and *in vitro* experiments. Taking advantage of the unique lipid bilayer structure (Figure 4.2A), SA-EVs delivered a variety of active pathogenic compounds, such as α-hemolysin (Figure 4.2C), via fusion and/or endocytosis into HaCaT cells without causing significant reduction of cell viability after 4 hr incubation (Figure 4.11A) [118]. Subsequently, vigorous inflammatory and immune responses were observed in both dorsal skin and skin draining lymph nodes of Balb/c mice, including significant upregulation of AD-related cytokines, chemokines, and skin barrier dysfunction (Figure 5.1B). The unique structure of EVs protected pathogenic compounds of *S. aureus* from the clearance by the host defensive system and retained their toxic function before arriving at the targeted location. As a result, α-hemolysin in the lumen of SA-EVs was effectively carried into the cytoplasm of HaCaT cells, whereas cell necrosis was induced, and further inflammatory responses occurred [115].

Clinically, atopic dermatitis can be categorized into three phases: acute atopic dermatitis (AAD), subacute atopic dermatitis (SAAD), and chronic atopic dermatitis (CAD), each of them harbors unique phenotypes [119]. Usually, AAD is characterized by short duration of rash, swelling, and erythema on the skin, along with overactive Th1- and Th2-driven immune responses. In contrast, CAD presents pigmentation and thickened skin, involving a complex interplay of Th1, Th22, and Th17 pathways. In our *in vivo* experiment, mice induced by 15 μg SA-EVs showed the most severe skin conditions with the thickest epidermis thickness among three groups (Figure 5.1C and 5.1D). From the differential gene expression profiles, two low-dosage SA-EVs established an acute AD model primarily driven by Th1 and Th2 immune cells, while 15 μg of SA-EVs developed a chronic AD model characterized by Th1- and Th17-dominated inflammatory responses (Figure 5.4) [120–122]. Apart from that, another typical marker of allergic reaction is total IgE level. Although three dosages of SA-EVs triggered hypersensitive reaction in Balb/c mice in a dose-dependent manners, only the highest dosage group showed statistical difference of total IgE level in serum compared to the control group. As the immune responses change rapidly within living organisms, the boundary between AAD and CAD is not easy to distinguish from one and the other. To maintain the stability of the disease state in subsequent experiments, a chronic disease model with a dose of 15 μg SA-EVs was selected for induction in the following animal experiments.

This chapter sought to establish an AD-like skin model utilizing the authentic pathogenic factor, SA-EVs, and to evaluate it against the gold standard DNCB induction from all perspectives. From the phenotypes of the two disease groups, continuous application of 15 μg of SA-EVs for 2 weeks successfully established a comparable AD-like skin model to the one induced by DNCB (Figure 5.5B-5.5D). Besides, SA-EVs also successfully triggered a systemic

allergic immune response with the significant increase of the hallmark associated with extrinsic AD in the serum (Figure 5.6B). SDLNs function as immune surveillance stations for the skin, modulating the activities of mature T and B cells. The enlarged size of SDLNs, indicative of an increase in immune cell activity, was observed in the mice, leading to the release of numerous inflammatory cytokines that exacerbate the persistence and severity of skin inflammation [115,123]. The differences between the two disease models started to appear in the aspect of T cell proliferation and inflammatory cytokines expression. Multi-signaling pathways were involved in the DNCB-induced AD development, such as T cells in the SDLNs proliferated into Treg and Th17 subsets (Figure 5.7A and 5.7C). Although the proportion of $CD4^{+}GATA3$ showed no significant increase in flow cytometry (Figure 5.7D), gene expression analysis revealed significantly upregulated *CCL17* and *IL4* in dorsal skin (Figure 5.8), indicating the participant of Th2. *CCL17* is vital for Th2-type immune responses as it recruits CCR4+ Th2-polarized memory and effector T cells to inflamed tissues, while also drawing Treg cells [124]. *IL4* contributes to the development of Th2-driven inflammatory diseases by promoting the differentiation of naïve CD4+ T cells through STAT6 activation [125] and influencing M2 macrophage polarization [126]. This result was a side proof Th2 cells and macrophage involved in inflammation development. On the contrary, SA-EVs only influenced the proliferation Th17 (Figure 5.7A). Unlike DNCB, it increased the gene expression level of chemokines (*CXCL5* and *CCL19*) and Th17-related cytokine (*IL17*) in the dorsal skins. *CXCL5* activates and recruits neutrophils by binding to CXCR2, potentially resulting in conditions such as AD [127]. *CCL19* is a homeostatic chemokine that interacts with CCR7, directing dendritic cells and T cells to SDLNs and maintaining a pro-inflammatory environment [128].

The contribution of skin microbiota to the formation of AD is often overlooked. Recent studies and clinical evidence revealed the crucial role of skin microbiome dysbiosis to AD [129,130]. DNCB significantly compromised the skin microbiome in terms of both richness and diversity, whereas SA-EVs only diminished a comparatively smaller quantity of skin microbiomes, maintaining diversity at the level comparable to the control (Figure 5 .9A, B, and E). Several reasons may explain this phenomenon. For instance, similar to the skin membrane, the cell membrane of the commensal skin microbiome were also damaged by DNCB, which prevents them from surviving in the hostile environment. Or it could be that DNCB disrupts the integrity of the stratum corneum, leading to transepidermal water loss [131]. These changes in moisture and pH may favor the overgrowth of pathogens (e.g. *Staphylococcus*, *Corynebacterium*) while suppressing the growth of commensal bacteria (e.g. *Streptococcus, Lachnospiraceae*) (Figure 5.9E and 5.9F). In summary, induction of SA-EVs increased the over colonization of pathogenic bacteria while mildly influenced the commensal skin microbiome. DNCB almost destroyed the skin microbiome and created an environment only durable to pathogens survival. This result indicated that the AD-like disease model developed by SA-EVs is more representative of the real-world pathophysiology.

Beyond the variation of skin microbiome composition between two disease models, the underlying mechanisms by which these two inducers trigger the inflammation and drive the

development of AD were also distinct. Transcriptome and proteome analysis of dorsal skin were included and combined to reveal the mystery hidden behind. Generally, the three groups were generally divided and formed unique groups at both gene and protein levels (Figure 5.10A and Figure 5.11A), suggesting that DNCB and SA-EVs affected and generated AD-like dorsal skin via highly different mechanisms. The gene expression profiler indicated that the most significant elevated genes in the dorsal skin due to DNCB were *Prss35*, *Sprr1b*, and *Lrrc15*. Those genes are all associated with the extracellular matrix (ECM) remodeling, tissue differentiation, and the immunological microenvironment, particularly in cancer and inflammation disorders. Their function is often studied in the context of cancer development and progression. *Prss35* is a secreted protease that functions as a tumor suppressor in hepatocellular carcinoma (HCC) by degrading CXCL2, which inhibits tumor progression. *Prss35* has a protective role against wound-induced skin tumorigenesis, as mice lacking *Prss35* were more susceptible to developing tumors after injury [132]. SPRR1B is a protein involved in the formation and maintenance of the epithelial barrier, providing mechanical strength and water resistance to the skin. It is a cross-linked structural protein in the cornified envelope of keratinocytes and plays a crucial role in wound healing. Recent research has also linked its regulation to the MAP kinase signaling pathway [133]. LRRC15 is a protein with roles in cell interactions, antiviral responses, and cancer biology. It binds to extracellular matrix proteins like collagen and laminin and can both inhibit viral entry and regulate cell migration [134].

Unlike DNCB, SA-EVs triggered the overexpression of genes such as *S100a8*, *S100a9*, and *261052A11RiK*. The *S100a8/a9 complex* comprises calcium-binding proteins that plays a major role in inflammation and immune responses [135]. Their functions include modulating the cytoskeleton during cell migration[136], activating NADPH oxidase for oxidative stress[137], binding to arachidonic acid, and regulating microbial infections [138]. It has been reported that S100a8/a9 induce NF-κB translocation and activates downstream inflammatory signaling pathways, which are crucial for NADPH oxidase complex assembly that is essential for generating reactive oxygen species during an immune response [139]. Besides, this complex could bind to the arachidonic acid and further regulate microbial infections by modulating the inflammatory response and exhibiting direct anti-microbial activity [138]. For the gene *261052A11RiK, its* main functions include attracting lymphocytes to the gut and skin, regulating skin barrier function, and influencing the inflammatory response in keratinocytes (skin cells). It has been linked to conditions like psoriasis and promotes keratinocyte proliferation. Taken together, both DNCB and SA-EVs produced inflammatory statues on the dorsal skin of mice, while those phenomena were obtained via distinct genes.

From the perspective of KEGG pathway analysis, apart from the overlapped pathway of *Staphylococcus aureus* infection, two omics methods both pointed to the fact that DNCB influenced the parasites related pathway, while SA-EVs affected IL-17 signaling pathway (Figure 5.10 C1&C2, Figure 5.11 C1&C2). This outcome is surprising, as numerous studies have focused on the phenotypic characterization of DNCB-induced inflammatory diseases, while few have elucidated the underlying causal mechanisms. If the underlying pathogenic

mechanisms differ, the corresponding therapeutic approaches will also differ substantially. Anti-parasitic therapy, such as Dormex, efficiently ameliorate inflammatory responses in DNCB groups [140], while IL-17 inhibitor, such as Secukinumab, is suitable for treating SA-EVs induced inflammation [141]. Sometimes, inappropriate treatment may even exacerbate the condition. As a result, establishing an AD-like disease model with the actual pathogenic factor is essential, as the functionality and efficacy of treatments developed from this model could be implemented in real-world applications, thereby benefiting society.

Chapter 6 Beneficial effects of live, heat-inactivated, and EVs of *B. longum* AC15 on AD

6.1 Introduction:

Existing literature indicates that modulation of the gut microbiome holds promise for attenuating human immune disorders, such as food allergies, allergic rhinitis, atopic dermatitis, and asthma [142]. Our previous cohort study in Chapter 3 aligned with those research findings that the abundance of *Bifidobacterium* spp. in infants' gut was inversely correlated with the incidence of illness. Subsequently, several *in vitro* experiments were conducted on both keratinocytes and macrophages in Chapter 4. The results further confirmed the beneficial effects of *Bifidobacterium* spp., including competitive inhibition of the colonization of pathogens, enhancement of gut barrier integrity via SCFAs production, and alleviation of inflammation aroused by SA-EVs, etc. Compared across multiple parameters, *B. longum* AC15 isolated from human breastmilk demonstrated superior performance and was selected as a representative candidate for the animal experiment in the following chapter. This strain exhibited the strongest adhesion to colon epithelial cells and the most potent inhibition of p65 phosphorylation of NF-κB signaling pathway amongst all. To better reflect real-world pathophysiology, SA-EVs, one of the critical factors leading to the development of AD, was used as inducer instead of DNCB. In Chapter 5, we comprehensively compared these two disease models across multiple dimensions. The results demonstrated that SA-EVs induced comparable disease phenotypes to DNCB, including epidermis thickening, robust immune responses, and preserved diversity of skin microbiome. However, multi-omics analyses revealed that the underlying mechanisms of the two inducers were distinct, leading to differential treatment efficacy. Given our objective to screen for effective interventions targeting clinically relevant pathogenic factors, the SA-EVs-induced AD model was adopted for subsequent experiments. Building upon this foundational work, the present chapter aims to elucidate the mechanisms underlying the beneficial effects of Bifidobacterium spp. by investigating both its probiotic and postbiotic properties.

The growing recognition of significance of both probiotics and postbiotics in human health underpins the experimental design of this study. To identify the specific components responsible for the observed bioactivity, this chapter presents a comparative investigation of three forms of *B. longum* AC15: (1) to optimize the dosages of live *B. longum* AC15 and its EVs to alleviate the disease manifestation in the SA-EV induced AD model.; (2) to investigate the beneficial effects of breastmilk-isolated *B. longum* AC15 on SA-EVs-induced AD mice; and (3) to decipher the underlying mechanism of live and HI *B. longum* AC15 and its EVs on preventing and treating AD. This tripartite treatment approach was designed to determine whether the biological effects are contingent upon bacterial viability or are mediated by structural and secretory components.

6.2 Optimization of Live *B. longum* AC15 on the SA-EVs induced AD mice

6.2.1 Live *B. longum* AC15 attenuated the SA-EVs induced symptoms

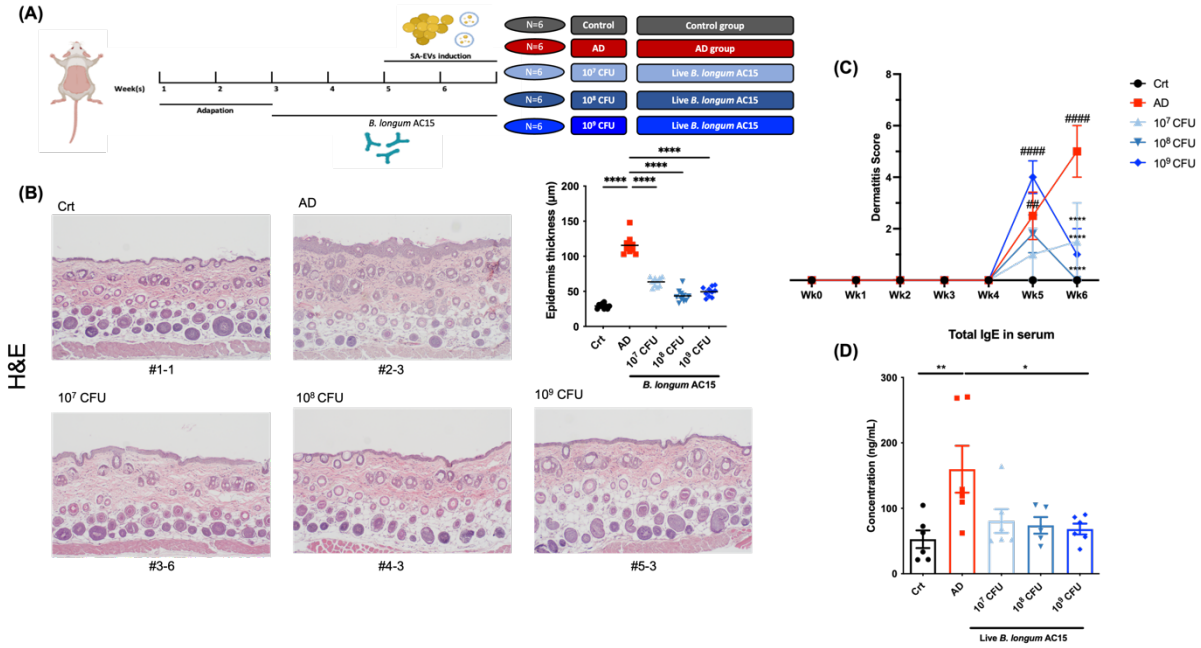

*Figure 6.1: Phenotypes of AD treated with live B. longum AC15. Titration of Live B. longum AC15 with dosage of 10^6, 10^7, 10^8 CFU/mouse on the AD mice. Timeline and design of animal experiment (A). Histological analysis of epidermal thickness with magnification of 400x (B). Dermatitis score of AD symptoms (C). Level of total IgE in serum (D). The statistical analysis was done by One-way ANOVA in Prism 9, #/*p<0.05, ##/**p<0.01, ###/***p<0.005, ####/****p<0.001. All results were shown as # and * as compared to the control and AD, respectively.*

As shown in the Figure 6.1A, 2-weeks of pre-treatment with three dosages (10^7 CFU/mouse, 10^8 CFU/mouse, and 10^9 CFU/mouse) of live *B. longum* AC15 successfully reduced AD symptoms on the Balb/c mice. According to the histological results (Figure 6.1B), the average epidermis thickness of the dorsal skin decreased by nearly two times (dropped from 115.6±13.2 μm to 52.2±11.2 μm) in treatment groups. After the first week of induction, mice from the highest dosage group (10^9 CFU/mouse) showed severe but not significant AD symptoms compared to the AD group. However, they recovered swiftly in the following week and demonstrated a significant difference from the AD group (Figure 6.1C). Additionally, the amount of total IgE in the serum from three groups decreased by half (ranging from 68.30±20 ng/mL to 80.52±40 ng/mL) while it increased three-times higher in the AD group (rising from 52.75±30.2 ng/mL to 159.71±80.2 ng/mL) (Figure 6.1D). In summary, consumption of live *B. longum* AC15 for 4 weeks at dosages ranging from 10^7 CFU to 10^9 CFU per mouse showed promising beneficial effects on preventing and alleviating AD symptoms induced by SA-EVs on Balb/c mice.

6.2.2 Anti-inflammatory effects of live *B. longum* AC15 on the dorsal skin of mice

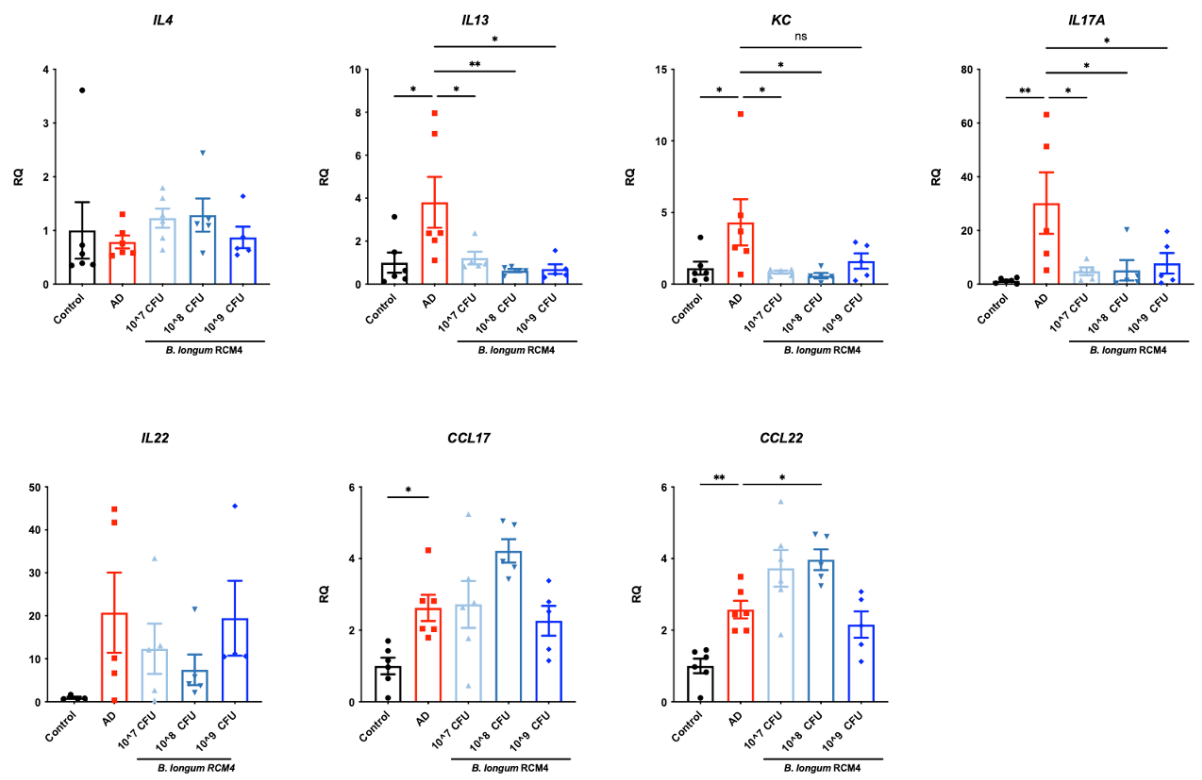

*Figure 6.2 Effects of live B. longum AC15 on the expression of inflammatory cytokines on the dorsal skin of Balb/c mice. Pretreatment of Balb/c mice with live B. longum AC15 for 2 weeks at dosages 107 CFU, 108 CFU, and 109 CFU per mice daily, followed by 2 weeks of SA-EVs induction and treatment. All groups were compared with *AD. Data was analysed by one-way ANOVA. Statistical significance is indicated as follows: ****P < 0.0001, *** P < 0.001, ** P <0.01, * P <0.05.*

To determine the most effective dosage of live *B. longum* AC15 for preventing or mitigating AD, it is essential to consider its ability of suppressing the expression of inflammatory cytokines and chemokines on the dorsal skin of mice. As shown in Figure 6.2, SA-EVs considerably increased the expression levels of *CCL17* and *CCL22* on the dorsal skin of AD mice, but the treatment groups' levels remained unchanged or were even greater than those of the disease. However, *B. longum* AC15 significantly decreased the cytokines of *KC*, *IL13*, and *IL17A* that SA-EVs induced in a dose-dependent manner. According to this result, 10^9 CFU/mouse is the most effective dosage of live *B. longum* AC15 that has favorable effects on attenuating AD, while treatment at the lowest dosage of 10^7 CFU/mouse began to show promising results. For our next experiment, these findings served as a dosage reference.

6.3 *B. longum* AC15 EVs Titration on AD

6.3.1 EVs of B. longum AC15 attenuated the SA-EVs induced symptoms

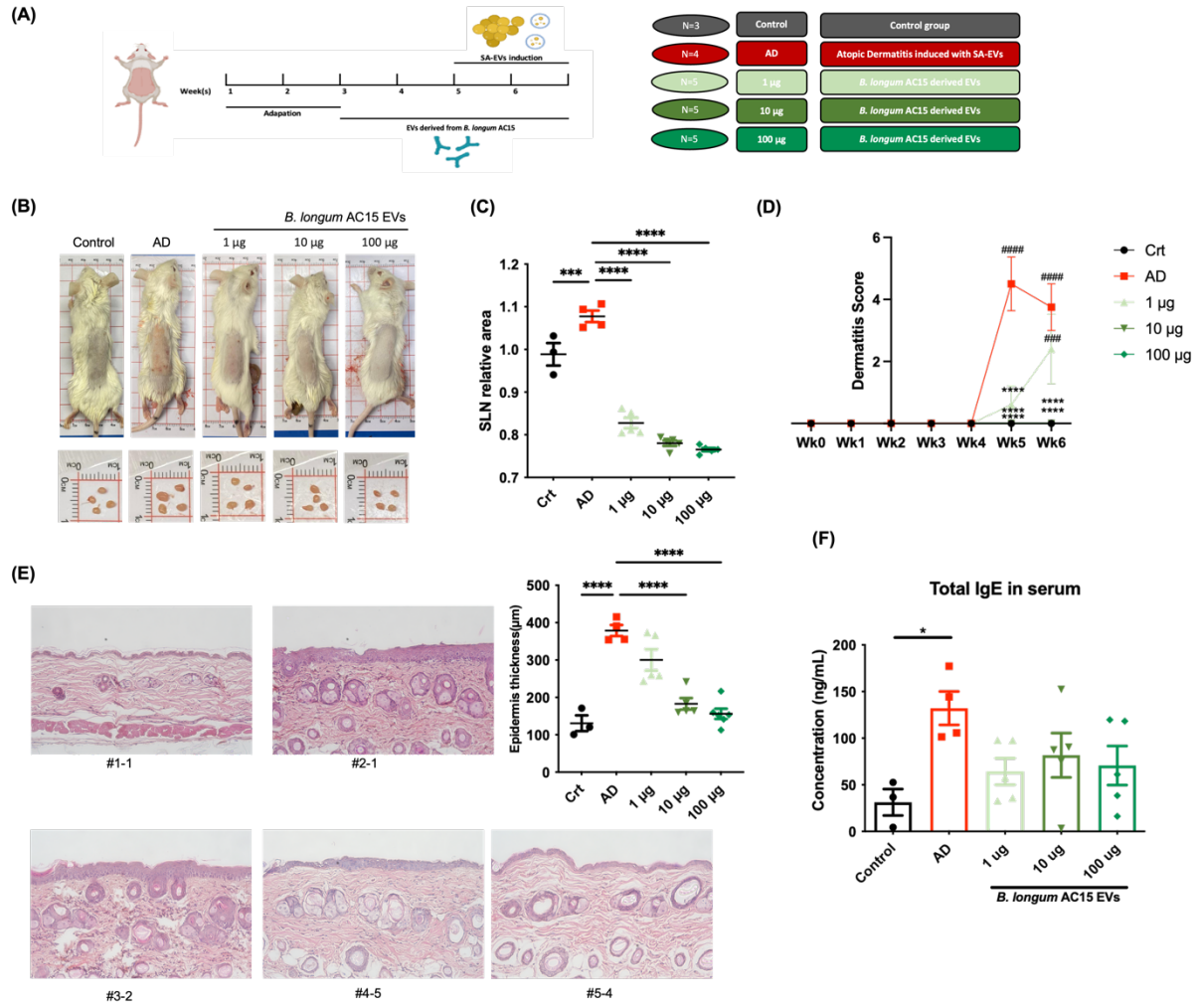

*Figure 6.3 Phenotypes of AD mice treated with EVs-derived from B. longum AC15 (BL15-EVs). Titration of BL15-EVs with dosage of 1 µg, 10 µg, 100 µg/mouse on the AD attenuation. Experiment timeline and design (A). Images of phenotype (B). Relative size of SDLN measures by ImageJ (C). Dermatitis score of AD (D). The dermatitis score of all groups was compared to control group. Histology analysis of epidermal thickness, magnification of 400x (E). Level of total IgE in serum (F). All compared to #control and *AD group. Statistically analysis was used One-way ANOVA in Prism 9, #/*p<0.05, ##/**p<0.01, ###/***p<0.005, ####/****p<0.001.*

In Figure 6.3, BL15-EVs showed a promising favourable effect on reducing AD-like symptoms in Balb/c mice in a dose-dependent manner, according to the results of phenotypic and important AD markers. As illustrated in Figure 6.3B, Balb/c mice developed a rash on their backs and enlarged size of SDLN after two-week induction of 15 µg/mouse SA-EVs, whereas the symptoms were reduced by administering with 10 µg/mouse and 100 µg/mouse of BL15-EVs prior to induction for 2 weeks. Mice from two higher dosage groups (10 µg and 100 µg)

displayed a considerably lower number in the dermatitis score compared to the AD and 1 μg groups. However, there was no discernible difference between the control group and the two higher dosage groups (Figure 6.3D). In the histology analysis, the level of epidermis thickness was increased from average of 130.8±36.4 μm to 379±29.7 μm after induction, while it decreased significantly and gradually after the dosage of BL15-EVs increased from 1 μg to 100 μg with the average reduction of 78.62±63.8 μm, 190.5±33.5 μm, and 234.9±18.7 μm, respectively (Figure 6.3E). The typical marker of allergic reaction was also analysis via ELISA. The level of total IgE in the serum showed a decreased trend in three treatment groups, though there was not significantly difference between disease and treatment groups, which probably due to the limited N number in each group (Figure 6.3F). To sum up, BL15-EVs had great potential for avoiding and reducing the development of AD raised by SA-EVs. This beneficial effect was shown in a dose-dependent manner and the best outcomes was obtained at the highest dose of 100 μg/mouse.

6.3.2 Anti-inflammation effects of EVs of *B. longum* AC15 on the dorsal skin of mice

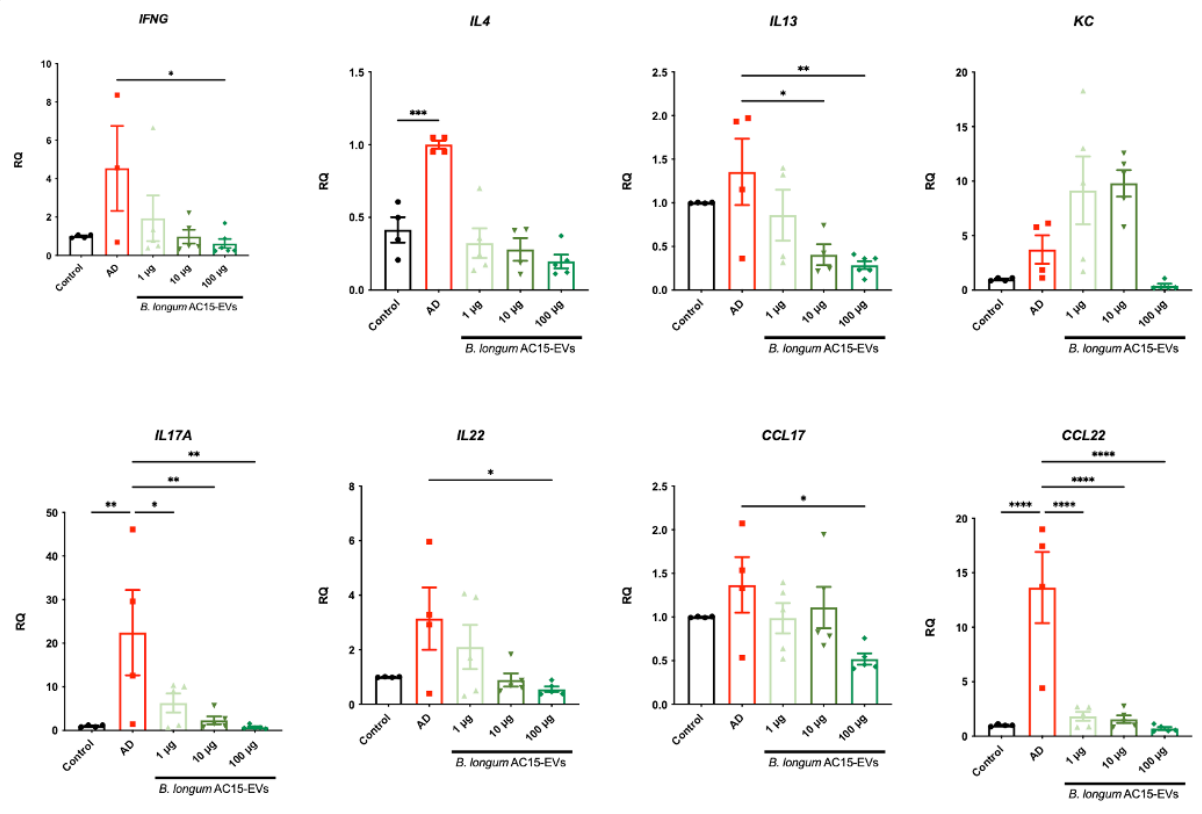

*Figure 6.4 Effects of BL15-EVs on the expression of inflammatory cytokines on the dorsal skin of Balb/c mice. Pretreatment Balb/c mice with BL15-EVs for 2 weeks at dosages 1 μg, 10 μg, and 100 μg/mice daily, followed by 2 weeks SA-EVs induction and treatment. All groups were compared with *AD. Data were analysed by one-way ANOVA. Statistical significance is indicated as follows: ****P < 0.0001, *** P < 0.001, ** P <0.01, * P <0.05.*

The expression of several of typical markers associated with AD was measured using RT-qPCR in order to determine whether BL15-EVs have any positive impact on attenuating the condition. Cytokines and chemokines, including *IFNG*, *IL4*, *IL13*, *IL17A*, *IL22*, *CCL17*, and *CCL22*, were overexpressed in the dorsal skin of AD mice, according to the findings in Figure 6.4. However, the secretion level of those makers was decreased in a dose-dependent manner when treatment BL15-EVs were added at dosages ranging from 1 μg to 100 μg. Although the expression of several markers did not be significantly suppressed after the treatment of BL15-EVs at dosages 1 μg and 10 μg, the decreasing trend was clearly observed. This circumstance might have arisen because each group's test size was insufficient. In conclusion, by inhibiting the release of inflammatory-related cytokines and chemokines, BL15-EVs demonstrated the capacity to prevent and mitigate the development of AD. The most promising dosage for preventing AD was oral gavage mice 100 μg of BL15-EVs daily for four weeks.

6.4 Validation the positive effects of Live/HI/EVs of B. longum AC15 on AD

6.4.1 Live/HI/EVs of *B. longum* AC15 attenuated AD symptoms

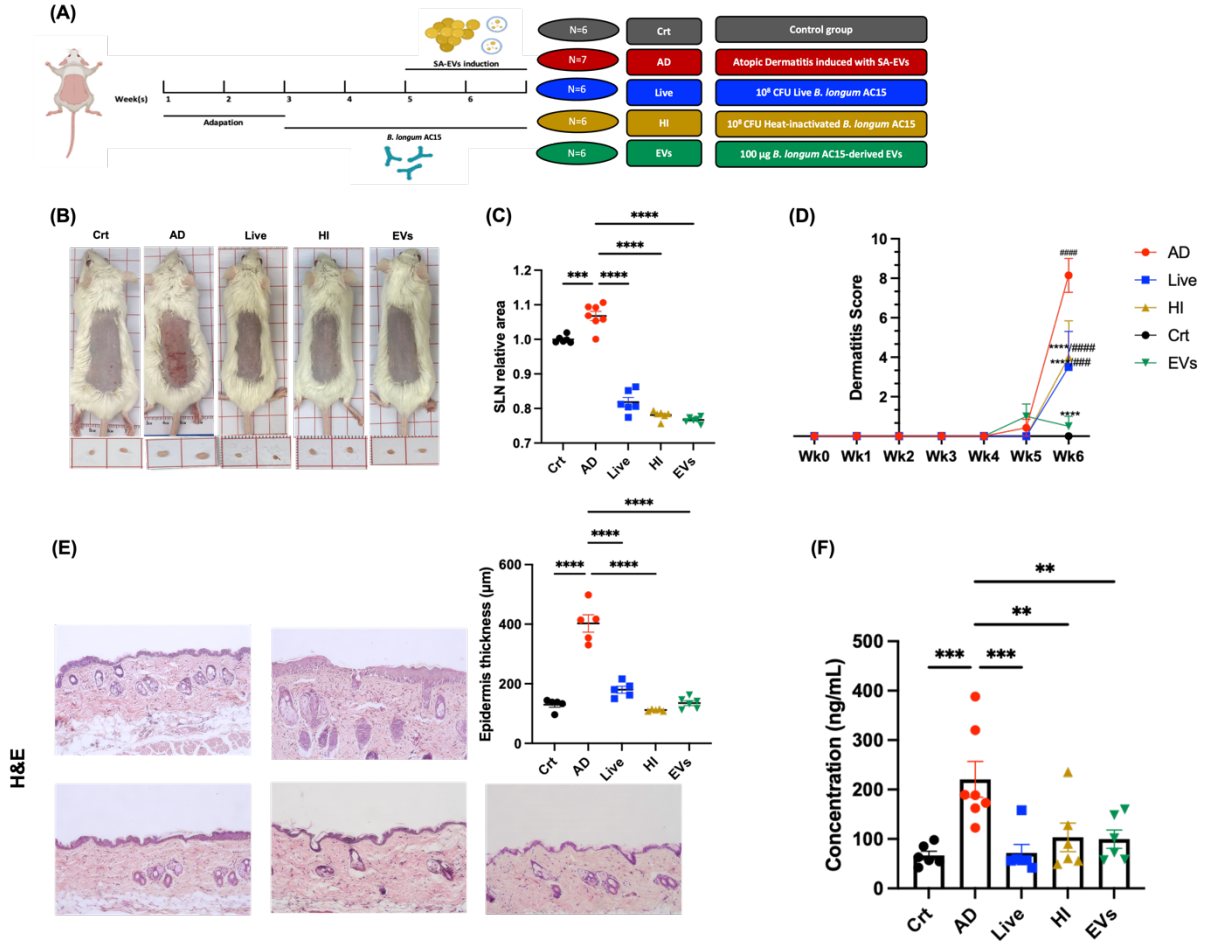

*Figure 6.5: In vivo effects of the most promising dosage of Live, heat-inactivated, EVs of B. longum AC15 on the AD attenuation. Experiment Timeline and design (A). Images of phenotype (B). Relative size of SDLN measures by ImageJ (C). Dermatitis score of AD (D). Histology analysis of epidermal thickness, magnification of 400x (E). Level of total IgE in serum (F). All compared to *AD group. Statistically analysis was used One-way ANOVA in Prism 9, *p<0.05, **p<0.01, ***p<0.005, ****p<0.001.*

According to previous two dosage optimization experiments, the most potent dosage of each treatment, including 10^9 CFU/mouse of both live and HI forms of *B. longum* AC15, and 100 µg/mouse of BL15-EVs, were used for the verification and comparison in the following experiment. From the phenotypes of dorsal skin and the size of SDLNs, three forms of *B. longum* AC15 presented repeatable excellent results in alleviating AD symptoms in this experiment. As shown in Figure 6.5D, although mice from treatment groups of live and HI *B. longum* AC15 started to show some severe AD symptoms in the final week (Week 6) compared to the control group, they were still in conditions that were better than the disease group. Amongst three treatment groups, mice from *B. longum* AC15 EVs group were kept in

the best condition throughout the whole experiment period. From the result of skin histology, the level of epidermis thickness increased by SA-EVs 2.2 times while decreased 2.23 to 3.60 times in three treatment groups (the average number of AD group decreased from 401.0±54.9 μm to the treatments groups of 177.6±23.7 μm, 111.3±3.2 μm, and 138.6±18.7 μm, respectively) and showed no significantly difference with the control group. This result indicated that all treatments prevented the dorsal skin epidermis thickness increasement caused by SA-EVs. Besides, the allergic marker of total IgE in serum were also suppressed and kept in the similar level of control groups in three treatment groups, indicating the effectiveness of three treatments in managing allergic responses and helped to stabilize immune function and reduce hypersensitivity reactions in the mice (Figure 6.5F).

6.4.2 Live/HI/EVs of *B. longum* AC15 suppressed the T cell proliferation in spleen

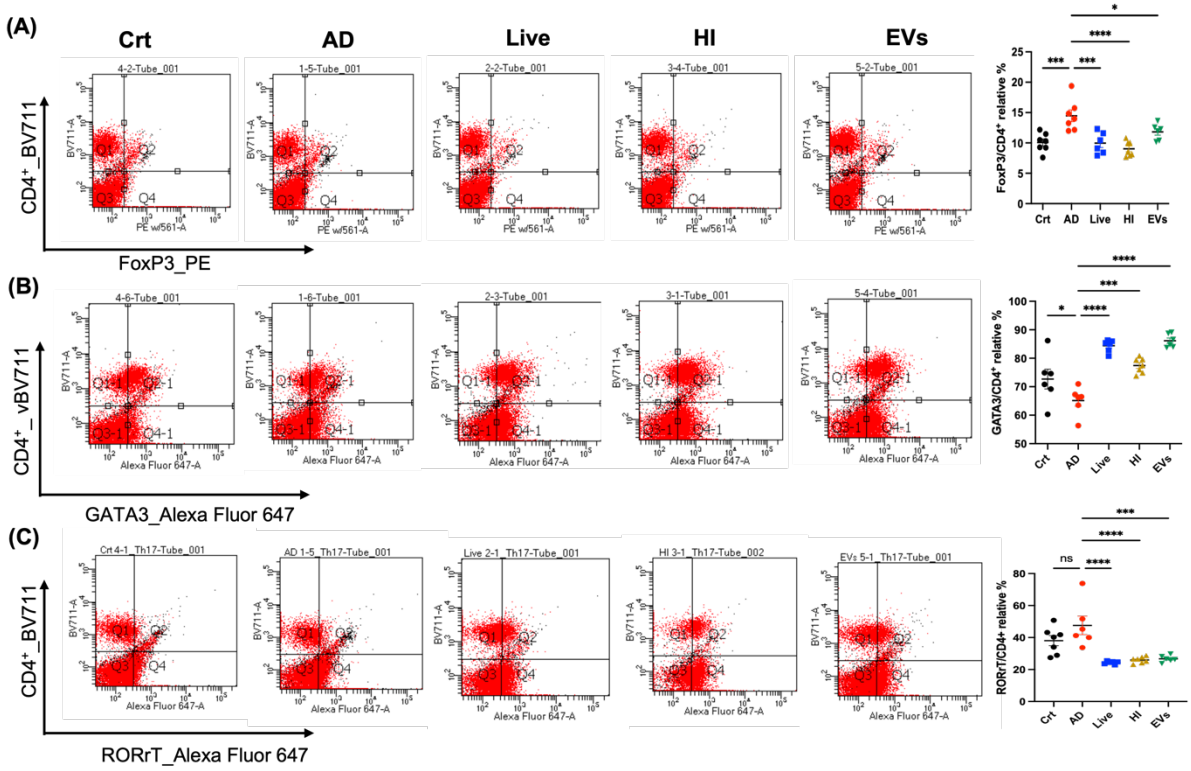

*Figure 6.6: Effects of live, HI, and EVs of B. longum AC15 on T cells proportion in spleen. Identification of Th1/Th2/Th17 and Treg in atopic dermatitis with flow cytometry. Flow cytometry assay were performed on CD4+ cells population isolated from spleen. CD4+ were labeled with BV711. FoxP3 were label with PE (A). GATA3 were labeled with Alexa 647 (B). RORγT were labeled with Alexa 647 (C). Statistical analysis was done by One-way ANOVA. *Compared with AD. Statistical significance is indicated as follows: *p<0.05, **p<0.01, ***p<0.005 and ****p<0.0001.*

To better understand how three treatments prevented hypersensitive reactions induced by SA-EVs in the host, T cells in spleen of Balb/c were collected for analysis. Key transcription factors of Treg (Foxp3), Th2 (GATA3) and Th17 (RORγT) were labelled with fluorescent dyes of PE, Alexa Fluor 647 respectively. The percentage of each T cell among CD4+ cells was quantified using flow cytometry. As shown in Figure 6.6A and 6.6C, the Treg and RORγT populations that increased in the SA-EVs group were reduced by the three treatment groups, while GATA3 exhibited the opposite trend. This result indicated that three treatments prevented the allergic responses through regulating the differentiation of T cells, suppressing Th17 and Treg, and increasing the number of Th2 cells.

6.4.3 Significant genes and signaling pathways suppressed by live/HI/EVs *B. longum* AC15

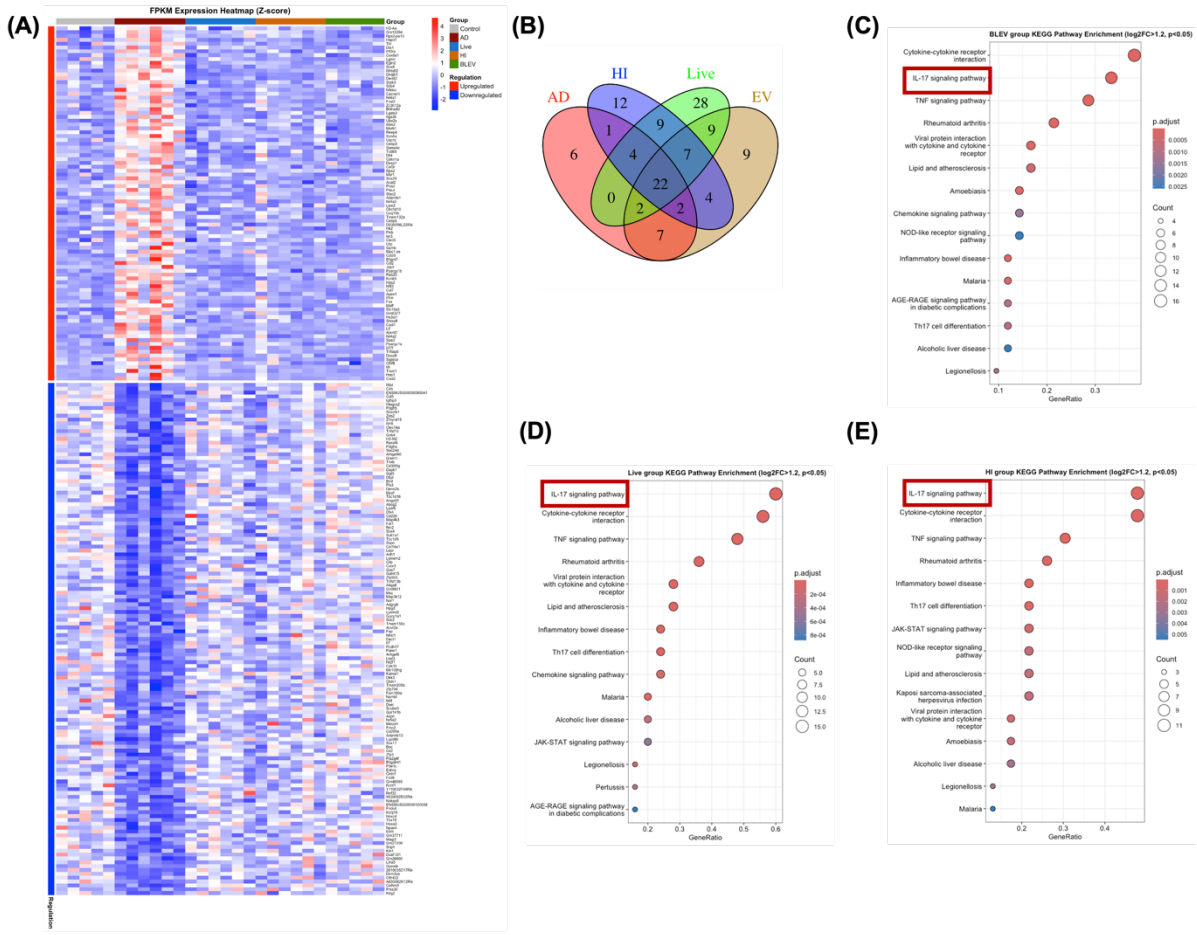

Figure 6.7: Differential genes and pathways analysis of SDLN via RNASeq. Significant genes between control, AD, and live/HI/EVs treatment groups (A). Venn diagram of overlapped KEGG pathways in three treatment groups (B). The top 15 significant signaling pathways of live (C), HI (D), and EVs (E) groups.

To deeply understand through which signaling pathways of those treatments played their function on suppressing the inflammatory responses in mice, transcriptome analysis was conducted to analyse genes and pathways contributing to those beneficial effects in the skin draining lymph nodes. Genes significantly upregulated or downregulated in disease groups, while brought back to the similar level to control group were plotted in heatmap (Figure 6.7 A). The number of significantly regulated KEGG pathways in AD, live, HI and EVs of *B. longum* AC15 groups were summarized in Venn diagram (Figure 6.7B), showing that they attenuated the AD symptoms through 22 shared signaling pathways, such as cytokine-cytokine receptor interactions, TNF signaling pathway, Th17 cell differentiation, etc (Figure 6.7C-E). The majority significantly changed genes from treatments groups took part in regulating IL-17 signaling pathway (Figure 6.7C-E), indicating suppressing the activation it might have the best outcomes for treating AD.

6.4.4 Validation of IL-17 signaling pathway via qPCR

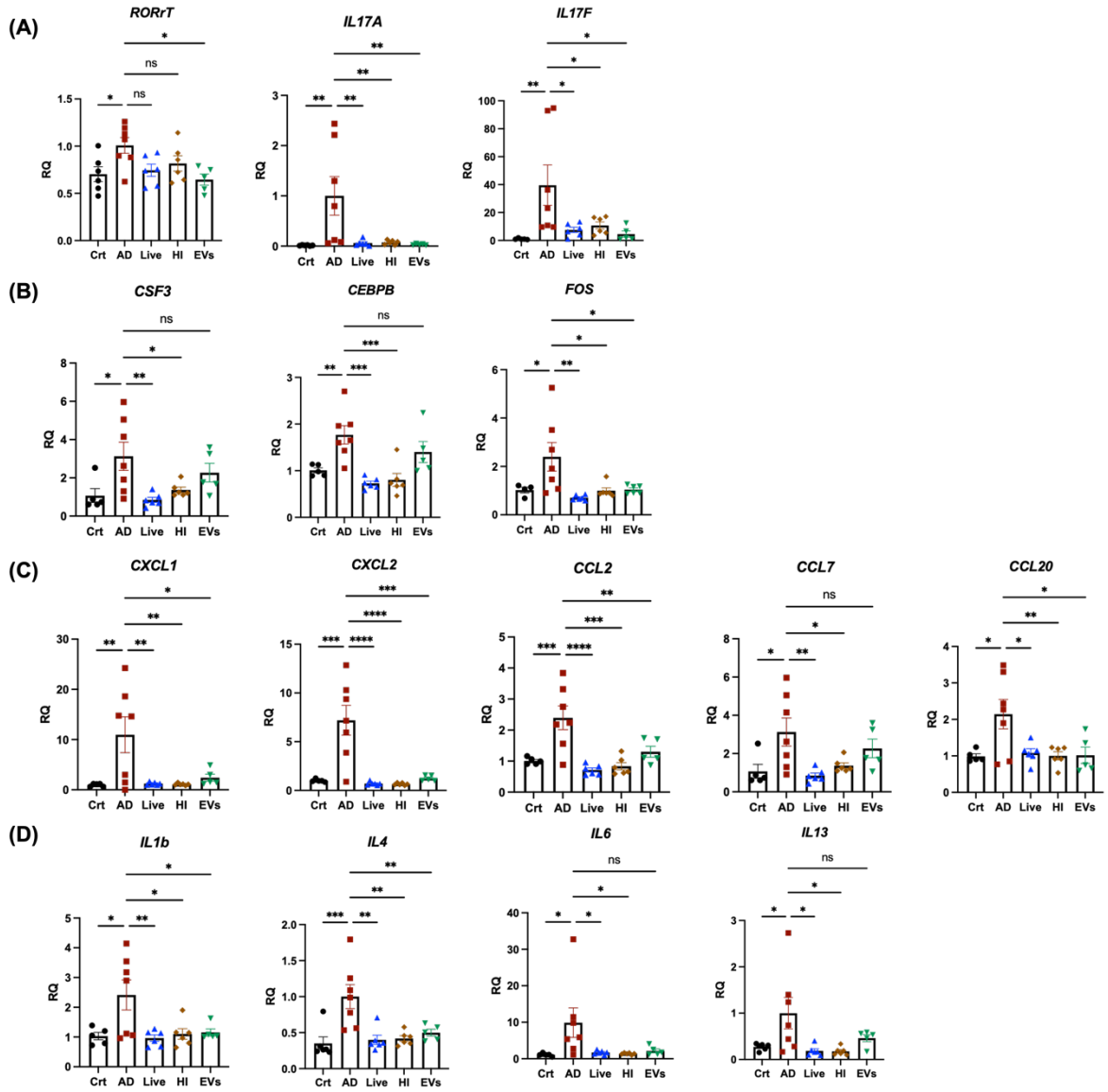

*Figure 6.8: Verification of key markers related to IL-17 signaling pathway-related at gene level. The effects of Live/HI/EVs of B. longum AC15 on the secretion of transcription factors, cytokines, and chemokines in skin draining lymph nodes. All groups were compared with *AD group. Data were analysed by one-way ANOVA. Statistical significance is indicated as follows: **** P < 0.0001, *** P < 0.001, ** P <0.01, * P <0.05.*

To further validate the result, expression level of genes related to IL-17 signaling pathway were quantified by RT-qPCR. The upstream, downstream, and transcription factors were measured. IL17A and IL17F, which are major contributors of activating IL-17 signaling pathways, were remarkably increased by SA-EVs while decreased in three treatment groups

(Figure 6.8A). And the level of three transcription factors downstream of IL-17 signaling pathway, CEBPB, and FOS, were also lower in treatment groups than disease group (Figure 6.8B). Furthermore, upregulated chemokines and cytokines in AD groups, which were attracting immune cells, monocytes, macrophages, and neutrophils and arising furious inflammatory responses, were also brough down to the similar level to control group (Figure 6.8C-D).

6.4.5 Validation of IL-17 signaling pathway key markers via ELISA

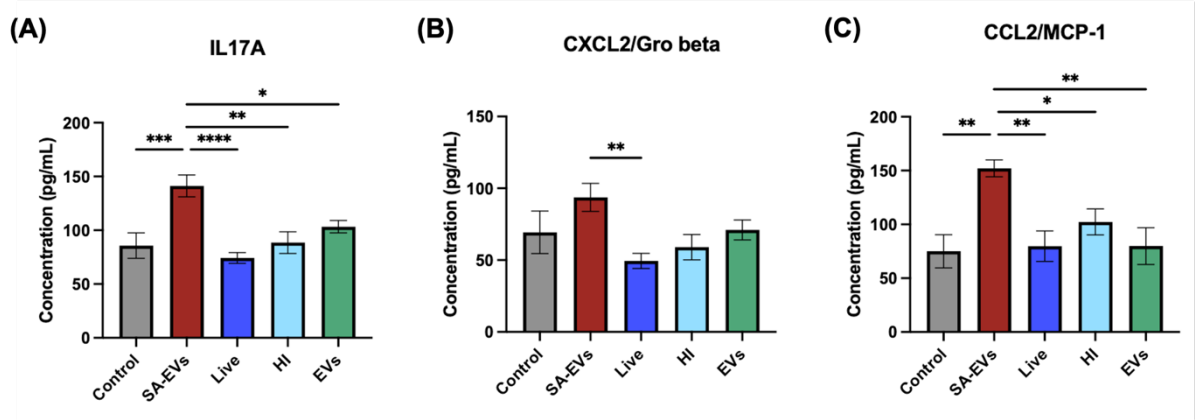

*Figure 6.9 Verification of three key targets related to IL-17 signaling pathway at protein level. The upstream marker of IL17 signaling pathway (A). The attractant of neutrophils and other immune cells (B). The attractants of monocytes, macrophages, T cells and other immune cells (C). *Compared with SA-EVs. *p<0.05, **p<0.01, ***p<0.005, and ****p<0.0001 by One-way ANOVA test.*

Continuously application of 15 μg SA-EVs daily for two weeks significantly increased the secretion of IL17A and CCL2 in the SDLNs, while the level of CXCL2 only raised slightly without significant differences. ELISA results showed that three treatments all suppressed the overexpression of IL-17A and CCL2 in SDLNs remarkably, while contradicted to the RNASeq result, the amount of CXCL2 did not have remarkable reduction in the SDLNs at protein level.

6.4.6 Correlation between the gene expression and the level of total IgE in serum

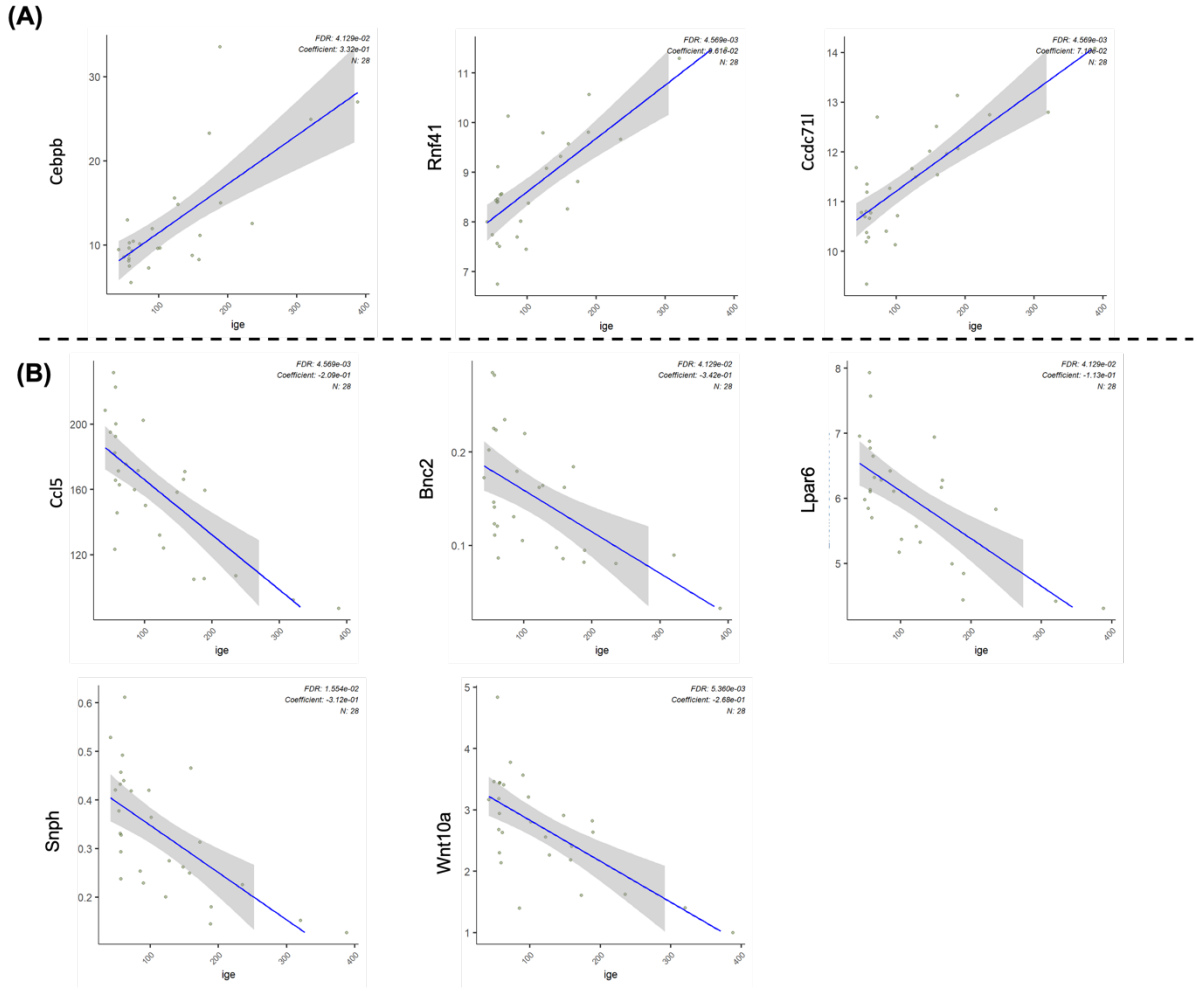

Figure 6.10 Genes in SDLNs positively and negatively association with systemic IgE levels (n=28). MaAsLin2 was used to identify gene expressed in SDLNs whose expression levels were significantly correlated with total serum IgE. Positive associations (A). Negative associations (B). All features shown have an FDR <0.05.

The analysis of RNASeq result of SDLNs for links to systemic IgE identified certain number of genes with statistically significant connections. Genes of *Cebpb*, *Rnf41*, and *CCdc71l* were characterized by a direct, positive corelation with IgE titers constituting a putative IgE-promoting signature (Figure 6.10A). *Cebpb* (CCAAT/enhancer-binding protein beta) is a key transcription factor central to inflammation, immune response, and cellular differentiation. It is critically involved in M2 polarization, Th2 cell differentiation, and regulation of acute phase genes [143]. *Rnf41* (Ring Finger Protein 41/NRDP1) is an E3 ubiquitin ligase that regulates protein degradation by the proteasome. Its immune-related targets including STAP-2 and MyD88/TRIF[144]. *Ccdc71l* (Colied-coli Domain Containing 71 Like) is the least characterized

genes which predicted to be involved in protein-protein interactions and cellular organization, yet it specific role in immunology is not well-defined [145].

By contract, genes including *Ccl5*, *Bnc2*, *Lpar6*, and *Wnt10a* were defined by a significant negative correlation, thereby comprising a candidate IgE-regulatory or suppressive signature (Figure 6.10B). *Ccl5*(C-C Motif Chemokine Ligand 5/RANTES) is a chemokine that acts as a potent chemoattractant for T cells, eosinophils, and basophils. It can produce IFN-r and directly inhibit Th2 cell proliferation and IgE class-switching, thereby suppressing IgE levels [146]. *Bnc2* (Basonuclin 2) is a transcription factor primarily studied in skin development. Collagen synthesis, and melanoma. It is a potential candidate gene for AD and other skin inflammation diseases [147]. Similarly, *Lpar6* (Lysophosphatidic acid receptor 6) is also indirectly linked to IgE, which is known for its critical role in hair follicle development and maintenance[148]. *Snph* (Syntaphilin) is a mitochondrial protein that anchors mitochondria to the cytoskeleton, regulating axonal transport in neurons [149]. *Wnt10a* (Wnt Family Member 10A) is a signaling molecule in the highly conserved Wnt pathway which is crucial for embryonic development, cell fate determination, and tissue homeostasis [150].

To sum up, the strong correlation with *Cebpb* suggests that this transcription factor is important for stimulating the IgE responses in SDLNs. Besides, *Rnf41* enhances this by modulating the innate signals that start this allergy cascade. Conversely, the genes that inverse correlated to IgE point to competing or regulating systems. Especially, the function of *Ccl5* which recruits CD8+ or Th1 T cell subsets that inhibit Th2-driven IgE production, with the help of *Wnt10a* and *Snph* impact on immune cell differentiation.

6.4.7 Effects of Live/HI/EVs *B. longum* AC15 on gut microbiota

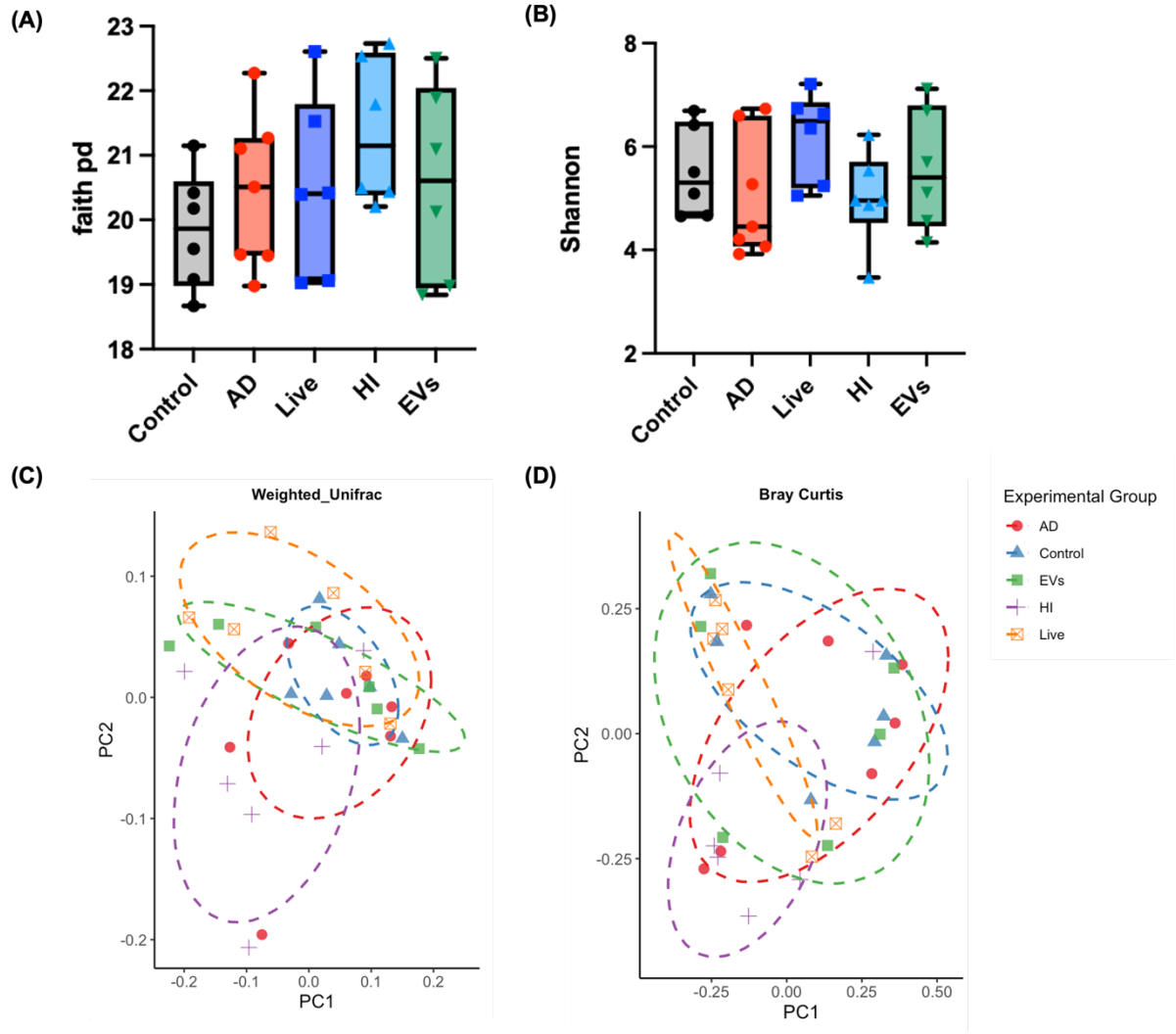

*Figure 6.11 Investigation the effects of three forms of B. longum AC15 on gut microbiota in five groups, Control, SA-EVs, Live, HI, and EVs of B. longum AC15. Shannon diversity index (A). Faith's phylogenetic diversity (B). Weighted UniFrac (C). Bray-Curtis (D). *Compared with control and #Compared with SA-EVs. #/*p<0.05, ##/**p<0.01, ###/***p<0.005, and ####/****p<0.0001 by One-way ANOVA test.*

Feces were collected at the end of a four-week oral gavage of live, HI, and EVs of *B. longum* AC15. As determined by faith pd and the Shannon, Figure 6.11A and 6.11B displayed the alpha diversity of gut microbiota among five groups. For faith pd, although there were no significant changes, it grew slightly after three treatments, with the HI group having the greatest value overall. These findings showed that after intervention, there was little variation in the phylogenetic distance of the gut microbiota of mice. For Shannon index, the number of five groups stayed constant and at a comparable level. These findings showed that the three

treatments had no effect on the gut microbiota's evenness or richness. The three treatments had no effect on the gut microbiota biodiversity of the five groups, as indicated by the weighted UniFrac and Bray-Curtis measurements of beta diversity, which are shown in Figures 48 (C) and (D). As they failed to separate well and form distinct clusters from each other, indicating that the phylogenetic diversity of the gut microbiome remained constant.

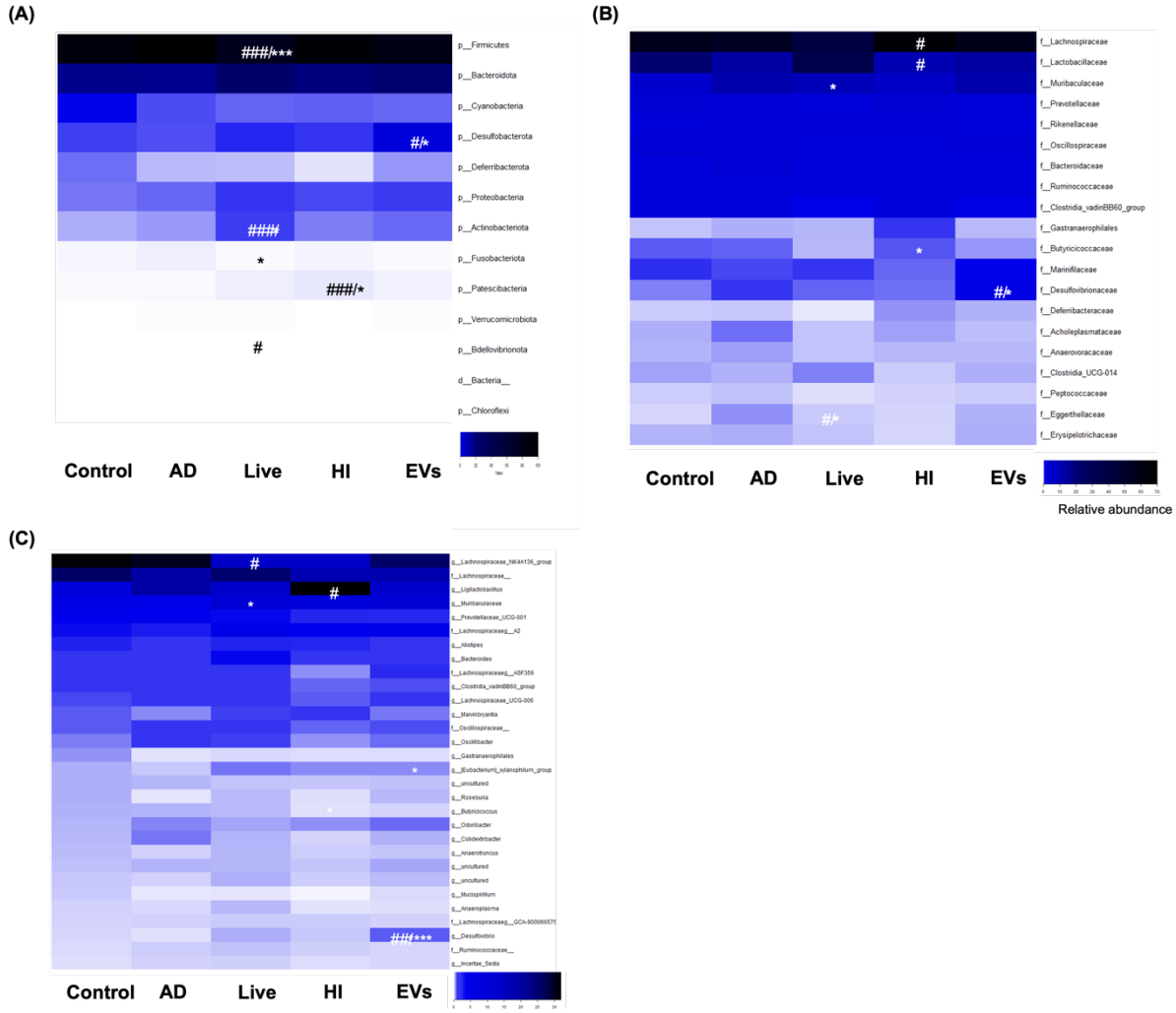

*Figure 6.12 Taxonomy analysis the gut microbiota among five groups at phylum (A), family (B), and genus (C) levels. T-test, *Compared with control and #Compared with SA-EVs. #/*p<0.05, ##/**p<0.01, ###/***p<0.005, and ####/****p<0.0001 by T test.*

Taxonomic analysis at the phylum, family, and genus levels revealed that SA-EVs had minimal effects on alteration of the gut microbiota in mice. While oral gavage mice with Live, HI, and EVs of *B. longum* AC15 for four weeks influenced their gut microbiota. At phylum level, compared to other groups, the relative abundance of *Firmicutes* and *Fusobacteriota* were only dramatically decreased in the Live *B. longum* AC15 group from average 99.64% to 78.09%, and 0.034% to 0.008%. *Firmicutes* are beneficial gut bacteria known for breaking down complex carbohydrates into SCFAs, which provide energy to gut cells and maintain the intestinal barrier [151]. In contrast, *Fusobacteria*, particularly *Fusobacterium nucleatum*, can act as an opportunistic pathogen, potentially promoting inflammation and contributing to inflammatory diseases [152]. However, *Antinobacteriota* was the only increased bacteria in the Live group. They are beneficial gut bacteria that play crucial roles in maintaining gut homeostasis and host health, despite being a minority group in the microbiota. Their functions include modulating the gut immune system, promoting gut barrier integrity, performing food fermentation, and even influencing drug absorption by producing specific inhibitors [153]. The situation in the HI group was different. *Proteobacteria* was the only increased bacteria in HI group. It is believed to be vital in preparing the gut for colonization by strict anaerobes essential for optimal gut function by depleting oxygen and reducing redox potential in the gut [154]. In the EVs group, *Desulfobacterota* was the only increased bacteria. It is a sulfate-reducing bacteria and has been associated with increased immune response and gut inflammation[155].

Further, we investigated the impacts of Live, HI, and EVs treatments on the development of mice gut microbiota at family level (Figure 6.12B). The relative abundance of *Muribaculaceae* and *Eggerthellaceae* were both doubled in the Live group compared to the AD group, rising from 5.52% to 11.88%, and 0.106% to 0.277%, respectively. The value of *Butyricicoccaceae* was only dropped in the HI group, which was reduced by half compared to the control group. In the EVs group, *Desulfovibrionaceae* was the only increased bacteria after intervention.

At the genus level, in comparison to the AD group, the relative abundance of *Muribaculaceae* doubled in the Live group, increasing from 5.44% to 11.50%. The value of *Butyricicoccus* in the HI group dropped dramatically from 0.38% to 0.16%. In the EVs group, the percentage of *Desulfovibrio* rose significantly from 0.16% to 0.81%.

6.5 Significance and Implications:

B. longum AC15, isolated from human breastmilk, was chosen for the study on animals based on its overall best outcomes of the *in vitro* tests in Chapter 5. Studies in Chapter 6 firstly determined the most effective dosages of both Live (10^9 CFU/mouse) and EVs (100 μg/mouse) of *B. longum* AC15 via dosage titration (Figures 6.1 and 6.3). As evidenced by the phenotypic outcomes from the two animal experiments, a clear dose-dependent amelioration of AD symptoms was observed. This therapeutic efficacy was demonstrated through a significant reduction in epidermal hyperplasia, leading to a thinner epidermis. Furthermore, the treated

groups exhibited a marked decrease in the incidence and severity of redness spots. Corroborating these phenotypes improvements, biochemical analysis revealed a substantial downregulation of total IgE levels in the serum. Collectively, these findings strongly implied that both treatments elicited pronounced positive effects in mitigating the pathological hallmarks of AD.

Apart from that, the typical pathogenetic markers related to AD were also assessed at molecular levels (Figure 6.2 and 6.4). The two treatments suppressed several common inflammatory cytokines, including *IL13* and *IL17A*, and also inhibited the overexpression of their unique targets. For instance, Live *B. longum* AC15 typically decreased the level of KC in the dorsal skin, whereas EVs neither suppressed nor reduced its expression, but rather enhanced it. On the contrary, BL15-EVs significantly reduced the expression of *IL22*, *CCL17*, and *CCL22* compared to AD group, but they remained mostly unaffected in the Live group. This result indicated that two treatments may alleviate AD via mitigating Th2- and Th17-mediated inflammation, which is essential for alleviating AD symptoms. However, they also modulated differential cytokines and chemokines with the immune system in distinct manners. Live *B. longum* AC15 seemed to work on the skin via stopping neutrophil-related inflammatory responses (*KC/CXCL1*) [156]. Conversely, BL15-EVs appeared to impact cytokines related to Th2 and Th22 (*IL22*, *CCL17*, *CCL22*) that are fundamental to the pathogenesis of AD [157].

To confirm the beneficial effects of Live and HI of *B. longum* AC15 on relief of AD, a validation trial was carried out using the most promising dosages and an enhanced N number for each group. Moreover, 10^9 CFU/mouse of the HI form of *B. longum* AC15 was added as a treatment with a dosage reference to the live group. In the validation experiment, three different forms of *B. longum* AC15 all demonstrated excellent efficacy in reducing AD symptoms in Balb/c mice. The beneficial effects of *B. longum* AC15 were confirmed by those reproducible results. In addition, it is worth mentioning that an interesting phenomenon observed during this experiment was that after 3 weeks of oral administration of BL15-EVs (the first induction week), mice began to experience some adverse reactions, with a slight allergic reaction to the skin on their backs. Then it suddenly disappears in the following week, accompanied by the slightest state of skin inflammation amongst all treatment groups at the end. These results piqued our curiosity regarding the potential role of BL15-EVs as immune adjuvants that enhance the immune response and help protect the host from invading pathogens [158]. However, additional research is necessary to confirm our hypothesis.

To investigate whether those treatments alleviated the AD symptoms through influencing immune systems or not, the proliferation of T cells in the spleen was also analysed. Results showed that application of 15 μg of SA-EVs for 2 weeks induced $CD4^+$ T cells to proliferate into Treg and Th17, while suppressing their proliferation into Th2 cells (Figure 6.6). Mice that received those treatments for two weeks in advance maintained a steady immune system. After the application of SA-EVs on dorsal skin, they were less susceptible to the effects by

those outside factors. As shown in Figure 6.6, the outcomes of three treatments were consistent in inhibiting the aberrant proliferation of $CD4^+$ cells and maintaining the equilibrium of various T cell percentages in the spleen. These results suggest that rebalancing $CD4^+$ T cells may be an important tactic for preventing the occurrence of AD symptoms.

From the profile of differential gene expression in SDLN, the effects of the three treatments on AD alleviation were carried out through comparable pathways to the immune system. As demonstrated in Figure 6.7, the top 3 significant influenced KEGG pathways were the IL-17 signaling pathway, cytokines-cytokine receptor interactions, and the TNF signaling pathway, which were closely associated with the inflammatory responses [159–161]. Those highly overlapped pathways modulation suggest that the three interventions ultimately target a common inflammatory axis. This convergence is significant and underscores the fundamental role of these specific pathways in the pathogenesis of AD. However, subtle differences in the degree of gene regulation within these pathways (e.g., stronger inhibition of specific cytokine receptors by a given treatment) may explain the differences in efficacy observed in our early phenotypic and immunological data.

Combining the results of disease model establishment in Chapter 5 and the performance of three treatments on AD in Chapter 6, the IL-17 signaling pathway was chosen for the pathway validation. As it was identified as the signature signaling pathway of SA-EVs-induced AD compared to DNCB-induced one through both proteome and transcriptome analysis. In addition, it was the most effective pathway shared by those three treatments on AD. Typical markers from both upstream and downstream of the IL-17 signaling pathway were verified at both gene and protein levels. In the upstream, the mRNA expression of *IL17A* and *IL17F* were verified, which was dramatically suppressed by the three treatments (Figure 6.8). These two targets, which can be produced by various innate immune cells, $CD4^+$, and $CD8^+$ T cells, are pro-inflammatory cytokines in the IL-17 family that contribute to host defense against pathogens and chronic inflammation in diseases like psoriasis and AD [162,163]. According to the results of flow cytometry (Figure 6.6) and transcriptome (Figure 6.7), the population of CD4+ RORγt+ cells increased in the AD group, and the Th17 differentiation pathway was remarkably affected by SA-EVs. We highly hypothesized that cytokines of *IL17A* and *IL17F* were secreted by immune cells, T helper 17. After SA-EVs invaded the host from the disrupted dorsal skin, they triggered the proliferation of T cells into Th17, and then they released cytokines of IL17A and IL17F to the skin and further led to the inflammatory statues of the skin. In the middle part, the three treatments presented excellent performance on inhibiting the activation of transcription factors, including *CEBPB*, and *FOS* (Figure 6.8B). *C/EBPβ* is a key transcription factor that is directly induced by IL-17 signaling and is essential for the transcription of many IL-17 target genes, such as IL-6 and LCN2 [164]. *FOS* is part of the AP-1 transcription factor. While the activation of AP-1 by IL-17 is complex, *FOS*, along with *c-Jun*, forms the AP-1 transcription factor [165]. Upon inhibiting these two transcription factors, the downstream effects that depend on those factors were also suppressed. In the downstream, the secretion of

neutrophils attractants, including *CXCL1* and *CXCL2*, was inhibited [166]. The level of *CCL2, CCL7* and *CCL20,* which could attract macrophages and monocytes, was also decreased by the three treatments [167,168]. Moreover, the expression of Th2-related Inflammatory cytokines (*IL4, IL13,* and *IL6),* and hypersensitivity marker (*IL1b*) were also suppressed by them.

From the outcomes of gut microbiota analysis, skin application of SA-EVs for 2 weeks showed limited impact on the modulation of gut microbiome in terms of composition and phylogenetic distances. However, three treatments of *B. longum* AC15 all showed unique influence on the alteration of mice's gut microbiome. They enhanced the growth of several beneficial bacteria in the gut. Live and HI *B. longum* AC15 both enhanced the growth of SCFAs producers, such as *Muribaculaceae* and *Butyricicoccus*, which provides energy to the colon cells and strengthening the gut barrier. BL15-EVs increased the sulfate-reducing bacteria like *Desulfovibrio* which is associated with increased immune responses. Overall, those beneficial bacteria maintained gut homeostasis and host health against invasion pathogens. However, the underlying mechanism of how those gut microbiota influenced the host immunity and further prevented the AD development is still not very demonstrated in this study. Further investigation is required to build the direct connection between those two.

Chapter 7 Summary and future perspectives

This thesis systematically investigated the interplay between early-life gut microbiota colonization and the therapeutic potential of *Bifidobacterium* strains and their extracellular vesicles in mitigating atopic dermatitis. The infant cohort study established that vaginal delivery and breastfeeding constitute the optimal strategy for establishing a diverse *Bifidobacterium* community, with *B. longum* dominating during exclusive breastfeeding before yielding to other bifidobacteria species upon dietary transition. Critically, delivery mode exerted transient effects that diminished postnatally, whereas feeding patterns persistently shaped microbial composition, underscoring the primacy of nutritional intervention over birth route.

Through rigorous *in vitro* characterization, *B. longum* AC15 isolated from human breastmilk emerged as the most promising probiotic candidate, demonstrating exceptional gastric and intestinal juice tolerance, superior adhesion to intestinal epithelial cells, potent pathogen exclusion, and significant anti-inflammatory capacity via NF-κB pathway suppression. Subsequent investigations established a clinically relevant AD model using *S. aureus*-derived extracellular vesicles, which authentically recapitulated human AD pathogenesis through IL-17 signaling pathway activation, fundamentally distinct from the conventional DNCB model's

parasite-associated pathways. This mechanistic divergence carries profound translational implications, as therapeutic strategies optimized using SA-EVs induction are more likely to succeed in clinical settings.

Oral administration of live, HI, and EV formulations of *B. longum* AC15 all demonstrated remarkable dose-dependent AD amelioration, characterized by reduced epidermal hyperplasia, suppressed IgE levels, and rebalanced CD4+ T cell homeostasis. Multi-omics analyses revealed convergent modulation of the IL-17 signaling axis as the central therapeutic mechanism, though each formulation exerted unique immunomodulatory fingerprints. Notably, BL15-EVs transiently stimulated immune responses before establishing durable tolerance, suggesting adjuvant-like properties warranting further investigation.

Future perspectives should prioritize translational validation through randomized controlled trials evaluating *B. longum* AC15 formulations in pediatric AD populations, with particular attention to strain-specific effects versus general bifidobacterial benefits. The mechanistic divergence between SA-EVs and DNCB models necessitates reevaluation of existing preclinical AD research, particularly regarding IL-17 versus anti-parasitic pathway engagement. Comprehensive proteomic and metabolomic characterization of BL15-EVs cargo is urgently required to identify the specific bioactive molecules responsible for immunomodulation, enabling development of cell-free biotherapeutics with standardized potency. Furthermore, the observed gut-skin axis modulation following oral administration demands mechanistic elucidation, specifically whether gut microbiota remodeling directly influences cutaneous immunity via metabolite translocation or whether systemic immune rebalancing occurs independently. Finally, the transient immune activation preceding tolerance induction by BL15-EVs presents an opportunity to harness controlled immunostimulant for enhancing vaccine efficacy or combating infectious diseases, representing an underexplored frontier in EV-based therapeutics.

Appendices:

Supplementary Table 1: Primers used for qPCR analysis of bacteria.

Target	ATCC strain	Forward (5'-3')	Reverse (5'-3')	Amplicon (bp)	Probe (if applicable)
Total *Bifidobacterium*		CGCGTCCGGTGTGAAAG	CCCCACATCCAGCATCCA	243	SYBR
B. breve M16-V		GGCCACCAGTATGGTCTTATCC	TCGTGCCATTCGCTATTGC	63	FAM-NFQ-MGB
B. breve	ATCC 15700	CCGGATGCTCCATCACAC	ACAAAGTGCCTTGCTCCCT	287	SYBR
B. bifidum	ATCC 29251	CCACATGATCGCATGTGATTG	CCGAAGGCTTGCTCCCAAA	277	SYBR
B. longum	ATCC 15707	GCCGTATCTCTACGACCGTCG	TATCGGGGAGCAAGCGAGAG	565	SYBR
Total bacteria		AGGATTAGATACCCTGGTA	CRRCACGAGCTGACGAC	294	SYBR

Supplementary Table 2 **Primer sequence used for RT-qPCR analysis of human samples:**

*Primer Name	Forward (5-3')	Reverse (5-3')
GAPDH	ACCCACTCCTCCACCTTTG	ATCTTGTGCTCTTGCTGGG
KART6	GGGTTTCAGTGCCAACTCAG	CCAGGCCATACAGACTGCGG
KRT1	CACTTATTCCGGAGTAACCAG	GAATAGGATGAGCTAGTGTAA
KRT10	GAGTCTTCATCTAAGGGACCA	AATGGTCTGTGTGAAGGGAGA
KRT14	CGCCAAATCCGCACCAAGGTC	GAAGCAGGGTCCAGCTGTGAA
KRT5	CAGCGTCAAATTTGTCTCCAC	TTGGTCTAGACTACTCTCCAG
TARC	CACGCAGCTCGAGGGACCAATGTG	TCAAGACCTCTCAAGGCTTTGCAGG
MDC	AGGACAGAGCATGGCTCGCCTACAGA	TAATGGCAGGGAGGTAGGGCTCCTGA
RANTES	CTGCCTCCCCATATTCCTCG	CTGCCTCCCCATATTCCTCG
IL8	ATGACTTCCAAGCTGGCCGTGGCT	TTATGAATTCTCAGCCCTCTTCAAAAA
IL1b	CTGTCGTGCGTGTTGAAAGA	TTCTGCTTGAGAGGTGCTGA
MCP-1/CCL2	GTTGGCTCAGCCAGATGCA	CCAGCCTACTCATTGGGATCA
IFNγ	GGGAAGCGAAAAAGGAGTCA	GGACAACCATTACTGGGATGCT
TNFA	AGCCGCATCGCCGTCTCCTA	CAGCGCTGAGTCGGTCACCC
MIP-1α	TCGCTCAGCCAGATGCAAT	TGGCCACAATGGTCTTGAAG
IL25	CGACCCAGATTAGGTGAGGA	TCCATCTTCACTGGCCCTAC

IL19	GGCAATGTCAGGAACAGAGG	AGCGGAATAAGACAGCCTGA
Filaggrin	GCAAGGTCAAGTCCAGGAGAA	CCCTCGGTTTCCACTGTCTC
Involucrin	GGGACTGCCTGAGCAAGAAT	GGGACTGCCTGAGCAAGAAT

Supplementary Table 3: **Primer sequence used for RT-qPCR analysis of mice samples:**

***PrimerName**	**Forward(5-3')**	**Reverse(5-3')**
Il22	AAGCATTGCCTTCTAGGTCTCC	TCAGAGATACACGAGCTGGTT
Il17f	GAGGATAACACTGTGAGAGTTGA	GAGTTCATGGTGCTGTCTTCC
Csf3	GCCACCTACAAGCTGTGTCACC	GCTGGCTTAGGCACTGTGTCTG
Ptgs2/COX2	CCAGAGCTCTTCCTCCTGTG	AAGCTGGTCCTCGTTCAAAA
Cxcl2/MIP-2	CGCCCAGACAGAAGTCATAG	TCCTCCTTTCCAGGTCAGTTA
Il6	TGTTCTCTGGGAAATCGTGGA	AAGTGCATCATCGTTGTTCATACA
Cxcl1/KC	TGGGATTCACCTCAAGAACA	TTTCTGAACCAAGGGAGCTT
Ccl2	CCACTCACCTGCTGCTACTCATTC	CTGCTGCTGGTGATCCTCTTGTAG
Ccl20	TGGGTACTGCTGGCTCACCT	CGAGAGGCAACAGTCGTAGTTG
Fos	CCTTCGGATTCTCCGTTTCTCT	CCTTCGGATTCTCCGTTTCTCT
Ccl7/MCP-3	TGGGAAGCTGTTATCTTCAAGACA	CTCGACCCACTTCTGATGGG
Cebpb	CGGGACTGACGCAACACA	CCGCAGGAACATCTTTAAGTGATTA
Ccl2	ACTGAAGCCAGCTCTCTCTTCCTC	TTCCTTCTTGGGGTCAGCACAGAC
Ccl7	CTGCTCATAGCTYCCTGGATCT	GGTGCTGAAGATCTTCTTTAGC
Ccl12	CAGGCAGCTCTCTCTTCCTCA	TGGGTTTGGGGTGGTTGTAG
Ccl20	CAGGTGCTGCTGTACATAGAC	GGAGGCAGGAAAGTTGATGC
Cxcl1	CTGGGATTCACCTCAAGAACATC	CAGGGTCAAGGCAAGCCTC
Cxcl2	CCACTCTCAAGGGCGGTCAA	GGTTGACAGCAGCCAGGTTC
Cxcl5	TGCGTTGTGTTTGCTTCCCT	TCCTTCTGGTCCAGTTTGGT

Cxcl10	GCTGCCGTCATTTTCTGCCT	TCTCACTGGAGCGAGTTTGG
Il1b	GCAACTGTTCCTGAACTCAACT	ATCTTTTGGGGTCCGTCAACT
Il6	TAGTCCTTCCTACCCCAATTTCC	TTGGTCCTTAGCCACTCCTTC
Il17a	TCCCTCTGTGATCTGGGAAG	AGCTTTCCCTCCGCATTGAC
Il17f	GGAGATCCTGGTGCTATTGC	TGGGTCTTCATTGCGGTAGA
Csf3	GCTGGAGACCTGTGAGGAAA	CAGGGTGGTGTGGTAAAGGA
Nfkbia	AGACGAGGAGTACGAGCAGAT	GTCGTAGCCAAGTCCAGGTC
Mapk11	GCTGGACACCAACATCACCT	TCCAGGTTGTCGTAGTCGTG
Mapk6	GGAAGAGGAGGAGGACGTGA	TCCAGGTAGGTGGCATTGAG
Fos	CTGGTGCAGCCCACTCTGGT	TGGCACTAGAGACGGACAGA
Jund	CAGCCAGCAAGAGGAAGACC	TGGTGGAGGTGGTGTAGAGG
Cebpb	TGGACAAGAACAGCAACGAG	TCATTGTCACTGGTCAGCTCC
S100a8	TGACAAGAAATCACCATGCCG	CTTTTGTTCCTCCGCTTATGG
S100a9	CAGAGCTGGAGAAAGGCAGAC	GGACAGTTTGTAGACGGGCT
NGF	catgctggacccaagctca	cctgcagggacattgctctc
SEMA3A	GAAGAGCCCTTATGATCCCAAAC	AGATAGCGAAGTCCCGTCCC
KLK3	GCATCAGGAACAAAAGCGTGA	CCTGAGGAATCGATTCTTCAG
KLK5	GCAGGTAGAGACTCCTGCCA	CACAAGGGTAATCTCCCCAG
KLK7	ACCCTCAGTGCTGGAGAAGA	ACTGGGTCAAAGGTGGTGAA
KLK8	AAGTGCACCGTCTCAGGC	TCCTCACACTTCTTCTGGGG
KLK10	CTCTGGCGAAGCTGCTG	ATAGGCTTCGGGGTCCAA
FLG	TCTTAAGAAGTGTTGTCACCATCA	GTGTCTGGATCATCTGGATTCTTC

JUN	CGACCAGAACGATGGACTT	CAGTTTGTAACCCCTCCCA
Fos	CCGGGCTGCACTACTTAC	TCAGGGAGTCGGAGGAG
MAPK1	CAAATGCTGACTCCAAAGC	CGTCCAACTCCATGTCAA
MAPK8	GCGTCCCATCTTTTAGTGA	TCATGCTCCAATTTCTGCT
MAPK14	AGCTGTTGACCGGAAGAA	GGGCCAGAGACTGAATGTA
NFKBIA(IKB)	CAGCCATGTTTCAGCCA	CCTTCACCATTTGCTCGT
Act1	TGCAGTAACCCAGAAGCC	CTTGCGTTCACCAGAGAGA
Ptgs2/COX2	TTGCTGTACAAGCAGTGGCAAAGG	AGGACAAACACCGGAGGGAATCTT
TNFA	AGCCAGGAGGGAGAACAGA	CAGTGAGTGAAAGGGACAGAAC
IL6	CAAGAAAGACAAAGCCAGAGTCCTT	TGGATGGTCTTGGTCCTTAGCC
CD80	TGGCTCTGCAAACACGGTTC	AGCAAATGTGCAAATCGTCCC
CD86	CTTACGGAAGCACCCACGAT	TGTAAATGGGCACGGCAGAT
CD206	GTGGAGTGATGGAACCCCAG	CTGTCCGCCCAGTATCCATC
Arg1	AGGGTCCACCCTGACCTATG	ACAGGTTGCCCATGCAGATT
CCL2	TGAAGTTGACCCGTAAATCTGAA	AGGCATCACAGTCCGAGTC
CCL5	CCTGCTGCTTTGCCTACCTCTC	ACACACTTGGCGGTTCCTTCGA
CCL11	GAATCACCAACAACAGATGCAC	ATCCTGGACCCACTTCTTCTT
CCL19	CCTGGGAACATCGTGAAAGC	TAGTGTGGTGAACACAACAGC
Cxcl2	CCAACCACCAGGCTACAGG	GCGTCACACTCAAGCTCTG
Cxcl5	GTTCCATCTCGCCATTCATGC	GCGGCTATGACTGAGGAAGG
Cxcl13	GGCCACGGTATTCTGGAAGC	ACCGACAACAGTTGAAATCACTC

Supplementary Figure 1

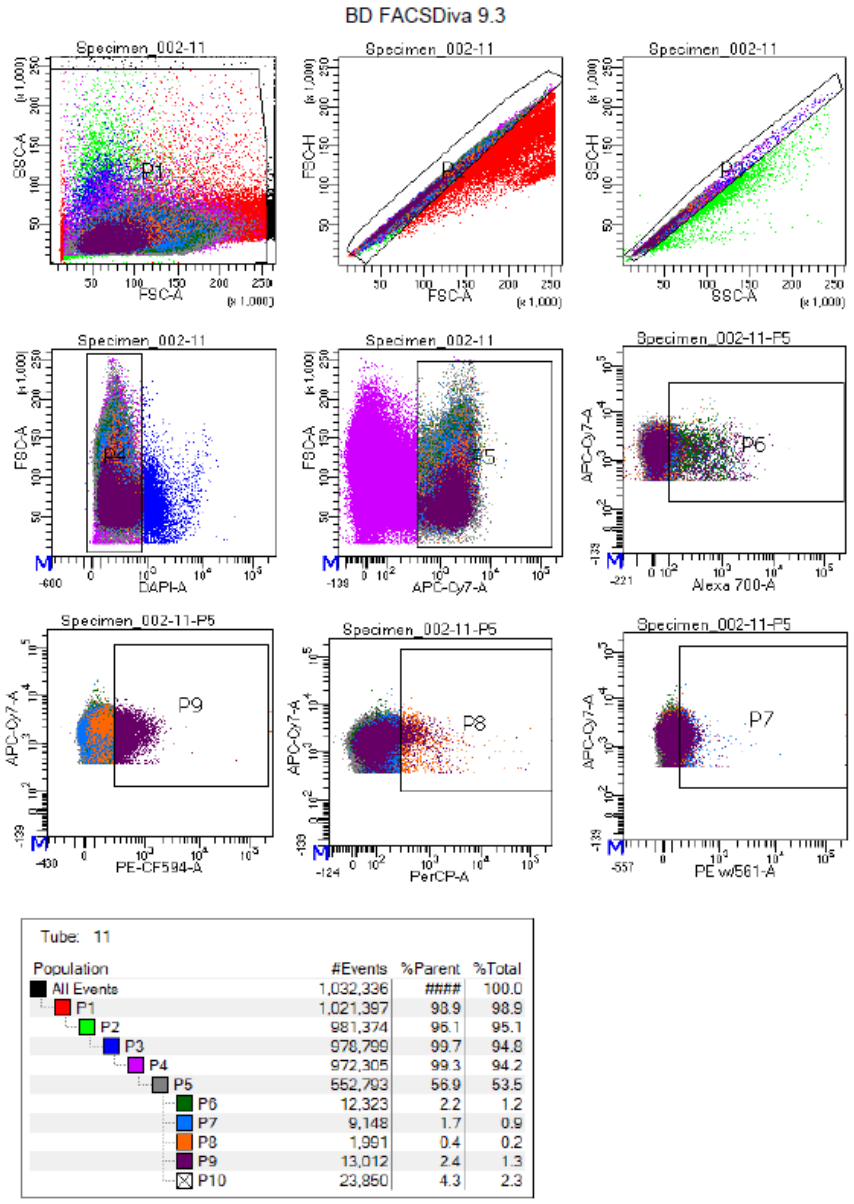

Tube: 11

Population	#Events	%Parent	%Total
All Events	1,032,336	####	100.0
P1	1,021,397	98.9	98.9
P2	981,374	96.1	95.1
P3	978,799	99.7	94.8
P4	972,305	99.3	94.2
P5	552,793	56.9	53.5
P6	12,323	2.2	1.2
P7	9,148	1.7	0.9
P8	1,991	0.4	0.2
P9	13,012	2.4	1.3
P10	23,850	4.3	2.3

Supplementary Figure 1: The gating strategy for CD4+ Treg/ Th1/Th2/Th17 cells in in skin draining lymph nodes of Balb/c mice (n=6).

Supplementary Figure 2

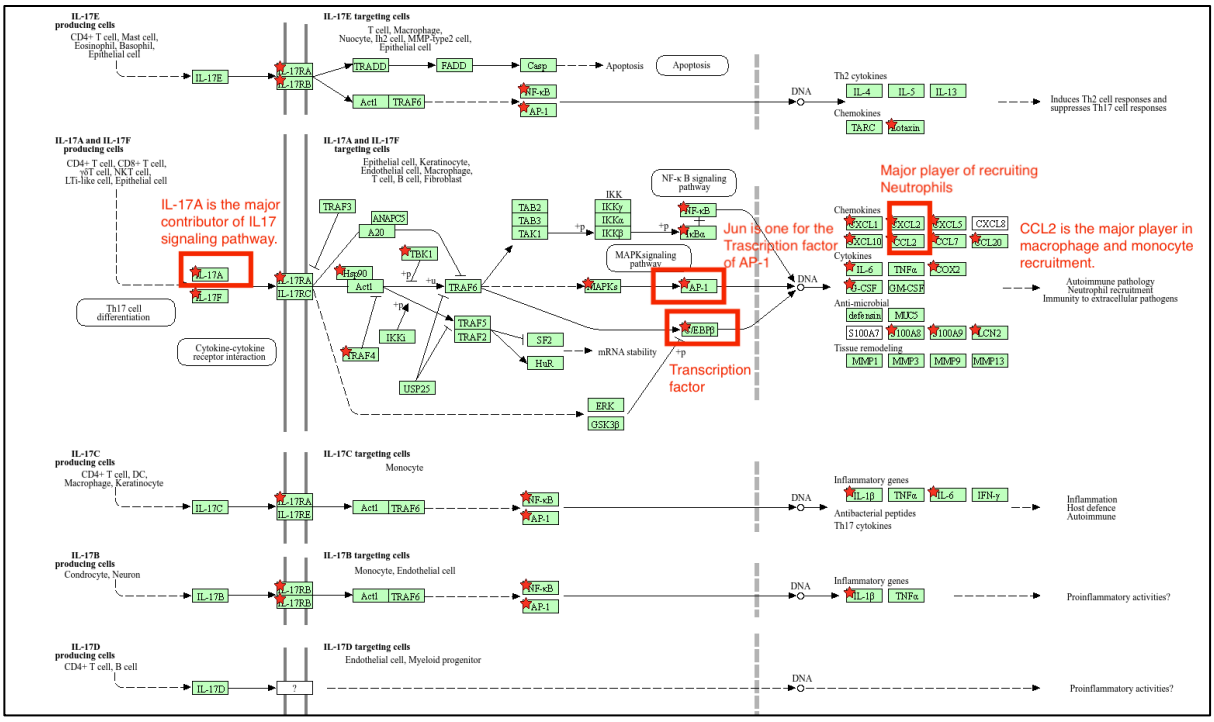

Supplementary Figure 2: The signaling map of IL-17 signaling pathway.

Reference

1. Postler, T. S. & Ghosh, S. Understanding the Holobiont: How microbial metabolites affect human health and shape the immune system. *Cell Metab* **26**, 110 (2017).

2. Mohammad, I. *et al.* Beyond Digestion: The Gut Microbiota as an Immune–Metabolic Interface in Disease Modulation. *Gastrointestinal Disorders 2025, Vol. 7,* **7**, (2025).

3. Ibrahem, K. H. The Role of Probiotics in Human Health: A Review. *Sana'a University Journal of Medicine and Health Sciences* **19**, 232–238 (2025).

4. Abeltino, A. *et al.* Unraveling the Gut Microbiota: Implications for Precision Nutrition and Personalized Medicine. *Nutrients* **16**, 100497 (2024).

5. Fuller, R. History and development of probiotics. *Probiotics* 1–8 (1992) doi:10.1007/978-94-011-2364-8_1.

6. Probiotics - International Scientific Association for Probiotics and Prebiotics (ISAPP). https://isappscience.org/topic/probiotics/.

7. Probiotics - International Scientific Association for Probiotics and Prebiotics (ISAPP). https://isappscience.org/topic/probiotics/.

8. Meena, K. K., Joshi, M., Gupta, L. & Meena, S. Comprehensive insights into postbiotics: Bridging the gap to real-world application. *Food Nutrition* **1**, 100024 (2025).

9. Latif, A. *et al.* Probiotics: mechanism of action, health benefits and their application in food industries. *Front Microbiol* **14**, 1216674 (2023).

10. Vijayaram, S. *et al.* Probiotics: A multifaceted approach to health promotion-from disease prevention to food enrichment and delivery systems. *AIMS Microbiol* **11**, 602 (2025).

11. Harnvoravongchai, P. *et al.* Gut commensal Bifidobacterium longum confers resistance to Salmonella Typhimurium and Shigella flexneri in a Caenorhabditis elegans model. *Microbiol Spectr* **14**, e01842-25 (2025).

12. Strain, R., Stanton, C. & Ross, R. P. Effect of diet on pathogen performance in the microbiome. *Microbiome Research Reports* **1**, 13 (2022).

13. Louis, P., Duncan, S. H., Sheridan, P. O., Walker, A. W. & Flint, H. J. Microbial lactate utilisation and the stability of the gut microbiome. *Gut Microbiome* **3**, e3 (2022).

14. Pinhal, S., Ropers, D., Geiselmann, J. & De Jong, H. Acetate Metabolism and the Inhibition of Bacterial Growth by Acetate. *J Bacteriol* **201**, e00147-19 (2019).

15. Martinez, F. A. C., Balciunas, E. M., Converti, A., Cotter, P. D. & De Souza Oliveira, R. P. Bacteriocin production by Bifidobacterium spp. A review. *Biotechnol Adv* **31**, 482–488 (2013).

16. Gavzy, S. J. *et al.* Bifidobacterium mechanisms of immune modulation and tolerance. *Gut Microbes* **15**, 2291164 (2023).

17. Lee, S. *et al.* Peptidoglycan from Bifidobacterium adolescentis enhances IL-10 production in regulatory B cells to alleviate gut inflammation. *Gut Microbes* **18**, 2611603 (2026).

18. Zhang, W., Mackay, C. R. & Gershwin, M. E. Immunomodulatory Effects of Microbiota-derived Short-Chain Fatty Acids in Autoimmune Liver Diseases. *J Immunol* **210**, 1629 (2023).

19. Abdulqadir, R., Engers, J. & Al-Sadi, R. Role of Bifidobacterium in Modulating the Intestinal Epithelial Tight Junction Barrier: Current Knowledge and Perspectives. *Curr Dev Nutr* **7**, 102026 (2023).

20. Terahara, M. *et al.* Effects of the intake of non-live Bifidobacterium bifidum on the faecal IgA of full-term infants: a double-blind, randomised, placebo-controlled study. *Biosci Microbiota Food Health* **40**, 196 (2021).

21. Furuyama, N. & Sircili, M. P. Outer Membrane Vesicles (OMVs) Produced by Gram-Negative Bacteria: Structure, Functions, Biogenesis, and Vaccine Application. *Biomed Res Int* **2021**, 1490732 (2021).

22. Li, Q. *et al.* Specific labeling of outer membrane vesicles with antibiotic-conjugated probe reveals early bacterial infections in blood. *Nature Communications 2025 16:1* **16**, 1–14 (2025).

23. Avila-Calderón, E. D. *et al.* Outer Membrane Vesicles of Gram-Negative Bacteria: An Outlook on Biogenesis. *Front Microbiol* **12**, 557902 (2021).

24. Kim, J. Y. *et al.* Gram-Negative Bacteria's Outer Membrane Vesicles. *Infect Chemother* **55**, 1 (2023).

25. Yang, J., Shin, T. S., Kim, J. S., Jee, Y. K. & Kim, Y. K. A new horizon of precision medicine: combination of the microbiome and extracellular vesicles. *Experimental & Molecular Medicine 2022 54:4* **54**, 466–482 (2022).

26. Li, Y. *et al.* Probiotic extracellular vesicles reprogram macrophage immunometabolism: From gut crosstalk to host health. *Gut Microbes* **18**, 2614115 (2026).

27. Domínguez Rubio, A. P., D'Antoni, C. L., Piuri, M. & Pérez, O. E. Probiotics, Their Extracellular Vesicles and Infectious Diseases. *Front Microbiol* **13**, 864720 (2022).

28. Wang, G., Wang, Y., Sheng, K. & Wang, Y. Effect of probiotic extracellular vesicles and their applications on health and disease. *J Sci Food Agric* **105**, 3539–3549 (2025).

29. Nishiyama, K. *et al.* Extracellular vesicles produced by Bifidobacterium longum export mucin-binding proteins. *Appl Environ Microbiol* **86**, (2020).

30. Domínguez Rubio, A. P., D'Antoni, C. L., Piuri, M. & Pérez, O. E. Probiotics, Their Extracellular Vesicles and Infectious Diseases. *Front Microbiol* **13**, 864720 (2022).

31. Morishita, M. *et al.* Activation of Host Immune Cells by Probiotic-Derived Extracellular Vesicles via TLR2-Mediated Signaling Pathways. *Biol Pharm Bull* **45**, 354–359 (2022).

32. Kim, W. *et al.* Lactobacillus plantarum-derived extracellular vesicles induce anti-inflammatory M2 macrophage polarization in vitro. *J Extracell Vesicles* **9**, 1793514 (2020).

33. López, P. *et al.* Treg-inducing membrane vesicles from Bifidobacterium bifidum LMG13195 as potential adjuvants in immunotherapy. *Vaccine* **30**, 825–829 (2012).

34. Yang, L. & Xia, J.-N. Beyond the Skin: Exploring the Gut-Skin Axis and Metabolic Pathways in Atopic Dermatitis Pathogenesis. *Int J Gen Med* **18**, 6123 (2025).

35. Kim, G. Il *et al.* Interconnection of the Gut-Skin Axis in NC/Nga Mouse with Atopic Dermatitis: Effects of the Three Types of Bifidobacterium bifidum CBT-BF3 (Probiotics, Postbiotics, and Cytosine-Phosphate-Guanine Oligodeoxynucleotide) on T Cell Differentiation and Gut Mi…. *Food Sci Anim Resour* **44**, 1417–1439 (2024).

36. Fang, Z. *et al.* Bifidobacterium longum mediated tryptophan metabolism to improve atopic dermatitis via the gut-skin axis. *Gut Microbes* **14**, 2044723 (2022).

37. Compliance Guide for Probiotic Food Products in China - ZMUni Compliance Centre. https://www.zmuni.com/en/news/complianceguideforprobioticfoodproductsinchina/ .

38. Principles for Safety Assessment of Novel Food Ingredients | ChemLinked. https://food.chemlinked.com/database/view/6755.

39. Part V (Food and Drugs) of the Public Health and Municipal Services Ordinance (Cap. 132) (Highlights). https://www.cfs.gov.hk/english/food_leg/food_leg_list.html.

40. Jun, S. H. *et al.* Staphylococcus aureus-derived membrane vesicles exacerbate skin inflammation in atopic dermatitis. *Clinical & Experimental Allergy* **47**, 85–96 (2017).

41. Wakarera, P. W., Ojola, P. & Njeru, E. M. Characterization and diversity of native Azotobacter spp. isolated from semi-arid agroecosystems of Eastern Kenya. *Biol Lett* **18**, (2022).

42. Abdelazez, A. *et al.* Verification of Lactobacillus brevis tolerance to simulated gastric juice and the potential effects of postbiotic gamma-aminobutyric acid in streptozotocin-induced diabetic mice. *Food Science and Human Wellness* **11**, 165–176 (2022).

43. Yadav, M. K. & Tiwari, S. K. Methods for Determination of Antimicrobial Activity of Bacteriocins of Lactic Acid Bacteria. *Microbiology 2023 92:6* **92**, 745–765 (2023).

44. Wongvibulsin, S. *et al.* Transcriptomic analysis of atopic dermatitis in African Americans is characterized by Th2/Th17-centered cutaneous immune activation. *Scientific Reports 2021 11:1* **11**, 1–11 (2021).

45. Cheung, M. K. *et al.* Development of the early-life gut microbiome and associations with eczema in a prospective Chinese cohort. *mSystems* **8**, (2023).

46. Pessemier, B. De *et al.* Gut–skin axis: Current knowledge of the interrelationship between microbial dysbiosis and skin conditions. *Microorganisms* **9**, 1–33 (2021).

47. Jeong, S. Factors influencing development of the infant microbiota: from prenatal period to early infancy. *Clin Exp Pediatr* **65**, 438 (2022).

48. Black, M. & Bhattacharya, S. Cesarean section in China, Taiwan, and Hong Kong—A safe choice for women and clinicians? *PLoS Med* **15**, (2018).

49. Chung, W. H., Kong, C. W. & To, W. W. K. Secular trends in caesarean section rates over 20 years in a regional obstetric unit in Hong Kong. *Hong Kong Medical Journal* **23**, 340–348 (2017).

50. Makino, H. *et al.* Mother-to-infant transmission of intestinal bifidobacterial strains has an impact on the early development of vaginally delivered infant's microbiota. *PLoS One* **8**, (2013).

51. Liu, Q., Jing, W. & Wang, W. Bifidobacterium lactis Ameliorates the Risk of Food Allergy in Chinese Children by Affecting Relative Percentage of Treg and Th17 Cells. *Canadian Journal of Infectious Diseases and Medical Microbiology* **2018**, (2018).

52. Pantazi, A. C. *et al.* Relationship between Gut Microbiota and Allergies in Children: A Literature Review. *Nutrients* **15**, (2023).

53. Yu, L. *et al.* Comparison of Gut Microbiota Between Infants with Atopic Dermatitis and Healthy Controls in Guangzhou, China. *J Asthma Allergy* **14**, 493–500 (2021).

54. Dattner, A. M. Breastfeeding and atopic dermatitis: protective or harmful? facts and controversies. *Clin Dermatol* **28**, 34–37 (2010).

55. Kim, J. H. Role of Breast-feeding in the Development of Atopic Dermatitis in Early Childhood. *Allergy Asthma Immunol Res* **9**, 285 (2017).

56. Enomoto, T. *et al.* Effects of Bifidobacterial Supplementation to Pregnant Women and Infants in the Prevention of Allergy Development in Infants and on Fecal Microbiota. *Allergology International* **63**, 575–585 (2014).

57. Freitas, A. C. & Hill, J. E. Bifidobacteria isolated from vaginal and gut microbiomes are indistinguishable by comparative genomics. *PLoS One* **13**, e0196290 (2018).

58. Matera, M. Bifidobacteria, Lactobacilli... when, how and why to use them. *Global Pediatrics* **8**, 100139 (2024).

59. Bakshani, C. R. & Crouch, L. I. Human milk oligosaccharides and Bifidobacterium species. *Trends Microbiol* **32**, 118–119 (2024).

60. Laursen, M. F. & Roager, H. M. Human milk oligosaccharides modify the strength of priority effects in the Bifidobacterium community assembly during infancy. *The ISME Journal 2023 17:12* **17**, 2452–2457 (2023).

61. Nishiyama, K. *et al.* Bifidobacterium bifidum Extracellular Sialidase Enhances Adhesion to the Mucosal Surface and Supports Carbohydrate Assimilation. *mBio* **8**, (2017).

62. Pan, K., Zhang, C. & Tian, J. The Effects of Different Modes of Delivery on the Structure and Predicted Function of Intestinal Microbiota in Neonates and Early Infants. *Pol J Microbiol* **70**, 45–55 (2021).

63. Long, G. *et al.* The Influence of Cesarean Section on the Composition and Development of Gut Microbiota During the First 3 Months of Life. *Front Microbiol* **12**, (2021).

64. Gila-Diaz, A. *et al.* A Review of Bioactive Factors in Human Breastmilk: A Focus on Prematurity. *Nutrients* **11**, (2019).

65. Saturio, S. *et al.* Role of Bifidobacteria on Infant Health. *Microorganisms* **9**, (2021).

66. Xiao, M. *et al.* Cross-feeding of bifidobacteria promotes intestinal homeostasis: a lifelong perspective on the host health. *NPJ Biofilms Microbiomes* **10**, 47 (2024).

67. Arboleya, S., Watkins, C., Stanton, C. & Ross, R. P. Gut Bifidobacteria Populations in Human Health and Aging. *Front Microbiol* **7**, (2016).

68. Tarracchini, C. *et al.* Phylogenomic disentangling of the Bifidobacterium longum subsp. infantis taxon. *Microb Genom* **7**, 000609 (2021).

69. Turroni, F. *et al.* Bifidobacterium bifidum: A Key Member of the Early Human Gut Microbiota. *Microorganisms* **7**, (2019).

70. Westermann, C., Gleinser, M., Corr, S. C. & Riedel, C. U. A critical evaluation of bifidobacterial adhesion to the host tissue. *Front Microbiol* **7**, 211780 (2016).

71. Fekete, E. E. *et al.* Multilevel Proteomic Profiling of Colorectal Adenocarcinoma Caco-2 Cell Differentiation to Characterize an Intestinal Epithelial Model. *J Proteome Res* **23**, 2561–2575 (2024).

72. Akhtar, M. *et al.* Gut microbiota-derived short chain fatty acids are potential mediators in gut inflammation. *Animal Nutrition* **8**, 350–360 (2022).

73. Fukuda, S., Toh, H., Taylor, T. D., Ohno, H. & Hattori, M. Acetate-producing bifidobacteria protect the host from enteropathogenic infection via carbohydrate transporters. *Gut Microbes* **3**, 449–454 (2012).

74. Li, T. *et al.* Bifidobacterium animalis subsp. lactis A12 prevents obesityassociated dyslipidemia by modulating gut microbiota-derived short-chain fatty acid production and energy metabolism in high-fat diet-fed mice. *Food Nutr Res* **66**, 8670 (2022).

75. Hodgkinson, K. *et al.* Butyrate's role in human health and the current progress towards its clinical application to treat gastrointestinal disease. *Clinical Nutrition* **42**, 61–75 (2023).

76. Rekha, K. *et al.* Short-chain fatty acid: An updated review on signaling, metabolism, and therapeutic effects. *Crit Rev Food Sci Nutr* **64**, 2461–2489 (2024).

77. Chen, S. *et al.* Macrophages in immunoregulation and therapeutics. *Signal Transduction and Targeted Therapy 2023 8:1* **8**, 207- (2023).

78. Piewngam, P. & Otto, M. Staphylococcus aureus colonisation and strategies for decolonisation. *Lancet Microbe* **5**, e606–e618 (2024).

79. Bennett, R. W., Hait, J. M. & Tallent, S. M. Staphylococcus aureus Infection. *Guide to Foodborne Pathogens, Second Edition* 26–44 (2025) doi:10.1002/9781118684856.ch2.

80. Chen, H. *et al.* Exploring the Role of Staphylococcus aureus in Inflammatory Diseases. *Toxins (Basel)* **14**, (2022).

81. Tartaglia, N. R. *et al.* Staphylococcus aureus extracellular vesicles elicit an immunostimulatory response in vivo on the murine mammary gland. *Front Cell Infect Microbiol* **8**, 393646 (2018).

82. Hong, S. W. *et al.* Extracellular vesicles derived from Staphylococcus aureus induce atopic dermatitis-like skin inflammation. *Allergy* **66**, 351 (2011).

83. Hong, S. W. *et al.* Extracellular vesicles derived from Staphylococcus aureus induce atopic dermatitis-like skin inflammation. *Allergy* **66**, 351 (2011).

84. Viegas, C., Seck, F. & Fonte, P. An insight on lipid nanoparticles for therapeutic proteins delivery. *J Drug Deliv Sci Technol* **77**, 103839 (2022).

85. Mazumdar, S., Chitkara, D. & Mittal, A. Exploration and insights into the cellular internalization and intracellular fate of amphiphilic polymeric nanocarriers. *Acta Pharm Sin B* **11**, 903–924 (2021).

86. Dell'Atti, F. *et al.* Probiotic-derived extracellular vesicles: the next breakthrough in postbiotics for rheumatoid arthritis. *Front Immunol* **16**, 1620185 (2025).

87. Wang, Y., Duan, C. & Yu, X. Extracellular vesicles of Gram-negative and Gram-positive probiotics. *Journal of Microbiology* **63**, e2506005 (2025).

88. Lee, K. S. *et al.* Human Probiotic Lactobacillus paracasei-Derived Extracellular Vesicles Improve Tumor Necrosis Factor-α-Induced Inflammatory Phenotypes in Human Skin. *Cells* **12**, 2789 (2023).

89. Wendel, U. Assessing Viability and Stress Tolerance of Probiotics—A Review. *Front Microbiol* **12**, (2021).

90. Bustos, A. Y., Saavedra, L., de Valdez, G. F., Raya, R. R. & Taranto, M. P. Relationship between bile salt hydrolase activity, changes in the internal pH and tolerance to bile acids in lactic acid bacteria. *Biotechnol Lett* **34**, 1511–1518 (2012).

91. Gorreja, F. & Walker, W. A. The potential role of adherence factors in probiotic function in the gastrointestinal tract of adults and pediatrics: a narrative review of experimental and human studies. *Gut Microbes* **14**, 2149214 (2022).

92. Collado, M. C., Gueimonde, M., Sanz, Y. & Salminen, S. Adhesion properties and competitive pathogen exclusion ability of bifidobacteria with acquired acid resistance. *J Food Prot* **69**, 1675–1679 (2006).

93. Yu, D. *et al.* Bifidobacterium longum subsp. infantis as widespread bacteriocin gene clusters carrier stands out among the Bifidobacterium. *Appl Environ Microbiol* **89**, (2023).

94. Cheikhyoussef, A. *et al.* COMPARISON OF THREE DIFFERENT METHODS FOR THE ISOLATION OF BACTERIOCIN-LIKE INHIBITORY SUBSTANCES FROM BIFIDOBACTERIUM INFANTIS BCRC 14602. *J Rapid Methods Autom Microbiol* **17**, 182–194 (2009).

95. Kim, M. H. *et al.* Lactobacillus plantarum-derived Extracellular Vesicles Protect Atopic Dermatitis Induced by Staphylococcus aureus-derived Extracellular Vesicles. *Allergy Asthma Immunol Res* **10**, 516 (2018).

96. Kim, M. R. *et al.* Staphylococcus aureus-derived extracellular vesicles induce neutrophilic pulmonary inflammation via both Th1 and Th17 cell responses. *Allergy* **67**, 1271–1281 (2012).

97. Kolb, L. & Ferrer-Bruker, S. J. Atopic Dermatitis. *StatPearls* https://www.ncbi.nlm.nih.gov/books/NBK448071/ (2023).

98. Mohd Kasim, V. N. K. *et al.* Management of Atopic Dermatitis Via Oral and Topical Administration of Herbs in Murine Model: A Systematic Review. *Front Pharmacol* **13**, 785782 (2022).

99. Fania, L. *et al.* Multiple Roles for Cytokines in Atopic Dermatitis: From Pathogenic Mediators to Endotype-Specific Biomarkers to Therapeutic Targets. *Int J Mol Sci* **23**, 2684 (2022).

100. Chong, A. C., Visitsunthorn, K. & Ong, P. Y. Genetic/Environmental Contributions and Immune Dysregulation in Children with Atopic Dermatitis. *J Asthma Allergy* **15**, 1681 (2022).

101. Hong, S. W. *et al.* Extracellular vesicles derived from Staphylococcus aureus induce atopic dermatitis-like skin inflammation. *Allergy* **66**, 351–359 (2011).

102. Gehrke, A. K. E., Giai, C. & Gómez, M. I. Staphylococcus aureus Adaptation to the Skin in Health and Persistent/Recurrent Infections. *Antibiotics* **12**, 1520 (2023).

103. Kengmo Tchoupa, A. & Peschel, A. Staphylococcus aureus Releases Proinflammatory Membrane Vesicles To Resist Antimicrobial Fatty Acids. *mSphere* **5**, (2020).

104. Tartaglia, N. R. *et al.* Staphylococcus aureus extracellular vesicles elicit an immunostimulatory response in vivo on the murine mammary gland. *Front Cell Infect Microbiol* **8**, 393646 (2018).

105. Jun, S. H. *et al.* Staphylococcus aureus-derived membrane vesicles exacerbate skin inflammation in atopic dermatitis. *Clinical & Experimental Allergy* **47**, 85–96 (2016).

106. Pinchuk, I. V., Beswick, E. J. & Reyes, V. E. Staphylococcal Enterotoxins. *Toxins (Basel)* **2**, 2177 (2010).

107. Roan, F., Obata-Ninomiya, K. & Ziegler, S. F. Epithelial cell-derived cytokines: more than just signaling the alarm. *J Clin Invest* **129**, 1441–1451 (2019).

108. Fujii, Y., Takeuchi, H., Sakuma, S., Sengoku, T. & Takakura, S. Characterization of a 2,4-dinitrochlorobenzene-induced chronic dermatitis model in rats. *Skin Pharmacol Physiol* **22**, 240–247 (2009).

109. Lu, C. *et al.* Inhibition of macrophage MAPK/NF-κB pathway and Th2 axis by mangiferin ameliorates MC903-induced atopic dermatitis. *Int Immunopharmacol* **133**, 112038 (2024).

110. Mohd Kasim, V. N. K. *et al.* Oral and topical administration of a geranyl acetophenone attenuates DNCB-induced atopic dermatitis-like skin lesions in BALB/c mice. *Scientific Reports 2024 14:1* **14**, 1–13 (2024).

111. Zhang, E. Y., Chen, A. Y. & Zhu, B. T. Mechanism of Dinitrochlorobenzene-Induced Dermatitis in Mice: Role of Specific Antibodies in Pathogenesis. *PLoS One* **4**, e7703 (2009).

112. Park, N. J. *et al.* Lobelia chinensis Extract and Its Active Compound, Diosmetin, Improve Atopic Dermatitis by Reinforcing Skin Barrier Function through SPINK5/LEKTI Regulation. *Int J Mol Sci* **23**, (2022).

113. Das, P. *et al.* Keratinocytes: An Enigmatic Factor in Atopic Dermatitis. *Cells 2022, Vol. 11, Page 1683* **11**, 1683 (2022).

114. Ryu, B. *et al.* Anti-Inflammatory Effects of M-MSCs in DNCB-Induced Atopic Dermatitis Mice. *Biomedicines* **8**, 439 (2020).

115. Hong, S. W. *et al.* An Important Role of α-Hemolysin in Extracellular Vesicles on the Development of Atopic Dermatitis Induced by Staphylococcus aureus. *PLoS One* **9**, e100499 (2014).

116. Heimall, J. & Spergel, J. M. New pathways for itching in patients with atopic dermatitis? *Journal of Allergy and Clinical Immunology* **140**, 393–394 (2017).

117. Gęgotek, A. & Skrzydlewska, E. The Role of ABC Transporters in Skin Cells Exposed to UV Radiation. *Int J Mol Sci* **24**, 115 (2022).

118. Joshi, B. S., de Beer, M. A., Giepmans, B. N. G. & Zuhorn, I. S. Endocytosis of Extracellular Vesicles and Release of Their Cargo from Endosomes. *ACS Nano* **14**, 4444–4455 (2020).

119. Girolomoni, G. *et al.* Nomenclature and clinical phenotypes of atopic dermatitis. *Ther Adv Chronic Dis* **12**, 20406223211002980 (2021).

120. Langan, S. M., Irvine, A. D. & Weidinger, S. Atopic dermatitis. *The Lancet* **396**, 345–360 (2020).

121. Park, K. D., Pak, S. C. & Park, K. K. The Pathogenetic Effect of Natural and Bacterial Toxins on Atopic Dermatitis. *Toxins 2017, Vol. 9, Page 3* **9**, 3 (2016).

122. Criado, P. R. *et al.* Update on the pathogenesis of atopic dermatitis. *An Bras Dermatol* **99**, 895–915 (2024).

123. Han, S. C. *et al.* 3-Bromo-4,5-dihydroxybenzaldehyde Attenuates Allergic Contact Dermatitis by Generating CD4+Foxp3+ T cells. *In Vivo (Brooklyn)* **39**, 201–209 (2025).

124. Tsunemi, Y. *et al.* CCL17 transgenic mice show an enhanced Th2-type response to both allergic and non-allergic stimuli. *Eur J Immunol* **36**, 2116–2127 (2006).

125. Zhu, J., Guo, L., Watson, C. J., Hu-Li, J. & Paul, W. E. Stat6 is necessary and sufficient for IL-4's role in Th2 differentiation and cell expansion. *J Immunol* **166**, 7276–7281 (2001).

126. Celik, M., Labuz, D., Keye, J., Glauben, R. & Machelska, H. IL-4 induces M2 macrophages to produce sustained analgesia via opioids. *JCI Insight* **5**, e133093 (2020).

127. Yin, C. *et al.* CXCL5 activates CXCR2 in nociceptive sensory neurons to drive joint pain and inflammation in experimental gouty arthritis. *Nat Commun* **15**, 3263 (2024).

128. Marsland, B. J. *et al.* CCL19 and CCL21 induce a potent proinflammatory differentiation program in licensed dendritic cells. *Immunity* **22**, 493–505 (2005).

129. Nakatsuji, T. & Gallo, R. L. The role of the skin microbiome in atopic dermatitis. *Ann Allergy Asthma Immunol* **122**, 263 (2018).

130. Williams, M. R. & Gallo, R. L. Evidence that Human Skin Microbiome Dysbiosis Promotes Atopic Dermatitis. *J Invest Dermatol* **137**, 2460 (2017).

131. Kim, Y. J. *et al.* Topical administration of EGF suppresses immune response and protects skin barrier in DNCB-induced atopic dermatitis in NC/Nga mice. *Scientific Reports 2018 8:1* **8**, 1–11 (2018).

132. Wang, T. *et al.* Secreted protease PRSS35 suppresses hepatocellular carcinoma by disabling CXCL2-mediated neutrophil extracellular traps. *Nature Communications 2023 14:1* **14**, 1513- (2023).

133. Michifuri, Y. *et al.* Small proline-rich protein-1B is overexpressed in human oral squamous cell cancer stem-like cells and is related to their growth through activation of MAP kinase signal. *Biochem Biophys Res Commun* **439**, 96–102 (2013).

134. Wan, Z., Wang, W., Peng, S. & Zhao, X. Assessing the role of LRRCl5 as a prognostic and therapeutic biomarker in glioblastoma. *Am J Transl Res* **17**, 6522–6541 (2025).

135. Averill, M. M., Kerkhoff, C. & Bornfeldt, K. E. S100A8 and S100A9 in Cardiovascular Biology and Disease. *Arterioscler Thromb Vasc Biol* **32**, 223 (2011).

136. Wang, S. *et al.* S100A8/A9 in inflammation. *Front Immunol* **9**, 371351 (2018).

137. Vlad, M. L. *et al.* Therapeutic S100A8/A9 inhibition reduces NADPH oxidase expression, reactive oxygen species production and NLRP3 inflammasome priming in the ischemic myocardium. *Eur J Pharmacol* **996**, (2025).

138. Zhou, H., Zhao, C., Shao, R., Xu, Y. & Zhao, W. The functions and regulatory pathways of S100A8/A9 and its receptors in cancers. *Front Pharmacol* **14**, 1187741 (2023).

139. Kim, M. J. *et al.* Effect of S100A8 and S100A9 on expressions of cytokine and skin barrier protein in human keratinocytes. *Mol Med Rep* **20**, 2476–2483 (2019).

140. Foti, C. *et al.* Allergic contact dermatitis with a fertilizer containing hydrogen cyanamide (Dormex). *Cutan Ocul Toxicol* **27**, 1–3 (2008).

141. Zundell, M. P., Gottlieb, A. B. & Stanger, R. Atopic Dermatitis as a Paradoxical Reaction to Secukinumab in a Patient With Plaque Psoriasis. *J Drugs Dermatol* **23**, 97–99 (2024).

142. Vijayan, S. *et al.* Probiotics in Allergy and Immunological Diseases: A Comprehensive Review. *Cureus* **16**, e55817 (2024).

143. Ruffell, D. *et al.* A CREB-C/EBPβ cascade induces M2 macrophage-specific gene expression and promotes muscle injury repair. *Proc Natl Acad Sci U S A* **106**, 17475–17480 (2009).

144. Wauman, J., De Ceuninck, L., Vanderroost, N., Lievens, S. & Tavernier, J. RNF41 (Nrdp1) controls type 1 cytokine receptor degradation and ectodomain shedding. *J Cell Sci* **124**, 921 (2011).

145. Zhang, Y. *et al.* CCDC71L as a novel prognostic marker and immunotherapy target via lipid metabolism in head and neck squamous cell carcinoma. *J Stomatol Oral Maxillofac Surg* **125**, (2024).

146. Paul, T. *et al.* Cytokine regulation by epidermal growth factor receptor inhibitors and epidermal growth factor receptor inhibitor associated skin toxicity in cancer patients. *Eur J Cancer* **50**, 1855–1863 (2014).

147. Orang, A. *et al.* Basonuclin-2 regulates extracellular matrix production and degradation. *Life Sci Alliance* **6**, e202301984 (2023).

148. Kiselev, A. & Park, S. Immune niches for hair follicle development and homeostasis. *Front Physiol* **15**, 1397067 (2024).

149. Mandal, A. & Drerup, C. M. Axonal Transport and Mitochondrial Function in Neurons. *Front Cell Neurosci* **13**, 373 (2019).

150. Xu, M. *et al.* WNT10A mutation causes ectodermal dysplasia by impairing progenitor cell proliferation and KLF4-mediated differentiation. *Nature Communications 2017 8:1* **8**, 15397- (2017).

151. Fusco, W. *et al.* Short-Chain Fatty-Acid-Producing Bacteria: Key Components of the Human Gut Microbiota. *Nutrients* **15**, 2211 (2023).

152. Fan, Z. *et al.* Fusobacterium nucleatum and its associated systemic diseases: epidemiologic studies and possible mechanisms. *J Oral Microbiol* **15**, 2145729 (2022).

153. Binda, C. *et al.* Actinobacteria: A relevant minority for the maintenance of gut homeostasis. *Digestive and Liver Disease* **50**, 421–428 (2018).

154. Moon, C. D., Young, W., Maclean, P. H., Cookson, A. L. & Bermingham, E. N. Metagenomic insights into the roles of Proteobacteria in the gastrointestinal microbiomes of healthy dogs and cats. *Microbiologyopen* **7**, e00677 (2018).

155. Rajput, M. *et al.* Determining the association between gut microbiota and its metabolites with higher intestinal Immunoglobulin A response. *Vet Anim Sci* **19**, 100279 (2022).

156. Riaz, B. & Sohn, S. Neutrophils in Inflammatory Diseases: Unraveling the Impact of Their Derived Molecules and Heterogeneity. *Cells* **12**, 2621 (2023).

157. Fania, L. *et al.* Multiple Roles for Cytokines in Atopic Dermatitis: From Pathogenic Mediators to Endotype-Specific Biomarkers to Therapeutic Targets. *Int J Mol Sci* **23**, 2684 (2022).

158. Morishita, M. *et al.* Characterizing Different Probiotic-Derived Extracellular Vesicles as a Novel Adjuvant for Immunotherapy. *Mol Pharm* **18**, 1080–1092 (2021).

159. Hu, H. qi *et al.* Yinqiao antipruritic formula attenuates atopic dermatitis-like skin lesions through modulating the cytokine-cytokine receptor interaction pathway. *Fitoterapia* **183**, 106529 (2025).

160. Oh, J. H. *et al.* Purpurin suppresses atopic dermatitis via TNF-α/IFN-γ-induced inflammation in HaCaT cells. *Int J Immunopathol Pharmacol* **36**, 03946320221111135 (2022).

161. Sugaya, M. The Role of Th17-Related Cytokines in Atopic Dermatitis. *International Journal of Molecular Sciences 2020, Vol. 21, Page 1314* **21**, 1314 (2020).

162. Mills, K. H. G. IL-17 and IL-17-producing cells in protection versus pathology. *Nature Reviews Immunology 2022 23:1* **23**, 38–54 (2022).

163. Sánchez-Rodríguez, G. & Puig, L. Pathogenic Role of IL-17 and Therapeutic Targeting of IL-17F in Psoriatic Arthritis and Spondyloarthropathies. *Int J Mol Sci* **24**, 10305 (2023).

164. Shen, F. *et al.* IL-17 receptor signaling inhibits C/EBPb by sequential phosphorylation of the regulatory 2 domain. *Sci Signal* **2**, (2009).

165. Li, J. K. *et al.* IL-17 mediates inflammatory reactions via p38/c-Fos and JNK/c-Jun activation in an AP-1-dependent manner in human nucleus pulposus cells. *J Transl Med* **14**, 1–10 (2016).

166. Chiang, C. C. *et al.* Neutrophils in Atopic Dermatitis. *Clin Rev Allergy Immunol* **67**, 21 (2024).

167. Shibuya, R. *et al.* CCL2–CCR2 Signaling in the Skin Drives Surfactant-Induced Irritant Contact Dermatitis through IL-1β–Mediated Neutrophil Accumulation. *Journal of Investigative Dermatology* **142**, 571-582.e9 (2022).

168. Vestergaard, C., Just, H., Baumgartner Nielsen, J., Thestrup-Pedersen, K. & Deleuran, M. Expression of CCR2 on monocytes and macrophages in chronically inflamed skin in atopic dermatitis and psoriasis. *Acta Derm Venereol* **84**, 353–358 (2004).

1. Postler, T. S. & Ghosh, S. Understanding the Holobiont: How microbial metabolites affect human health and shape the immune system. *Cell Metab* **26**, 110 (2017).

2. Mohammad, I. *et al.* Beyond Digestion: The Gut Microbiota as an Immune–Metabolic Interface in Disease Modulation. *Gastrointestinal Disorders 2025, Vol. 7,* **7**, (2025).

3. Ibrahem, K. H. The Role of Probiotics in Human Health: A Review. *Sana'a University Journal of Medicine and Health Sciences* **19**, 232–238 (2025).

4. Abeltino, A. *et al.* Unraveling the Gut Microbiota: Implications for Precision Nutrition and Personalized Medicine. *Nutrients* **16**, 100497 (2024).

5. Fuller, R. History and development of probiotics. *Probiotics* 1–8 (1992) doi:10.1007/978-94-011-2364-8_1.

6. Probiotics - International Scientific Association for Probiotics and Prebiotics (ISAPP). https://isappscience.org/topic/probiotics/.

7. Probiotics - International Scientific Association for Probiotics and Prebiotics (ISAPP). https://isappscience.org/topic/probiotics/.

8. Meena, K. K., Joshi, M., Gupta, L. & Meena, S. Comprehensive insights into postbiotics: Bridging the gap to real-world application. *Food Nutrition* **1**, 100024 (2025).

9. Latif, A. *et al.* Probiotics: mechanism of action, health benefits and their application in food industries. *Front Microbiol* **14**, 1216674 (2023).

10. Vijayaram, S. *et al.* Probiotics: A multifaceted approach to health promotion-from disease prevention to food enrichment and delivery systems. *AIMS Microbiol* **11**, 602 (2025).

11. Harnvoravongchai, P. *et al.* Gut commensal Bifidobacterium longum confers resistance to Salmonella Typhimurium and Shigella flexneri in a Caenorhabditis elegans model. *Microbiol Spectr* **14**, e01842-25 (2025).

12. Strain, R., Stanton, C. & Ross, R. P. Effect of diet on pathogen performance in the microbiome. *Microbiome Research Reports* **1**, 13 (2022).

13. Louis, P., Duncan, S. H., Sheridan, P. O., Walker, A. W. & Flint, H. J. Microbial lactate utilisation and the stability of the gut microbiome. *Gut Microbiome* **3**, e3 (2022).

14. Pinhal, S., Ropers, D., Geiselmann, J. & De Jong, H. Acetate Metabolism and the Inhibition of Bacterial Growth by Acetate. *J Bacteriol* **201**, e00147-19 (2019).

15. Martinez, F. A. C., Balciunas, E. M., Converti, A., Cotter, P. D. & De Souza Oliveira, R. P. Bacteriocin production by Bifidobacterium spp. A review. *Biotechnol Adv* **31**, 482–488 (2013).

16. Gavzy, S. J. *et al.* Bifidobacterium mechanisms of immune modulation and tolerance. *Gut Microbes* **15**, 2291164 (2023).

17. Lee, S. *et al.* Peptidoglycan from Bifidobacterium adolescentis enhances IL-10 production in regulatory B cells to alleviate gut inflammation. *Gut Microbes* **18**, 2611603 (2026).

18. Zhang, W., Mackay, C. R. & Gershwin, M. E. Immunomodulatory Effects of Microbiota-derived Short-Chain Fatty Acids in Autoimmune Liver Diseases. *J Immunol* **210**, 1629 (2023).

19. Abdulqadir, R., Engers, J. & Al-Sadi, R. Role of Bifidobacterium in Modulating the Intestinal Epithelial Tight Junction Barrier: Current Knowledge and Perspectives. *Curr Dev Nutr* **7**, 102026 (2023).

20. Terahara, M. *et al.* Effects of the intake of non-live Bifidobacterium bifidum on the faecal IgA of full-term infants: a double-blind, randomised, placebo-controlled study. *Biosci Microbiota Food Health* **40**, 196 (2021).

21. Furuyama, N. & Sircili, M. P. Outer Membrane Vesicles (OMVs) Produced by Gram-Negative Bacteria: Structure, Functions, Biogenesis, and Vaccine Application. *Biomed Res Int* **2021**, 1490732 (2021).

22. Li, Q. *et al.* Specific labeling of outer membrane vesicles with antibiotic-conjugated probe reveals early bacterial infections in blood. *Nature Communications 2025 16:1* **16**, 1–14 (2025).

23. Avila-Calderón, E. D. *et al.* Outer Membrane Vesicles of Gram-Negative Bacteria: An Outlook on Biogenesis. *Front Microbiol* **12**, 557902 (2021).

24. Kim, J. Y. *et al.* Gram-Negative Bacteria's Outer Membrane Vesicles. *Infect Chemother* **55**, 1 (2023).

25. Yang, J., Shin, T. S., Kim, J. S., Jee, Y. K. & Kim, Y. K. A new horizon of precision medicine: combination of the microbiome and extracellular vesicles. *Experimental & Molecular Medicine 2022 54:4* **54**, 466–482 (2022).

26. Li, Y. *et al.* Probiotic extracellular vesicles reprogram macrophage immunometabolism: From gut crosstalk to host health. *Gut Microbes* **18**, 2614115 (2026).

27. Domínguez Rubio, A. P., D'Antoni, C. L., Piuri, M. & Pérez, O. E. Probiotics, Their Extracellular Vesicles and Infectious Diseases. *Front Microbiol* **13**, 864720 (2022).

28. Wang, G., Wang, Y., Sheng, K. & Wang, Y. Effect of probiotic extracellular vesicles and their applications on health and disease. *J Sci Food Agric* **105**, 3539–3549 (2025).

29. Nishiyama, K. *et al.* Extracellular vesicles produced by Bifidobacterium longum export mucin-binding proteins. *Appl Environ Microbiol* **86**, (2020).

30. Domínguez Rubio, A. P., D'Antoni, C. L., Piuri, M. & Pérez, O. E. Probiotics, Their Extracellular Vesicles and Infectious Diseases. *Front Microbiol* **13**, 864720 (2022).

31. Morishita, M. *et al.* Activation of Host Immune Cells by Probiotic-Derived Extracellular Vesicles via TLR2-Mediated Signaling Pathways. *Biol Pharm Bull* **45**, 354–359 (2022).

32. Kim, W. *et al.* Lactobacillus plantarum-derived extracellular vesicles induce anti-inflammatory M2 macrophage polarization in vitro. *J Extracell Vesicles* **9**, 1793514 (2020).

33. López, P. *et al.* Treg-inducing membrane vesicles from Bifidobacterium bifidum LMG13195 as potential adjuvants in immunotherapy. *Vaccine* **30**, 825–829 (2012).

34. Yang, L. & Xia, J.-N. Beyond the Skin: Exploring the Gut-Skin Axis and Metabolic Pathways in Atopic Dermatitis Pathogenesis. *Int J Gen Med* **18**, 6123 (2025).

35. Kim, G. Il *et al.* Interconnection of the Gut-Skin Axis in NC/Nga Mouse with Atopic Dermatitis: Effects of the Three Types of Bifidobacterium bifidum CBT-BF3 (Probiotics, Postbiotics, and Cytosine-Phosphate-Guanine Oligodeoxynucleotide) on T Cell Differentiation and Gut Mi…. *Food Sci Anim Resour* **44**, 1417–1439 (2024).

36. Fang, Z. *et al.* Bifidobacterium longum mediated tryptophan metabolism to improve atopic dermatitis via the gut-skin axis. *Gut Microbes* **14**, 2044723 (2022).

37. Compliance Guide for Probiotic Food Products in China - ZMUni Compliance Centre. https://www.zmuni.com/en/news/complianceguideforprobioticfoodproductsinchina/ .

38. Principles for Safety Assessment of Novel Food Ingredients | ChemLinked. https://food.chemlinked.com/database/view/6755.

39. Part V (Food and Drugs) of the Public Health and Municipal Services Ordinance (Cap. 132) (Highlights). https://www.cfs.gov.hk/english/food_leg/food_leg_list.html.

40. Jun, S. H. *et al.* Staphylococcus aureus-derived membrane vesicles exacerbate skin inflammation in atopic dermatitis. *Clinical & Experimental Allergy* **47**, 85–96 (2017).

41. Wakarera, P. W., Ojola, P. & Njeru, E. M. Characterization and diversity of native Azotobacter spp. isolated from semi-arid agroecosystems of Eastern Kenya. *Biol Lett* **18**, (2022).

42. Abdelazez, A. *et al.* Verification of Lactobacillus brevis tolerance to simulated gastric juice and the potential effects of postbiotic gamma-aminobutyric acid in streptozotocin-induced diabetic mice. *Food Science and Human Wellness* **11**, 165–176 (2022).

43. Yadav, M. K. & Tiwari, S. K. Methods for Determination of Antimicrobial Activity of Bacteriocins of Lactic Acid Bacteria. *Microbiology 2023 92:6* **92**, 745–765 (2023).

44. Wongvibulsin, S. *et al.* Transcriptomic analysis of atopic dermatitis in African Americans is characterized by Th2/Th17-centered cutaneous immune activation. *Scientific Reports 2021 11:1* **11**, 1–11 (2021).

45. Cheung, M. K. *et al.* Development of the early-life gut microbiome and associations with eczema in a prospective Chinese cohort. *mSystems* **8**, (2023).

46. Pessemier, B. De *et al.* Gut–skin axis: Current knowledge of the interrelationship between microbial dysbiosis and skin conditions. *Microorganisms* **9**, 1–33 (2021).

47. Jeong, S. Factors influencing development of the infant microbiota: from prenatal period to early infancy. *Clin Exp Pediatr* **65**, 438 (2022).

48. Black, M. & Bhattacharya, S. Cesarean section in China, Taiwan, and Hong Kong—A safe choice for women and clinicians? *PLoS Med* **15**, (2018).

49. Chung, W. H., Kong, C. W. & To, W. W. K. Secular trends in caesarean section rates over 20 years in a regional obstetric unit in Hong Kong. *Hong Kong Medical Journal* **23**, 340–348 (2017).

50. Makino, H. *et al.* Mother-to-infant transmission of intestinal bifidobacterial strains has an impact on the early development of vaginally delivered infant's microbiota. *PLoS One* **8**, (2013).

51. Liu, Q., Jing, W. & Wang, W. Bifidobacterium lactis Ameliorates the Risk of Food Allergy in Chinese Children by Affecting Relative Percentage of Treg and Th17 Cells. *Canadian Journal of Infectious Diseases and Medical Microbiology* **2018**, (2018).

52. Pantazi, A. C. *et al.* Relationship between Gut Microbiota and Allergies in Children: A Literature Review. *Nutrients* **15**, (2023).

53. Yu, L. *et al.* Comparison of Gut Microbiota Between Infants with Atopic Dermatitis and Healthy Controls in Guangzhou, China. *J Asthma Allergy* **14**, 493–500 (2021).

54. Dattner, A. M. Breastfeeding and atopic dermatitis: protective or harmful? facts and controversies. *Clin Dermatol* **28**, 34–37 (2010).

55. Kim, J. H. Role of Breast-feeding in the Development of Atopic Dermatitis in Early Childhood. *Allergy Asthma Immunol Res* **9**, 285 (2017).

56. Enomoto, T. *et al.* Effects of Bifidobacterial Supplementation to Pregnant Women and Infants in the Prevention of Allergy Development in Infants and on Fecal Microbiota. *Allergology International* **63**, 575–585 (2014).

57. Freitas, A. C. & Hill, J. E. Bifidobacteria isolated from vaginal and gut microbiomes are indistinguishable by comparative genomics. *PLoS One* **13**, e0196290 (2018).

58. Matera, M. Bifidobacteria, Lactobacilli... when, how and why to use them. *Global Pediatrics* **8**, 100139 (2024).

59. Bakshani, C. R. & Crouch, L. I. Human milk oligosaccharides and Bifidobacterium species. *Trends Microbiol* **32**, 118–119 (2024).

60. Laursen, M. F. & Roager, H. M. Human milk oligosaccharides modify the strength of priority effects in the Bifidobacterium community assembly during infancy. *The ISME Journal 2023 17:12* **17**, 2452–2457 (2023).

61. Nishiyama, K. *et al.* Bifidobacterium bifidum Extracellular Sialidase Enhances Adhesion to the Mucosal Surface and Supports Carbohydrate Assimilation. *mBio* **8**, (2017).

62. Pan, K., Zhang, C. & Tian, J. The Effects of Different Modes of Delivery on the Structure and Predicted Function of Intestinal Microbiota in Neonates and Early Infants. *Pol J Microbiol* **70**, 45–55 (2021).

63. Long, G. *et al.* The Influence of Cesarean Section on the Composition and Development of Gut Microbiota During the First 3 Months of Life. *Front Microbiol* **12**, (2021).

64. Gila-Diaz, A. *et al.* A Review of Bioactive Factors in Human Breastmilk: A Focus on Prematurity. *Nutrients* **11**, (2019).

65. Saturio, S. *et al.* Role of Bifidobacteria on Infant Health. *Microorganisms* **9**, (2021).

66. Xiao, M. *et al.* Cross-feeding of bifidobacteria promotes intestinal homeostasis: a lifelong perspective on the host health. *NPJ Biofilms Microbiomes* **10**, 47 (2024).

67. Arboleya, S., Watkins, C., Stanton, C. & Ross, R. P. Gut Bifidobacteria Populations in Human Health and Aging. *Front Microbiol* **7**, (2016).

68. Tarracchini, C. *et al.* Phylogenomic disentangling of the Bifidobacterium longum subsp. infantis taxon. *Microb Genom* **7**, 000609 (2021).

69. Turroni, F. *et al.* Bifidobacterium bifidum: A Key Member of the Early Human Gut Microbiota. *Microorganisms* **7**, (2019).

70. Westermann, C., Gleinser, M., Corr, S. C. & Riedel, C. U. A critical evaluation of bifidobacterial adhesion to the host tissue. *Front Microbiol* **7**, 211780 (2016).

71. Fekete, E. E. *et al.* Multilevel Proteomic Profiling of Colorectal Adenocarcinoma Caco-2 Cell Differentiation to Characterize an Intestinal Epithelial Model. *J Proteome Res* **23**, 2561–2575 (2024).

72. Akhtar, M. *et al.* Gut microbiota-derived short chain fatty acids are potential mediators in gut inflammation. *Animal Nutrition* **8**, 350–360 (2022).

73. Fukuda, S., Toh, H., Taylor, T. D., Ohno, H. & Hattori, M. Acetate-producing bifidobacteria protect the host from enteropathogenic infection via carbohydrate transporters. *Gut Microbes* **3**, 449–454 (2012).

74. Li, T. *et al.* Bifidobacterium animalis subsp. lactis A12 prevents obesityassociated dyslipidemia by modulating gut microbiota-derived short-chain

fatty acid production and energy metabolism in high-fat diet-fed mice. *Food Nutr Res* **66**, 8670 (2022).

75. Hodgkinson, K. *et al.* Butyrate's role in human health and the current progress towards its clinical application to treat gastrointestinal disease. *Clinical Nutrition* **42**, 61–75 (2023).

76. Rekha, K. *et al.* Short-chain fatty acid: An updated review on signaling, metabolism, and therapeutic effects. *Crit Rev Food Sci Nutr* **64**, 2461–2489 (2024).

77. Chen, S. *et al.* Macrophages in immunoregulation and therapeutics. *Signal Transduction and Targeted Therapy 2023 8:1* **8**, 207- (2023).

78. Piewngam, P. & Otto, M. Staphylococcus aureus colonisation and strategies for decolonisation. *Lancet Microbe* **5**, e606–e618 (2024).

79. Bennett, R. W., Hait, J. M. & Tallent, S. M. Staphylococcus aureus Infection. *Guide to Foodborne Pathogens, Second Edition* 26–44 (2025) doi:10.1002/9781118684856.ch2.

80. Chen, H. *et al.* Exploring the Role of Staphylococcus aureus in Inflammatory Diseases. *Toxins (Basel)* **14**, (2022).

81. Tartaglia, N. R. *et al.* Staphylococcus aureus extracellular vesicles elicit an immunostimulatory response in vivo on the murine mammary gland. *Front Cell Infect Microbiol* **8**, 393646 (2018).

82. Hong, S. W. *et al.* Extracellular vesicles derived from Staphylococcus aureus induce atopic dermatitis-like skin inflammation. *Allergy* **66**, 351 (2011).

83. Hong, S. W. *et al.* Extracellular vesicles derived from Staphylococcus aureus induce atopic dermatitis-like skin inflammation. *Allergy* **66**, 351 (2011).

84. Viegas, C., Seck, F. & Fonte, P. An insight on lipid nanoparticles for therapeutic proteins delivery. *J Drug Deliv Sci Technol* **77**, 103839 (2022).

85. Mazumdar, S., Chitkara, D. & Mittal, A. Exploration and insights into the cellular internalization and intracellular fate of amphiphilic polymeric nanocarriers. *Acta Pharm Sin B* **11**, 903–924 (2021).

86. Dell'Atti, F. *et al.* Probiotic-derived extracellular vesicles: the next breakthrough in postbiotics for rheumatoid arthritis. *Front Immunol* **16**, 1620185 (2025).

87. Wang, Y., Duan, C. & Yu, X. Extracellular vesicles of Gram-negative and Gram-positive probiotics. *Journal of Microbiology* **63**, e2506005 (2025).

88. Lee, K. S. *et al.* Human Probiotic Lactobacillus paracasei-Derived Extracellular Vesicles Improve Tumor Necrosis Factor-α-Induced Inflammatory Phenotypes in Human Skin. *Cells* **12**, 2789 (2023).

89. Wendel, U. Assessing Viability and Stress Tolerance of Probiotics—A Review. *Front Microbiol* **12**, (2021).

90. Bustos, A. Y., Saavedra, L., de Valdez, G. F., Raya, R. R. & Taranto, M. P. Relationship between bile salt hydrolase activity, changes in the internal pH and tolerance to bile acids in lactic acid bacteria. *Biotechnol Lett* **34**, 1511–1518 (2012).

91. Gorreja, F. & Walker, W. A. The potential role of adherence factors in probiotic function in the gastrointestinal tract of adults and pediatrics: a narrative review of experimental and human studies. *Gut Microbes* **14**, 2149214 (2022).

92. Collado, M. C., Gueimonde, M., Sanz, Y. & Salminen, S. Adhesion properties and competitive pathogen exclusion ability of bifidobacteria with acquired acid resistance. *J Food Prot* **69**, 1675–1679 (2006).

93. Yu, D. *et al.* Bifidobacterium longum subsp. infantis as widespread bacteriocin gene clusters carrier stands out among the Bifidobacterium. *Appl Environ Microbiol* **89**, (2023).

94. Cheikhyoussef, A. *et al.* COMPARISON OF THREE DIFFERENT METHODS FOR THE ISOLATION OF BACTERIOCIN-LIKE INHIBITORY SUBSTANCES FROM BIFIDOBACTERIUM INFANTIS BCRC 14602. *J Rapid Methods Autom Microbiol* **17**, 182–194 (2009).

95. Kim, M. H. *et al.* Lactobacillus plantarum-derived Extracellular Vesicles Protect Atopic Dermatitis Induced by Staphylococcus aureus-derived Extracellular Vesicles. *Allergy Asthma Immunol Res* **10**, 516 (2018).

96. Kim, M. R. *et al.* Staphylococcus aureus-derived extracellular vesicles induce neutrophilic pulmonary inflammation via both Th1 and Th17 cell responses. *Allergy* **67**, 1271–1281 (2012).

97. Kolb, L. & Ferrer-Bruker, S. J. Atopic Dermatitis. *StatPearls* https://www.ncbi.nlm.nih.gov/books/NBK448071/ (2023).

98. Mohd Kasim, V. N. K. *et al.* Management of Atopic Dermatitis Via Oral and Topical Administration of Herbs in Murine Model: A Systematic Review. *Front Pharmacol* **13**, 785782 (2022).

99. Fania, L. *et al.* Multiple Roles for Cytokines in Atopic Dermatitis: From Pathogenic Mediators to Endotype-Specific Biomarkers to Therapeutic Targets. *Int J Mol Sci* **23**, 2684 (2022).

100. Chong, A. C., Visitsunthorn, K. & Ong, P. Y. Genetic/Environmental Contributions and Immune Dysregulation in Children with Atopic Dermatitis. *J Asthma Allergy* **15**, 1681 (2022).

101. Hong, S. W. *et al.* Extracellular vesicles derived from Staphylococcus aureus induce atopic dermatitis-like skin inflammation. *Allergy* **66**, 351–359 (2011).

102. Gehrke, A. K. E., Giai, C. & Gómez, M. I. Staphylococcus aureus Adaptation to the Skin in Health and Persistent/Recurrent Infections. *Antibiotics* **12**, 1520 (2023).

103. Kengmo Tchoupa, A. & Peschel, A. Staphylococcus aureus Releases Proinflammatory Membrane Vesicles To Resist Antimicrobial Fatty Acids. *mSphere* **5**, (2020).

104. Tartaglia, N. R. *et al.* Staphylococcus aureus extracellular vesicles elicit an immunostimulatory response in vivo on the murine mammary gland. *Front Cell Infect Microbiol* **8**, 393646 (2018).

105. Jun, S. H. *et al.* Staphylococcus aureus-derived membrane vesicles exacerbate skin inflammation in atopic dermatitis. *Clinical & Experimental Allergy* **47**, 85–96 (2016).

106. Pinchuk, I. V., Beswick, E. J. & Reyes, V. E. Staphylococcal Enterotoxins. *Toxins (Basel)* **2**, 2177 (2010).

107. Roan, F., Obata-Ninomiya, K. & Ziegler, S. F. Epithelial cell-derived cytokines: more than just signaling the alarm. *J Clin Invest* **129**, 1441–1451 (2019).

108. Fujii, Y., Takeuchi, H., Sakuma, S., Sengoku, T. & Takakura, S. Characterization of a 2,4-dinitrochlorobenzene-induced chronic dermatitis model in rats. *Skin Pharmacol Physiol* **22**, 240–247 (2009).

109. Lu, C. *et al.* Inhibition of macrophage MAPK/NF-κB pathway and Th2 axis by mangiferin ameliorates MC903-induced atopic dermatitis. *Int Immunopharmacol* **133**, 112038 (2024).

110. Mohd Kasim, V. N. K. *et al.* Oral and topical administration of a geranyl acetophenone attenuates DNCB-induced atopic dermatitis-like skin lesions in BALB/c mice. *Scientific Reports 2024 14:1* **14**, 1–13 (2024).

111. Zhang, E. Y., Chen, A. Y. & Zhu, B. T. Mechanism of Dinitrochlorobenzene-Induced Dermatitis in Mice: Role of Specific Antibodies in Pathogenesis. *PLoS One* **4**, e7703 (2009).

112. Park, N. J. *et al.* Lobelia chinensis Extract and Its Active Compound, Diosmetin, Improve Atopic Dermatitis by Reinforcing Skin Barrier Function through SPINK5/LEKTI Regulation. *Int J Mol Sci* **23**, (2022).

113. Das, P. *et al.* Keratinocytes: An Enigmatic Factor in Atopic Dermatitis. *Cells 2022, Vol. 11, Page 1683* **11**, 1683 (2022).

114. Ryu, B. *et al.* Anti-Inflammatory Effects of M-MSCs in DNCB-Induced Atopic Dermatitis Mice. *Biomedicines* **8**, 439 (2020).

115. Hong, S. W. *et al.* An Important Role of α-Hemolysin in Extracellular Vesicles on the Development of Atopic Dermatitis Induced by Staphylococcus aureus. *PLoS One* **9**, e100499 (2014).

116. Heimall, J. & Spergel, J. M. New pathways for itching in patients with atopic dermatitis? *Journal of Allergy and Clinical Immunology* **140**, 393–394 (2017).

117. Gęgotek, A. & Skrzydlewska, E. The Role of ABC Transporters in Skin Cells Exposed to UV Radiation. *Int J Mol Sci* **24**, 115 (2022).

118. Joshi, B. S., de Beer, M. A., Giepmans, B. N. G. & Zuhorn, I. S. Endocytosis of Extracellular Vesicles and Release of Their Cargo from Endosomes. *ACS Nano* **14**, 4444–4455 (2020).

119. Girolomoni, G. *et al.* Nomenclature and clinical phenotypes of atopic dermatitis. *Ther Adv Chronic Dis* **12**, 20406223211002980 (2021).

120. Langan, S. M., Irvine, A. D. & Weidinger, S. Atopic dermatitis. *The Lancet* **396**, 345–360 (2020).

121. Park, K. D., Pak, S. C. & Park, K. K. The Pathogenetic Effect of Natural and Bacterial Toxins on Atopic Dermatitis. *Toxins 2017, Vol. 9, Page 3* **9**, 3 (2016).

122. Criado, P. R. *et al.* Update on the pathogenesis of atopic dermatitis. *An Bras Dermatol* **99**, 895–915 (2024).

123. Han, S. C. *et al.* 3-Bromo-4,5-dihydroxybenzaldehyde Attenuates Allergic Contact Dermatitis by Generating CD4+Foxp3+ T cells. *In Vivo (Brooklyn)* **39**, 201–209 (2025).

124. Tsunemi, Y. *et al.* CCL17 transgenic mice show an enhanced Th2-type response to both allergic and non-allergic stimuli. *Eur J Immunol* **36**, 2116–2127 (2006).

125. Zhu, J., Guo, L., Watson, C. J., Hu-Li, J. & Paul, W. E. Stat6 is necessary and sufficient for IL-4's role in Th2 differentiation and cell expansion. *J Immunol* **166**, 7276–7281 (2001).

126. Celik, M., Labuz, D., Keye, J., Glauben, R. & Machelska, H. IL-4 induces M2 macrophages to produce sustained analgesia via opioids. *JCI Insight* **5**, e133093 (2020).

127. Yin, C. *et al.* CXCL5 activates CXCR2 in nociceptive sensory neurons to drive joint pain and inflammation in experimental gouty arthritis. *Nat Commun* **15**, 3263 (2024).

128. Marsland, B. J. *et al.* CCL19 and CCL21 induce a potent proinflammatory differentiation program in licensed dendritic cells. *Immunity* **22**, 493–505 (2005).

129. Nakatsuji, T. & Gallo, R. L. The role of the skin microbiome in atopic dermatitis. *Ann Allergy Asthma Immunol* **122**, 263 (2018).

130. Williams, M. R. & Gallo, R. L. Evidence that Human Skin Microbiome Dysbiosis Promotes Atopic Dermatitis. *J Invest Dermatol* **137**, 2460 (2017).

131. Kim, Y. J. *et al.* Topical administration of EGF suppresses immune response and protects skin barrier in DNCB-induced atopic dermatitis in NC/Nga mice. *Scientific Reports 2018 8:1* **8**, 1–11 (2018).

132. Wang, T. *et al.* Secreted protease PRSS35 suppresses hepatocellular carcinoma by disabling CXCL2-mediated neutrophil extracellular traps. *Nature Communications 2023 14:1* **14**, 1513- (2023).

133. Michifuri, Y. *et al.* Small proline-rich protein-1B is overexpressed in human oral squamous cell cancer stem-like cells and is related to their growth through activation of MAP kinase signal. *Biochem Biophys Res Commun* **439**, 96–102 (2013).

134. Wan, Z., Wang, W., Peng, S. & Zhao, X. Assessing the role of LRRCl5 as a prognostic and therapeutic biomarker in glioblastoma. *Am J Transl Res* **17**, 6522–6541 (2025).

135. Averill, M. M., Kerkhoff, C. & Bornfeldt, K. E. S100A8 and S100A9 in Cardiovascular Biology and Disease. *Arterioscler Thromb Vasc Biol* **32**, 223 (2011).

136. Wang, S. *et al.* S100A8/A9 in inflammation. *Front Immunol* **9**, 371351 (2018).

137. Vlad, M. L. *et al.* Therapeutic S100A8/A9 inhibition reduces NADPH oxidase expression, reactive oxygen species production and NLRP3 inflammasome priming in the ischemic myocardium. *Eur J Pharmacol* **996**, (2025).

138. Zhou, H., Zhao, C., Shao, R., Xu, Y. & Zhao, W. The functions and regulatory pathways of S100A8/A9 and its receptors in cancers. *Front Pharmacol* **14**, 1187741 (2023).

139. Kim, M. J. *et al.* Effect of S100A8 and S100A9 on expressions of cytokine and skin barrier protein in human keratinocytes. *Mol Med Rep* **20**, 2476–2483 (2019).

140. Foti, C. *et al.* Allergic contact dermatitis with a fertilizer containing hydrogen cyanamide (Dormex). *Cutan Ocul Toxicol* **27**, 1–3 (2008).

141. Zundell, M. P., Gottlieb, A. B. & Stanger, R. Atopic Dermatitis as a Paradoxical Reaction to Secukinumab in a Patient With Plaque Psoriasis. *J Drugs Dermatol* **23**, 97–99 (2024).

142. Vijayan, S. *et al.* Probiotics in Allergy and Immunological Diseases: A Comprehensive Review. *Cureus* **16**, e55817 (2024).

143. Ruffell, D. *et al.* A CREB-C/EBPβ cascade induces M2 macrophage-specific gene expression and promotes muscle injury repair. *Proc Natl Acad Sci U S A* **106**, 17475–17480 (2009).

144. Wauman, J., De Ceuninck, L., Vanderroost, N., Lievens, S. & Tavernier, J. RNF41 (Nrdp1) controls type 1 cytokine receptor degradation and ectodomain shedding. *J Cell Sci* **124**, 921 (2011).

145. Zhang, Y. *et al.* CCDC71L as a novel prognostic marker and immunotherapy target via lipid metabolism in head and neck squamous cell carcinoma. *J Stomatol Oral Maxillofac Surg* **125**, (2024).

146. Paul, T. *et al.* Cytokine regulation by epidermal growth factor receptor inhibitors and epidermal growth factor receptor inhibitor associated skin toxicity in cancer patients. *Eur J Cancer* **50**, 1855–1863 (2014).

147. Orang, A. *et al.* Basonuclin-2 regulates extracellular matrix production and degradation. *Life Sci Alliance* **6**, e202301984 (2023).

148. Kiselev, A. & Park, S. Immune niches for hair follicle development and homeostasis. *Front Physiol* **15**, 1397067 (2024).

149. Mandal, A. & Drerup, C. M. Axonal Transport and Mitochondrial Function in Neurons. *Front Cell Neurosci* **13**, 373 (2019).

150. Xu, M. *et al.* WNT10A mutation causes ectodermal dysplasia by impairing progenitor cell proliferation and KLF4-mediated differentiation. *Nature Communications 2017 8:1* **8**, 15397- (2017).

151. Fusco, W. *et al.* Short-Chain Fatty-Acid-Producing Bacteria: Key Components of the Human Gut Microbiota. *Nutrients* **15**, 2211 (2023).

152. Fan, Z. *et al.* Fusobacterium nucleatum and its associated systemic diseases: epidemiologic studies and possible mechanisms. *J Oral Microbiol* **15**, 2145729 (2022).

153. Binda, C. *et al.* Actinobacteria: A relevant minority for the maintenance of gut homeostasis. *Digestive and Liver Disease* **50**, 421–428 (2018).

154. Moon, C. D., Young, W., Maclean, P. H., Cookson, A. L. & Bermingham, E. N. Metagenomic insights into the roles of Proteobacteria in the gastrointestinal microbiomes of healthy dogs and cats. *Microbiologyopen* **7**, e00677 (2018).

155. Rajput, M. *et al.* Determining the association between gut microbiota and its metabolites with higher intestinal Immunoglobulin A response. *Vet Anim Sci* **19**, 100279 (2022).

156. Riaz, B. & Sohn, S. Neutrophils in Inflammatory Diseases: Unraveling the Impact of Their Derived Molecules and Heterogeneity. *Cells* **12**, 2621 (2023).

157. Fania, L. *et al.* Multiple Roles for Cytokines in Atopic Dermatitis: From Pathogenic Mediators to Endotype-Specific Biomarkers to Therapeutic Targets. *Int J Mol Sci* **23**, 2684 (2022).

158. Morishita, M. *et al.* Characterizing Different Probiotic-Derived Extracellular Vesicles as a Novel Adjuvant for Immunotherapy. *Mol Pharm* **18**, 1080–1092 (2021).

159. Hu, H. qi *et al.* Yinqiao antipruritic formula attenuates atopic dermatitis-like skin lesions through modulating the cytokine-cytokine receptor interaction pathway. *Fitoterapia* **183**, 106529 (2025).

160. Oh, J. H. *et al.* Purpurin suppresses atopic dermatitis via TNF-α/IFN-γ-induced inflammation in HaCaT cells. *Int J Immunopathol Pharmacol* **36**, 03946320221111135 (2022).

161. Sugaya, M. The Role of Th17-Related Cytokines in Atopic Dermatitis. *International Journal of Molecular Sciences 2020, Vol. 21, Page 1314* **21**, 1314 (2020).

162. Mills, K. H. G. IL-17 and IL-17-producing cells in protection versus pathology. *Nature Reviews Immunology 2022 23:1* **23**, 38–54 (2022).

163. Sánchez-Rodríguez, G. & Puig, L. Pathogenic Role of IL-17 and Therapeutic Targeting of IL-17F in Psoriatic Arthritis and Spondyloarthropathies. *Int J Mol Sci* **24**, 10305 (2023).

164. Shen, F. *et al.* IL-17 receptor signaling inhibits C/EBPb by sequential phosphorylation of the regulatory 2 domain. *Sci Signal* **2**, (2009).

165. Li, J. K. *et al.* IL-17 mediates inflammatory reactions via p38/c-Fos and JNK/c-Jun activation in an AP-1-dependent manner in human nucleus pulposus cells. *J Transl Med* **14**, 1–10 (2016).

166. Chiang, C. C. *et al.* Neutrophils in Atopic Dermatitis. *Clin Rev Allergy Immunol* **67**, 21 (2024).

167. Shibuya, R. *et al.* CCL2–CCR2 Signaling in the Skin Drives Surfactant-Induced Irritant Contact Dermatitis through IL-1β–Mediated Neutrophil Accumulation. *Journal of Investigative Dermatology* **142**, 571-582.e9 (2022).

168. Vestergaard, C., Just, H., Baumgartner Nielsen, J., Thestrup-Pedersen, K. & Deleuran, M. Expression of CCR2 on monocytes and macrophages in chronically inflamed skin in atopic dermatitis and psoriasis. *Acta Derm Venereol* **84**, 353–358 (2004).